

**SYNTHESIS AND BIOLOGICAL STUDIES OF NICKEL(II)
COMPLEXES OF THIOSEMICARBAZONES**

S SAVINA A/P SAVIR

**FACULTY OF SCIENCE
UNIVERSITY OF MALAYA
KUALA LUMPUR**

2021

**SYNTHESIS AND BIOLOGICAL STUDIES OF
NICKEL(II) COMPLEXES OF THIOSEMICARBAZONES**

S SAVINA A/P SAVIR

**DISSERTATION SUBMITTED IN FULFILMENT OF THE
REQUIREMENTS FOR THE DEGREE OF MASTER OF
SCIENCE**

**DEPARTMENT OF CHEMISTRY
FACULTY OF SCIENCE
UNIVERSITI MALAYA
KUALA LUMPUR**

2021

UNIVERSITI MALAYA

ORIGINAL LITERARY WORK DECLARATION

Name of Candidate: **S SAVINA A/P SAVIR**

Matric No: **SMA180012**

Name of Degree: **MASTER OF SCIENCE**

Title of Thesis (“this work”):

**SYNTHESIS AND BIOLOGICAL STUDIES OF NICKEL(II) COMPLEXES
OF THIOSEMICARBAZONES**

Field of Study:

INORGANIC CHEMISTRY

I do solemnly and sincerely declare that:

- (1) I am the sole author/writer of this Work;
- (2) This Work is original;
- (3) Any use of any work in which copyright exists was done by way of fair dealing and for permitted purposes and an excerpt or extract from, or reference to or reproduction of any copyright work has been disclosed expressly and sufficiently and the title of the Work and its authorship have been acknowledged in this Work;
- (4) I do not have any actual knowledge nor do I ought reasonably to know that the making of this work constitutes an infringement of any copyright work;
- (5) I hereby assign all and every rights in the copyright to this Work to the University of Malaya (“UM”), who henceforth shall be owner of the copyright in this Work and that any reproduction or the used in any form or by any means whatsoever is prohibited without the written consent of UM having been first had and obtained;
- (6) I am fully aware that if in the course of making this Work I have infringed any copyright whether intentionally or otherwise, I may be subject to legal action or any other action as may be determined by UM.

Candidate’s Signature

Date: 25/7/2021

Subscribed and solemnly declared before,

Witness’s Signature

Date: 25/7/2021

Name:

Designation:

SYNTHESIS AND BIOLOGICAL STUDIES OF NICKEL(II) COMPLEXES OF THIOSEMICARBAZONES

ABSTRACT

Eleven Schiff base ligands have been prepared from the condensation of N3-substituted thiosemicarbazide with fluorene-2-carboxaldehyde (**L1-L3**), 2,3,4-trihydroxybenzaldehyde (**L4-L7**) and 2,5-dihydroxybenzaldehyde (**L8-L11**). Their corresponding nickel complexes have been synthesized with two general formulations of $[\text{Ni}(\text{L})_2]$ (**1-3**) (where **L**= **L1-L3**) and $[\text{Ni}(\text{L})\text{PPh}_3]$ (**4-11**) (where **L**= **L4-L11**). The compounds were characterised by FT-IR, ^1H NMR, ^{13}C NMR, and single crystal X-ray diffraction. The results suggested that the thiosemicarbazone ligands behaved as bidentate (**L1-L3**) and tridentate (**L4-L11**) ligands which were coordinated to the Ni(II) ion *via* their N,S atoms displaying a square planar geometry (**1-3**) and their O,N,S atoms displaying a distorted square planar geometry (**4-11**), respectively. Among the compounds tested, ligands **L3** and **L5**, complexes **1** and **4** showed higher cytotoxicity against HCT 116 human colorectal carcinoma cell line than cisplatin. It is noteworthy that ligands **L6**, **L7** and **L8** showed higher cytotoxic activity against PC-3 human prostate cancer cell line than cisplatin. In addition, complexes **2**, **3**, **5** and **6** exhibited moderate *in vitro* antimalarial activity. In general, the antimalarial activity of the compound increases as the size of the substituent increases. However, this may not always be the case as anomalies in trend may occur. Our findings revealed that complex **6** displayed the highest antimalarial activity probably due to the more hydrophobic substituent attached at the N(3) position.

Keywords: Anticancer, Antimalarial, Nickel complexes, Schiff Base, Thiosemicarbazones

SINTESIS DAN KAJIAN BIOLOGI KOMPLEKS NIKEL(II) TIOSEMIKARBAZON

ABSTRAK

Sebelas ligan asas Schiff telah disediakan dari pemeluwapan thiosemicarbazide yang diganti N3 dengan fluorene-2-karboksaldehid (**L1-L3**), 2,3,4-trihydroxybenzaldehyde (**L4-L7**) dan 2,5-dihydroxybenzaldehyde (**L8-L11**). Kompleks nikel yang sesuai telah disintesis dengan dua formulasi umum $[\text{Ni}(\text{L})_2]$ (**1-3**) (di mana **L** = **L1-L3**) dan $[\text{Ni}(\text{L})\text{PPh}_3]$ (**4-11**) (di mana **L** = **L4-L11**). Sebatian tersebut dicirikan oleh FT-IR, ¹H NMR, ¹³C NMR, dan difraksi sinar-X kristal tunggal. Hasil kajian menunjukkan bahawa ligan thiosemikarbazone berkelakuan sebagai ligan bidentate (**L1-L3**) dan tridentate (**L4-L11**) yang diselaraskan ke ion Ni(II) melalui atom N, S mereka yang menunjukkan geometri satah segiempat (**1-3**) dan O, N, S atom masing-masing memaparkan geometri satah persegi yang terdistorsi (**4-11**). Di antara sebatian yang diuji, ligan **L3** dan **L5**, kompleks **1** dan **4** menunjukkan sitotoksiti yang lebih tinggi terhadap garis sel karsinoma kolorektal manusia HCT 116 daripada cisplatin. Perlu diperhatikan bahawa ligan **L6**, **L7** dan **L8** menunjukkan aktiviti sitotoksik yang lebih tinggi terhadap barisan sel barah prostat manusia PC-3 daripada cisplatin. Sebagai tambahan, kompleks **2**, **3**, **5** dan **6** menunjukkan aktiviti antimalarial in vitro sederhana. Secara amnya, aktiviti antimalarial sebatian meningkat seiring dengan peningkatan ukuran substituen. Walau bagaimanapun, ini tidak selalu berlaku kerana kecenderungan kecenderungan mungkin berlaku. Hasil kajian kami menunjukkan bahawa kompleks **6** menunjukkan aktiviti antimalarial yang paling tinggi mungkin disebabkan oleh substituen hidrofobik yang lebih melekat pada kedudukan N(3).

Kata Kunci: Antikanser, Antimalarial, Kompleks nikel, Asas Schiff, Thiosemikarbazon

ACKNOWLEDGEMENTS

First and foremost, all glory and honor be unto God who enabled me to complete my thesis successfully despite all the hardships I was going through.

I also express my heartfelt gratitude to my supervisors, Associate Professor Dr Tan Kong Wai and Associate Professor Dr Sim Kae Shin for giving me an opportunity to carry out my master studies with their group. I would like to thank them for their guidance, suggestions and comments during the research.

I am indebted to the Malaysian Government for funding and supporting me throughout the entire course of study by providing me the MyBrain Science scholarship (FRGS-FP006-2015A). I also thank Universiti Malaya for their support financially through research grants (RP033A-17AFR).

I owe my deepest gratitude to my mother, K Santhena Mary for her continuous love, support and encouragement. I could not have done it without her by my side.

Last but not least, I would like to thank my friends Nur Amira Solehah and Sophia Saging for being there with me through thick and thin. I would also like to remember lab mates Lee Shiaw Xian, Gan Chun Hao and Cheah Poh Wei for their help.

TABLE OF CONTENTS

ABSTRACT.....	iii
ABSTRAK.....	iv
ACKNOWLEDGEMENTS.....	v
TABLE OF CONTENTS.....	vi
LIST OF FIGURES.....	xi
LIST OF TABLES.....	xiv
LIST OF SYMBOLS AND ABBREVIATIONS.....	xvi
CHAPTER 1: INTRODUCTION.....	1
1.1 Introduction.....	1
1.2 Problem Statement.....	5
1.3 Research Objectives.....	5
CHAPTER 2: LITERATURE REVIEW.....	7
2.1 Importance of metal ions in biological systems.....	7
2.2 Biological roles of Nickel.....	11
2.3 Metal complexes in cancer therapy.....	13
2.3.1 Modifications in the structures of cisplatin.....	14
2.3.2 Use of prodrug as delivery strategy.....	19
2.3.3 Non-platinum anticancer drugs.....	20
2.4 Evolution of drugs for malaria.....	24
2.4.1 Chronological order of drug development for malaria.....	25
2.4.2 Targets of antimalarial drugs.....	26
2.4.3 Transition metal complexes for malaria.....	27

2.5	Thiosemicarbazone as a whole.....	28
2.5.1	Thiosemicarbazones and their metal complexes for cancer treatment.....	30
2.5.2	Antimalarial properties of thiosemicarbazones and their metal complexes.....	32
2.5.3	Fluorene-2-carboxaldehyde and polyhydroxybenzaldehyde thiosemicarbazones.....	34
2.5.4	Nickel complexes of thiosemicarbazones.....	35
CHAPTER 3: METHODOLOGY.....		37
3.1	Materials and Solutions.....	37
3.2	Physical Measurements.....	37
3.3	Syntheses.....	37
3.3.1	Synthesis of fluorene-2-carboxaldehyde thiosemicarbazone (L1).....	37
3.3.2	Synthesis of fluorene-2-carboxaldehyde-4-methyl-3-thiosemicarbazone(L2).....	38
3.3.3	Synthesis of fluorene-2-carboxaldehyde-4-ethyl-3-thiosemicarbazone (L3).....	39
3.3.4	Synthesis of bis(fluorene-2-carboxaldehyde thiosemicarbazone)nickel(II) complex [Ni(L1) ₂], (1).....	39
3.3.5	Synthesis of bis(fluorene-2-carboxaldehyde-4-methyl-3-thiosemicarbazone)nickel(II) complex [Ni(L2) ₂], (2).....	40
3.3.6	Synthesis of bis(fluorene-2-carboxaldehyde-4-ethyl-3-thiosemicarbazone)nickel(II) complex [Ni(L3) ₂], (3).....	41
3.3.7	Synthesis of 2,3,4-trihydroxybenzaldehyde-4-methyl-3-thiosemicarbazone (L4).....	41
3.3.8	Synthesis of 2,3,4-trihydroxybenzaldehyde-4-ethyl-3-thiosemicarbazone (L5).....	42
3.3.9	Synthesis of 2,3,4-trihydroxybenzaldehyde-4-phenyl-3-thiosemicarbazone (L6).....	43
3.3.10	Synthesis of 2,3,4-trihydroxybenzaldehyde-4-(4-ethylphenyl)-3-thiosemicarbazone (L7).....	43

3.3.11	Synthesis of (2,3,4-trihydroxybenzaldehyde-4-methyl-3-thiosemicarbazonato)-(triphenylphosphine)nickel(II) chloride [Ni(L4)PPh ₃]Cl, (4).....	44
3.3.12	Synthesis of (2,3,4-trihydroxybenzaldehyde-4-ethyl-3-thiosemicarbazonato)-(triphenylphosphine)nickel(II) chloride [Ni(L5)PPh ₃]Cl, (5).....	45
3.3.13	Synthesis of (2,3,4-trihydroxybenzaldehyde-4-phenyl-3-thiosemicarbazonato)-(triphenylphosphine)nickel(II) [Ni(L6)PPh ₃], (6).....	45
3.3.14	Synthesis of (2,3,4-trihydroxybenzaldehyde-4-(4-ethylphenyl)-3-thiosemicarbazonato)-(triphenylphosphine)nickel(II) [Ni(L7)PPh ₃], (7).....	46
3.3.15	Synthesis of 2,5-dihydroxybenzaldehyde thiosemicarbazone (L8).....	46
3.3.16	Synthesis of 2,5-dihydroxybenzaldehyde-4-methyl-3-thiosemicarbazone (L9).....	47
3.3.17	Synthesis of 2,5-dihydroxybenzaldehyde-4-ethyl-3-thiosemicarbazone (L10).....	47
3.3.18	Synthesis of 2,5-dihydroxybenzaldehyde-4-phenyl-3-thiosemicarbazone (L11).....	48
3.3.19	Synthesis of (2,5-dihydroxybenzaldehyde thiosemicarbazonato)-(triphenylphosphine)nickel(II) [Ni(L8)PPh ₃], (8).....	48
3.3.20	Synthesis of (2,5-dihydroxybenzaldehyde-4-methyl-3-thiosemicarbazonato)-(triphenylphosphine)nickel(II) [Ni(L9)PPh ₃], (9).....	49
3.3.21	Synthesis of (2,5-dihydroxybenzaldehyde-4-ethyl-3-thiosemicarbazonato)-(triphenylphosphine)nickel(II) chloride [Ni(L10)PPh ₃]Cl, (10).....	50
3.3.22	Synthesis of (2,5-dihydroxybenzaldehyde-4-phenyl-3-thiosemicarbazonato)-(triphenylphosphine)nickel(II) [Ni(L11)PPh ₃], (11).....	50
3.4	X-ray crystallography.....	51
3.5	Biological assays.....	51
3.5.1	MTT cytotoxicity assay.....	51
3.5.2	Determination of antimalarial activity by testing on <i>Plasmodium falciparum</i> culture.....	52

CHAPTER 4: RESULTS AND DISCUSSION.....	54
4.1 Synthesis of ligands and metal complexes.....	54
4.1.1 Synthesis of fluorene-2-carboxaldehyde-N4 thiosemicarbazone ligands (L1-L3) and their metal complexes (1-3).....	54
4.1.2 Synthesis of 2,3,4-trihydroxybenzaldehyde-N4 thiosemicarbazone ligands (L4-L7) and their metal complexes (4-7).....	56
4.1.3 Synthesis of 2,5-dihydroxybenzaldehyde-N4 thiosemicarbazone ligands (L8-L11) and their metal complexes (8-11).....	58
4.2 Infrared spectra.....	60
4.2.1 Infrared spectra of fluorene-2-carboxaldehyde-N4 thiosemicarbazone ligands (L1-L3) and their metal complexes (1-3).....	60
4.2.2 Infrared spectra of 2,3,4-trihydroxybenzaldehyde-N4 thiosemicarbazone ligands (L4-L7) and their metal complexes (4-7).....	63
4.2.3 Infrared spectra of 2,5-dihydroxybenzaldehyde-N4 thiosemicarbazone ligands (L8-L11) and their metal complexes (8-11).....	66
4.3 ¹ H NMR and ¹³ C NMR spectra.....	69
4.3.1 ¹ H NMR and ¹³ C NMR spectra of fluorene-2-carboxaldehyde-N4 thiosemicarbazone ligands (L1-L3) and their metal complexes (1-3).....	69
4.3.2 ¹ H NMR and ¹³ C NMR spectra of fluorene-2-carboxaldehyde-N4 thiosemicarbazone ligands (L4-L7) and their metal complexes (4-7).....	75
4.3.3 ¹ H NMR and ¹³ C NMR spectra of fluorene-2-carboxaldehyde-N4 thiosemicarbazone ligands (L8-L11) and their metal complexes (8-11).....	81
4.4 Crystal structures.....	87
4.4.1 Crystal structures of fluorene-2-carboxaldehyde-N4 thiosemicarbazone ligands (L1-L3) and their metal complexes (1-3).....	87
4.4.2 Crystal structures of Nickel complexes of 2,3,4-trihydroxybenzaldehyde thiosemicarbazone derivatives and triphenylphosphine.....	100

4.4.3	Crystal structures of Nickel complexes of 2,5-dihydroxybenzaldehyde thiosemicarbazone derivatives and triphenylphosphine.....	108
4.5	Biological activities of ligands and metal complexes.....	116
4.5.1	Cytotoxic activity of ligands and metal complexes.....	116
4.5.2	Antiplasmodium activity of ligands and metal complexes.....	122
CHAPTER 5: CONCLUSION AND RECOMMENDATIONS.....		126
REFERENCES.....		128
LIST OF PUBLICATIONS AND PAPERS PRESENTED.....		151
LIST OF APPENDICES.....		152

LIST OF FIGURES AND SCHEMES

Figure 2.1	: Preparation of new nickel(II) complexes (Kalaivani et al., 2014).....	13
Figure 2.2	: Structures of platinum-based anticancer drugs (Johnstone et al., 2013).....	14
Figure 2.3	: Monofunctional platinum complexes (Johnstone et al., 2013).....	15
Figure 2.4	: Synthesis of the acrydinylthioureas and their platinum conjugates (Ackley et al., 2004).....	16
Figure 2.5	: Molecular docking of the FC60 to P-gp and MRP-1. (a) Hypothetical geometry image of the FC60 binding to P-gp in four potential positions: 1,2,3 and 4; (b) potential binding site for FC60 binding to MRP-1; (c) potential binding site for FC60 binding to MRP-2 (Prylutska et al., 2017).....	18
Figure 2.6	: Structures of octahedral gallium (III) complexes (Dabrowiak., 2017).....	24
Figure 4.1	: Proposed structures of ligands (L1-L3) and complexes (1-3)	55
Scheme 4.1	: Schematic representation for the synthesis of ligands (L1-L3) and metal complexes (1-3).....	55
Figure 4.2	: Proposed structures of ligands (L4-L7) and complexes (4-7)	56
Scheme 4.2	: Schematic representation for the synthesis of ligands (L4-L7) and metal complexes (4-7).....	57
Figure 4.3	: Proposed structures of ligands (L8-L11) and complexes (8-11).....	58
Scheme 4.3	: Schematic representation for the synthesis of ligands (L8-L11) and metal complexes (8-11).....	59
Figure 4.4	: Infrared spectra of ligand L1.....	61
Figure 4.5	: Infrared spectra of complex 1.....	62
Figure 4.6	: Infrared spectra of ligand L4.....	64
Figure 4.7	: Infrared spectra of complex 4.....	65
Figure 4.8	: Infrared spectra of ligand L8.....	67
Figure 4.9	: Infrared spectra of complex 8.....	68
Figure 4.10	: ¹ H NMR spectra of ligand L1.....	71

Figure 4.11	:	^{13}C NMR spectra of ligand L1	72
Figure 4.12	:	^1H NMR spectra of complex 1	72
Figure 4.13	:	^{13}C NMR spectra of complex 1	73
Figure 4.14	:	^1H NMR spectra of ligand L4	78
Figure 4.15	:	^{13}C NMR spectra of ligand L4	78
Figure 4.16	:	^1H NMR spectra of complex 4	79
Figure 4.17	:	^{13}C NMR spectra of complex 4	79
Figure 4.18	:	^1H NMR spectra of ligand L8	83
Figure 4.19	:	^{13}C NMR spectra of ligand L8	84
Figure 4.20	:	^1H NMR spectra of complex 8	84
Figure 4.21	:	^{13}C NMR spectra of complex 8	85
Figure 4.22	:	Ellipsoid plot of ligand L1 drawn at 50 % probability level.	88
Figure 4.23	:	Unit cell packing diagram of ligand L1 viewed along axis b. Water molecules bridge the adjacent ligands forming O-H--S and N-H--O hydrogen bonding interactions.....	88
Figure 4.24	:	Ellipsoid plot of ligand L3 drawn at 50 % probability level.	90
Figure 4.25	:	Unit cell packing diagram of ligand L3 viewed along axis a. Vivid N-H--S hydrogen bonding interaction is observed.....	90
Figure 4.26	:	Ellipsoid plot of complex 1 drawn at 50 % probability level. Hydrogen atoms are omitted for clarity.....	93
Figure 4.27	:	Unit cell packing diagram of complex 1 viewed along axis a. N-H--S hydrogen bonding interaction is observed.....	93
Figure 4.28	:	Ellipsoid plot of complex 2 drawn at 50 % probability level.	95
Figure 4.29	:	Unit cell packing diagram of complex 2 viewed along axis b	95
Figure 4.30	:	Ellipsoid plot of complex 3 drawn at 50 % probability level.	98
Figure 4.31	:	Unit cell packing diagram of complex 3 viewed along axis a	98
Figure 4.32	:	Ellipsoid plot of complex 4 drawn at 50 % probability level.	102
Figure 4.33	:	Unit cell packing diagram of complex 4 viewed along axis c. Intermolecular and intramolecular O-H--Cl, O-H--O and N-H--Cl hydrogen bonding interactions are displayed. Also, water molecules were found to bridge adjacent ligands.	102

Figure 4.34	:	Ellipsoid plot of complex 5 drawn at 50 % probability level.	104
Figure 4.35	:	Unit cell packing diagram of complex 5 viewed along axis b. N-H--Cl and O-H--Cl hydrogen bonding interactions are observed. Water molecules were found to bridge adjacent ligands.....	104
Figure 4.36	:	Ellipsoid plot of complex 6 drawn at 50 % probability level.	106
Figure 4.37	:	Unit cell packing diagram of complex 6 viewed along axis c. N-H, S-H and O-H--O hydrogen bonding interactions are observed.....	106
Figure 4.38	:	Ellipsoid plot of complex 8 drawn at 50 % probability level.	110
Figure 4.39	:	Unit cell packing diagram of complex 8 viewed along axis c. Intermolecular N-H--N hydrogen bonding interactions are observed.....	110
Figure 4.40	:	Ellipsoid plot of complex 9 drawn at 50 % probability level.	112
Figure 4.41	:	Unit cell packing diagram of complex 9 viewed along axis b. Intermolecular N-H--O and O-H--O hydrogen bonding interactions are observed. Water molecules were found to bridge adjacent ligands.....	112
Figure 4.42	:	Ellipsoid plot of complex 10 drawn at 50 % probability level.....	114
Figure 4.43	:	Unit cell packing diagram of complex 10 viewed along axis a. Intermolecular N-H--Cl, N-H--O and O-H--Cl hydrogen bonding interactions are observed. Water molecules and chloride ions were found to bridge adjacent ligands.....	114

LIST OF TABLES

Table 4.1	: Infrared spectra of ligands (L1-L3) and complexes (1-3).....	62
Table 4.2	: Infrared spectra of ligands (L4-L7) and complexes (4-7).....	65
Table 4.3	: Infrared spectra of ligands (L8-L11) and complexes (8-11)....	68
Table 4.4	: ¹ H NMR spectra of ligands (L1-L3) and complexes (1-3).....	73
Table 4.5	: ¹³ C NMR spectra of ligands (L1-L3) and complexes (1-3).....	74
Table 4.6	: ¹ H NMR spectra of ligands (L4-L7) and complexes (4-7).....	80
Table 4.7	: ¹³ C NMR spectra of ligands (L4-L7) and complexes (4-7).....	80
Table 4.8	: ¹ H NMR spectra of ligands (L8-L11) and complexes (8-11)....	86
Table 4.9	: ¹³ C NMR spectra of ligands (L8-L11) and complexes (8-11)...	86
Table 4.10	: Crystallographic data summary for ligand L1	89
Table 4.11	: Selected bond lengths (Å) and bond angles (°) for ligand L1 ...	89
Table 4.12	: Crystallographic data summary for ligand L3	91
Table 4.13	: Selected bond lengths (Å) and bond angles (°) for ligand L3 ...	91
Table 4.14	: Crystallographic data summary for complex 1	94
Table 4.15	: Selected bond lengths (Å) and bond angles (°) for complex 1 ..	94
Table 4.16	: Crystallographic data summary for complex 2	96
Table 4.17	: Selected bond lengths (Å) and bond angles (°) for complex 2 ..	97
Table 4.18	: Crystallographic data summary for complex 3	99
Table 4.19	: Selected bond lengths (Å) and bond angles (°) for complex 3 .	99
Table 4.20	: Crystallographic data summary for complex 4	103
Table 4.21	: Selected bond lengths (Å) and bond angles (°) for complex 4 ..	103
Table 4.22	: Crystallographic data summary for complex 5	105
Table 4.23	: Selected bond lengths (Å) and bond angles (°) for complex 5 ..	105
Table 4.24	: Crystallographic data summary for complex 6	107
Table 4.25	: Selected bond lengths (Å) and bond angles (°) for complex 6 ..	107
Table 4.26	: Crystallographic data summary for complex 8	111
Table 4.27	: Selected bond lengths (Å) and bond angles (°) for complex 8 ..	111

Table 4.28	:	Crystallographic data summary for complex 9	113
Table 4.29	:	Selected bond lengths (Å) and bond angles (°) for complex 9 ..	113
Table 4.30	:	Crystallographic data summary for complex 10	115
Table 4.31	:	Selected bond lengths (Å) and bond angles (°) for complex 10	115
Table 4.32	:	<i>In Vitro</i> cytotoxic activity (IC ₅₀ values) of ligands (L1-L3) and complexes (1-3) against three human cancer cell lines.....	117
Table 4.33	:	<i>In Vitro</i> cytotoxic activity (IC ₅₀ values) of ligands (L4-L7) and complexes (4-7) against three human cancer cell lines.....	119
Table 4.34	:	<i>In Vitro</i> cytotoxic activity (IC ₅₀ values) of ligands (L8-L11) and complexes (8-11) against three human cancer cell lines....	121
Table 4.35	:	Antiplasmodium activity (IC ₅₀ (μM) values) of ligands (L1- L3) and metal complexes (1-3) for <i>P. falciparum</i> 3D7.....	123
Table 4.36	:	Antiplasmodium activity (IC ₅₀ (μM) values) of ligands (L4- L7) and metal complexes (4-7) for <i>P. falciparum</i> 3D7.....	124
Table 4.37	:	Antiplasmodium activity (IC ₅₀ (μM) values) of ligands (L8- L11) and metal complexes (8-11) for <i>P. falciparum</i> 3D7.....	125

LIST OF SYMBOLS AND ABBREVIATIONS

Å	: Angstrom
μ	: micro
DNA	: Deoxyribonucleic acid
CQ	: Chloroquine
TSC	: Thiosemicarbazone
TPP	: Triphenylphosphine
DMSO	: Dimethyl sulfoxide
GLOBOAN	: Global Cancer Incidence, Mortality and Prevalence
WHO	: World Health Organisation
PPT 1	: Palmitoyl-protein thioesterase 1
PC-3	: Human prostate cancer
A375	: Human malignant melanoma
MCF7	: Human breast cancer
HCT 116	: Human colorectal carcinoma
H413	: Carcinoma-derived human oral keratinocyte
RNA	: Ribonucleic acid
ATP	: Adenosine triphosphate
ROS	: Reactive oxygen species
CT-DNA	: Calf thymus deoxyribonucleic acid
MIC	: Minimum inhibitory concentration
DMF	: Dimethyl formamide
ATCC	: American Type Culture Collection

LIST OF APPENDICES

Appendix A	:	IR spectra of ligands and complexes.....	152
Appendix B	:	^1H NMR spectra of ligands and complexes.....	161
Appendix C	:	^{13}C NMR spectra of ligands and complexes.....	178

Universiti Malaya

CHAPTER 1: INTRODUCTION

1.1 Introduction

This research focuses on the synthesis and characterisation of Ni(II) complexes coordinated to bidentate fluorene-2-carboxaldehyde thiosemicarbazone ligands *via* their N,S atoms and tridentate polyhydroxybenzaldehyde ligands *via* their O,N,S atoms. The structure and biological activities of transition metal complexes with nitrogen/sulfur donor ligands have made them important. Metal complexation of the N/S donor ligands was seen to improve their biological properties. Since nickel forms bond with soft and hard ligands, bonding of nickel with N/S donor ligands form compounds with various geometries, coordination numbers and oxidation states. Hence, it would be interesting to synthesise nickel complexes from N, S and O, N, S donor ligands.

The cytotoxicity and antimalarial activities of the ligands and their nickel complexes were studied in the current study. Transition metal complexes with planar and aromatic functional group ligands can intercalate DNA base pairs. Hence, ligands and complexes from fluorene-2-carboxaldehyde were synthesised to serve their purpose as DNA intercalators. Ligands and complexes from polyhydroxybenzaldehyde were also synthesised due to the presence of uncomplexed hydroxyl group which enhances solubility of the compound and ease biological testing. Besides, the substituent group at the N3 position of thiosemicarbazone was varied because a slight structural change can bring about a great difference in biological activity. Studies of new drugs with cytotoxic activity is crucial to curb increasing death rate due to cancer.

A report obtained by using GLOBOCAN 2018 to estimate cancer occurrence showed that death caused by cancer worldwide in 2018 was about 9.6 million (Bray et al., 2018). Anticancer drugs are rapidly being synthesised to overcome the issues in cancer therapy. For instance, compounds derived from platinum such as cisplatin, oxaliplatin and

carboplatin were once vital anticancer agents (Gao et al., 2020). However, platinum based compounds were found to cause significant and irreversible side effects such as ototoxicity, nephrotoxicity and peripheral neuropathy (Calvert, 2019; Tserga et al., 2019). In which case, new anticancer agents have to constantly be synthesised to address the issues caused by previous drugs. Previous studies have shown that pyrimethamine which is an antimalarial drug, is able to induce apoptosis of cancer cells, acting as an antitumor drug simultaneously (Liu et al., 2019). Thus, it would be enthralling if the compounds studied in this work could have cytotoxic activity and act as antimalarial drugs at the same time.

Malaria is an illness that can be caused by four species of protozoan parasites of the genus *Plasmodium*, i.e. *Plasmodium falciparum*, *Plasmodium vivax*, *Plasmodium ovale* and *Plasmodium malariae*. Among them, *P. falciparum* has been found to cause the most severe form of malaria (Koram & Molyneux, 2007). It is noted that malaria infection activates immune-responsive genes during the critical transition states of the parasites' life cycle (Dimopoulos et al., 1998). Data provided by WHO European region from 1990-2016 shows that malaria is prevalent among children aged 5-14 years (Kyu et al., 2018). Discoveries of chloroquine followed by artemisinin were able to ward off malarial infection for some time until the parasite acquired resistance towards these drugs (Chinappi et al., 2010; Tilley et al., 2016). Therefore, the therapeutic potential of metal-based antimalarial agents were extensively explored ever since the discovery of ferroquine which was once considered the most potent organometallic antimalarial drug (Atteke et al., 2003). However, ferroquine exhibited clinical adverse effects such as gastrointestinal and nervous system disorders (Mombo-Ngoma et al., 2011). Hence, the need for the discovery of new drugs that can overcome the resistance issue is always there. Interestingly, recent studies on chloroquine have proved that it is able to act as an autophagy inhibitor by targeting the palmitoyl-protein thioesterase 1 (*PPT 1*) enzyme

causing apoptosis of cancer cells (Rebecca et al., 2019). Thus, it would be fascinating if the compounds that are being studied in this paper could be cytotoxic and act as antimalarial drugs at the same time.

Thiosemicarbazones (RNH-CS-NH-NHR', tsc) are widely used as ligands in studying the cytotoxicity and antimalarial activity of metal complexes due to their rich biological, medicinal and pharmacological properties (Chandra et al., 2009; Güveli et al., 2016). They can coordinate to metal as neutral molecules or as anionic ligands and can adopt a variety of different coordination. Thiosemicarbazones bind through their sulphur and hydrazine nitrogen atom with transition metal ion, making them good chelating agents (Chandra et al., 2013).

Triphenylphosphine (TPP) is used as secondary ligand in this study because phosphine based compounds have widespread pharmacological applications such as antiviral, antioxidant, antifungal, anticarcinogenic, antitumor and antibacterial by nature (Kaya et al., 2020). Explicitly, phosphine based nickel(II) and palladium(II) complexes have been reported to possess significant bioactivities (Shabbir et al., 2017). In cancer treatment, TPP, which is a mitochondriotropic ligand is expected to transfer the metal ion into the cancer cells (Chrysouli et al., 2018). Besides, TPP is used in the metal complexation process because it acts as a catalyst in the synthesis of organic and inorganic compounds to speed up the rate of a chemical reaction (Aswin et al., 2014). Thus, it is believed to speed up the rate of a chemical reaction. An important factor that influences the antimalarial activity of a compound is its hydrophobicity. The higher the hydrophobicity, the more potent its activity (Deshpande et al., 2009; Navarro et al., 2011). Hence, the hydrophobic aromatic rings in TPP are hoped to enhance the antimalarial activity of the synthesised compounds.

Focus was given to develop nickel complexes of thiosemicarbazones because nickel complexes have shown to exhibit potent cytotoxic and antimalarial activities (Shawish et al., 2014). Besides, metal free ligands show little or no cytotoxic and antimalarial activities, but metal complexes were believed to exhibit potent activities mentioned earlier. Hence, metal chelating abilities account for the cytotoxic and antimalarial activities of a metal complex (Chellan et al., 2010). In addition, complexation of the ligand with a metal helps with the cellular uptake process of the parasite due to the lipophilic nature of the metal complex as it aids in the transportation of the metal-free thiosemicarbazones into cellular components (Bahl et al., 2010). In a nutshell, metal chelators can deprive parasites from metal ions crucial for their survival and utilize the newly formed metal-chelator hybrid (complex) to induce oxidative insult to the parasites.

Previous research on citronellal thiosemicarbazone derivatives suggested that bis complexes of nickel where the ligand was coordinated to the metal centre *via* its bidentate N, S atom was exceedingly efficacious towards several cancer cell lines (Bisceglie et al., 2019). However, not much has been studied on ligands and complexes derived from fluorene-2-carboxaldehyde. Hence, taking into consideration works previously done using this group of compounds (Heng et al., 2015), this research reports on the synthesis, characterisation and biological studies of ligands and Nickel(II) complexes derived from fluorene-2-carboxaldehyde.

Also, previous research on polyhydroxybenzaldehyde thiosemicarbazone derivatives suggested that complexes of nickel where the ligand was coordinated to the metal centre *via* its tridentate O,N,S atom was effective towards several cancer cell lines (Human prostate cancer (PC3), human malignant melanoma (A375), human breast cancer (MCF 7) and carcinoma-derived human oral keratinocyte (H413)) (Shawish et al., 2014). Although some ligands of the 2,3,4-trihydroxybenzaldehyde and 2,5-dihydroxybenzaldehyde derivatives have been synthesised and reported, further

characterisation and biological studies could still be conducted on their metal complexes. Therefore, this research also reports the synthesis, characterisation and biological studies of ligands and complexes derived from 2,3,4-trihydroxybenzaldehyde and 2,5-dihydroxybenzaldehyde.

1.2 Problem Statement

Malaria is caused by the *Plasmodium* species parasite. The parasites are transmitted to humans by the *Anopheles* species mosquitoes. Artemisinin once became the essential component for the treatment of malaria. It is able to put to death the young malaria parasites which are found within the red blood cells. Hence, it prevents the development of the parasites to mature stages. Therefore, new antimalarials are continuously developed to overcome drug resistance.

On the other hand, compounds derived from platinum such as cisplatin, oxaliplatin and carboplatin were once vital anticancer agents. However, platinum based compounds were found to cause significant and irreversible side effects such as ototoxicity, nephrotoxicity and peripheral neuropathy. Besides, the cancer cells were found to develop resistance towards drugs derived from platinum. Hence, new anticancer agents need to be constantly synthesised to address the issues caused by previous drugs.

1.3 Research Objectives

The main objective is to synthesise Nickel complexes with anticancer and antimalarial properties. This is achieved through the following sub-objectives:

- i. To synthesise and characterise Nickel complexes of thiosemicarbazones
- ii. To determine the antimalarial activities of the synthesised compounds

- iii. To evaluate the growth inhibitory properties of the synthesised compounds against selected human cancer cell lines
- iv. To investigate the potency of these chelators and Nickel complexes in treatment of malaria and cancer

Universiti Malaya

CHAPTER 2: LITERATURE REVIEW

2.1 Importance of metal ions in biological systems

The maintenance of lifespan of plants, animals and humans depend on metal ions which are the fundamental elements. Growth disorders, severe malfunction, carcinogenesis or death may result from the absence of metal ions. The cellular and subcellular functions of metal ions are highly recognised. Calcium is one of the metal ions which is needed to lead a healthy lifestyle. Apart from building strong bones and teeth, it helps to quell muscle cramps and trigger a number of chemical reactions that the human body needs (Anastassopoulou & Theophanides, 1995). Calcium ion (Ca^{2+}) is needed for muscle contraction and tissue survival as well. Besides, it plays vital roles in secretion, glycolysis, gluconeogenesis, ion transport, cell division and growth. It is also known for its significant roles outside cells. For instance, the Ca^{2+} ion forms links between individual cells and maintains the rigidity of the whole seaweed plant. Whereas, in the blood plasma of mammals, this ions function to join proteins with membrane surfaces of circulating cells. On the other hand, Ca^{2+} ions are found in quite a number of the extracellular enzymes to elevate their functioning abilities (Forsen & Kordel, 1994). Calcium deficiency may result in hypocalcaemia which will lead to osteoporosis and dental caries. Meanwhile, excess level of calcium in the blood may result in hypercalcaemia which in the long run will weaken the bones, create kidney stones and obstruct the normal function of heart and brain (Dorozhkin & Epple, 2002). Thus, a normal level of calcium must be maintained for a healthy lifestyle.

Interestingly, another metal ion that works hand in hand with Ca^{2+} ion for the sustenance of a stable internal environment is the magnesium ion (Mg^{2+}). It functions to modulate and control the entry and exit of Ca^{2+} from sarcoplasmic and endoplasmic reticular membranes. Being the fourth most abundant cation in the body, it plays an

important role in physiological functions. Its balance is maintained by renal regulation of magnesium reabsorption (Swaminathan, 2003). Besides, it regulates intermediary metabolism, DNA and RNA synthesis, cell growth, reproduction and membrane structure. The Mg^{2+} ion also controls neuronal activity, cardiac excitability, neuromuscular transmission, muscular contraction, vasomotor tone, blood pressure and peripheral blood flow (Altura & Altura, 1996). Apart from their known functions, it was later discovered that Mg^{2+} plays a vital role in brain biochemistry, is safe to be consumed and has a vast history in treating depression and mental health issues. Its use for the treatment of depression was recognised in homeopathic medicine. For instance, magnesium chloride was able to alleviate anxiety, apathy, aversions, despair, depression, discontent, headaches, insecurities, irritability, over sensitiveness, restlessness, sulkiness, talkativeness and uncertainty. It is interesting to note that the first use of magnesium to secure a fracture involving the bones of the lower leg was reported by Lambotte in 1970, confirming the use of magnesium and its alloys as orthopaedic biomaterials. Subsequent discoveries were able to prove the non-toxic attribute of magnesium which made it suitable as an orthopaedic biomaterial since it possesses bone healing properties (Lambotte, 1932; Staiger et al., 2006). On the other hand, various neuromuscular symptoms could result from magnesium deficiency. Moreover, lack of magnesium can cause hypocalcaemia, hypokalaemia, hinder cardiac and neurological manifestations. However, a lack of magnesium is all the time neurotic and not psychotic (Eby & Eby, 2006).

Sodium (Na^+) and potassium (K^+) are some of the metal ions worth the discussion. These ions serve to main cellular homeostasis and affect most metabolic processes. The balance of these ions in the cells are important to maintain osmotic pressure and water distribution in the body. The maintenance of proper pH, regulation of heart rate and proper functioning of muscles depend strongly on the level of these ions in the body. In

addition, they take part in electron transport reactions and function as cofactor for enzymes in catalysis reactions. Both ions are equally important but are found in different cellular environments. The Na^+ ions are found mostly at the extracellular fluid whereas the K^+ ions are found mostly at the intracellular fluid. Hence, these ions are in constant movement between intracellular and extracellular body compartments to maintain internal fluid and electrolyte balance. They also play vital role in the renal regulation of acid-base balance. Besides, the conduction of nerve impulses is possible through the generation of electric potential by the sodium-potassium flux. As a result of this electric potential gradient, muscle contraction is generated, and heartbeat is regulated. Hence, nerve cells could respond to stimuli and transmit impulses accurately. However, unusual levels of these ions in the body could lead to several pathological disorders such as oedema, headache, muscle spasms, nausea, vomiting, fatigue, arrhythmia and muscle weakness (Pohl et al., 2013; Sigel et al., 2013). Thus, it is important to keep these electrolytes in balance to ensure proper functioning of the cells.

It is noteworthy that copper is a significant metal ion in the biological system. Known as the third most abundant transition metal, it serves as an element for all organisms that have an oxidative metabolism due to its ability to interconvert between two oxidation states. It is well known as a cofactor for several enzymes in physiological reactions to maintain homeostasis. Moreover, biological processes such as angiogenesis, response to hypoxia and neuromodulation are dependent on the levels of copper in the cell (Scheiber et al., 2013). On the other hand, it is important to address the vital role played by zinc in the body. This colourless trace metal serves as a cofactor of at least 3000 human proteins. Zinc is given importance due to its functions in metalloenzyme and transcription factor. Apart from this, its role in protein structure and protein-protein interactions are highly significant. Simply put, as an enzymatic catalysis and regulator of protein, its molecular role is based on its interaction with proteins (Maret, 2013). It was found to affect and

interfere with homeostasis, immune function, oxidative stress and apoptosis. Zinc deficiency occurring simultaneously with chronic diseases such as atherosclerosis, neurological disorder, autoimmune diseases, aging, age-related degenerative diseases and Wilson's disease was found to complicate clinical features, affect immunological status, increase oxidative stress, and generate inflammatory cytokines (Chasapis et al., 2012). Previous studies have shown that zinc deficiencies may cause retarded growth, immune dysfunction and cognitive impairment (Chasapis et al., 2012).

Yet, another essential metal ion in the biological system is iron (Fe^{3+}). Its ability to participate in electron transport reactions makes it remarkable. It is often found in ferritin, hemosiderin, myoglobin and erythrocytes. Hence, it is not freely available in the human body (Bullen et al., 1978). Furthermore, an optimum level of iron has to be maintained in the body to avoid complications. This is because, iron overload was found to cause abnormal glucose metabolism, increasing the occurrence of type 2 diabetes. However, through phlebotomy and iron chelation therapy, a reduction in iron overload was achieved and lead to improvement in diabetes (Swaminathan et al., 2007). Iron is vital for oxygen consumption and ATP production. The rate of oxygen consumption in the brain is relatively high. Cells in the central nervous system (CNS) that stains for iron is the oligodendrocytes. These cells, known as the neuroglia, accumulates iron in order to function better (Todorich et al., 2009). In addition, studies have shown that iron and its derivatives required for the ROS-enzymes to function optimally. It is noteworthy that ROS-dependent cell damage and death are caused by both iron-dependent ROS-producing enzyme and labile iron (Dixon & Stockwell, 2014). Thus, iron functions as catalyst to produce ROS species within the cell, leading to apoptosis of the cell.

2.2 Biological roles of Nickel

Nickel, being the 24th most abundant element in earth's crust exist as either insoluble particles such as dusts, sulfides and oxides or water-soluble nickel compounds such as chloride salts of nickel, sulfate salts of nickel and nitrate salts of nickel. Nickel and its complexes suit applications in the modern industry due to their low thermal and electrical conductivities, high resistance to corrosion and oxidation, outstanding thermal strength and toughness and potential to be magnetised. Several experiments on animal models have highlighted the necessity of nickel for optimal reproductive function, bone composition and strength, energy metabolism and sensory function. Nickel complexes were reported to cause genotoxic effects on the structure of DNA, resulting in immense DNA damage in the genome region. It causes oxidative damage to DNA by generating oxides and reactive species that produce crosslinks between DNA and protein (Sigel et al., 2013; Zambelli & Ciurli, 2013).

Previous study stated that nickel acts as a co-factor in the absorption of iron from the intestine (Schneegg & Kirchgessner, 1976). Later, a study by Kumar and co-workers (2016) proved that nickel increased the absorption of iron in iron-deficient rats, but this only occurs under certain specified conditions. For instance, iron absorption occurred only when iron was in ferric form, not ferrous or ferric sulphates forms (Kumar & Trivedi, 2016).

A study on biological evaluation of nickel complexes carried out by Kalaivani and co-workers (2014) on nickel(II) metallates showed binding by intercalation mode between the complexes and CT-DNA. **Figure 2.1** shows the preparation of nickel complexes. The binding studies deduced that complex 4 which is Ni(Msal-ptsc)(PPh₃), in which the ligand contains the -phenyl substituent was the most active. Besides, cytotoxicity test was carried out on human lung adenocarcinoma (A549) cells *in vitro* with the synthesised complexes.

At given experimental conditions, the newly synthesised nickel complexes displayed potent cytotoxic activity. Factors such as lactate dehydrogenase (LDH) leakage and release of nitric oxide into the extracellular medium were used to indicate level of cytotoxicity displayed by the nickel complexes. Once the membrane integrates due to apoptosis, LDH which is a stable cytoplasmic enzyme will be released into the medium culture. The synthesised nickel complexes were found to cause LDH leakage in the culture medium of A549 cells even at a low dosage and increased LDH leakage in a dose-dependent manner. Whereas, the third isoform of NO synthase which is the iNOS produces nitric oxide (NO) during oxidative stress. DNA and protein are damaged by the extremely unstable nitric oxide when it is in excess. Compared with control cells, the A549 cells treated with complexes showed an increase in nitric oxide release. The levels of both LDH and NO released into the A549 culture medium indicated that complex 3 with ethyl substituent at the N3 position was the most cytotoxic. Furthermore, the findings concluded that apoptosis was induced by the nickel complexes through ROS hypergeneration, in which the complex with the ethyl substituent (complex 3) was found to be the most efficient.

This study also revealed that the nickel complexes induced apoptosis in the A549 cells through mitochondria-mediated pathway. On the other hand, migration of cancer cell studied by conducting wound migration assay showed the suppression of A549 cell migration by nickel complexes, indicating that the complexes are antimetastatic (Kalaivani et al., 2014). Thus, nickel complexes could intercalate to DNA, generate ROS species and lead to cell death in a mitochondria-mediated pathway. Having said that, nickel complexes have great potential to be developed into an anticancer drug.

On the other hand, a study on the antimalarial activity of metal complexes from primaquine and sulphamethoxazole by Nandal and co-workers (2019) proved that nickel complexes displayed better activity than the standard drug primaquine (Nandal et al., 2019). Whereas, another study by Adediji et al. reported that nickel complexes of mefloquine and pyrimethamine showed improved antimalarial activity (Adediji et al., 2012; Singh, 2019). Nickel complexes have significant potential to be developed as drug for malaria. Thus, derivatives of nickel complexes need to be synthesised and tested to obtain the mode of action of the complexes in order to function as effective antimalarial compounds in the future.

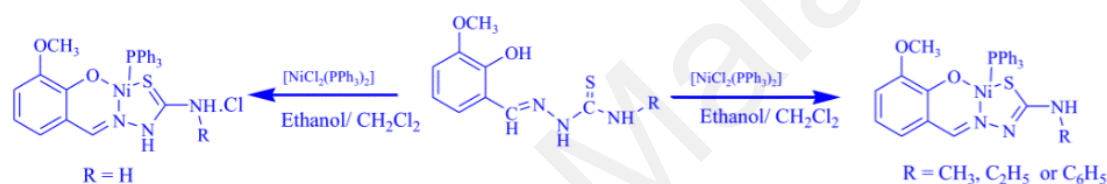


Figure 2.1 Preparation of new nickel(II) complexes (Copyright permission from Kalaivani et al., 2014).

2.3 Metal complexes in cancer therapy

Although there are many metal complexes around the world, platinum complexes are the most remarkable metals in medicine. The most familiar platinum-based drug, cisplatin and its anticancer activity was serendipitously discovered by Rosenberg in 1969 (Rosenberg et al., 1969). Soon after, various forms of platinum-based drugs such as carboplatin, oxaliplatin, nedaplatin, lobaplatin and heptaplatin were prepared and examined for their antitumor properties and ability to cause cell death. **Figure 2.2** shows the structures of platinum based anticancer drugs. Cisplatin undoubtedly prevails as the most efficacious than the rest, especially in the treatment of testicular cancer.

Unfortunately, dose-limiting side effects such as gastrointestinal toxicity, neurotoxicity and nephrotoxicity caused a decline in the use of cisplatin. Other than that, the limited use of cisplatin as an anticancer drug is due to its high rate of chemoresistance (Galluzzi et al., 2012). However, the therapeutic effects of cisplatin and its role as anticancer agent cannot be ignored completely. Several approaches have been considered to address the issues of toxicity and drug resistance. For instance, proposing a modification in the structure of the platinum drug, using prodrug as a delivery strategy and developing non-platinum drugs as anticancer agents.

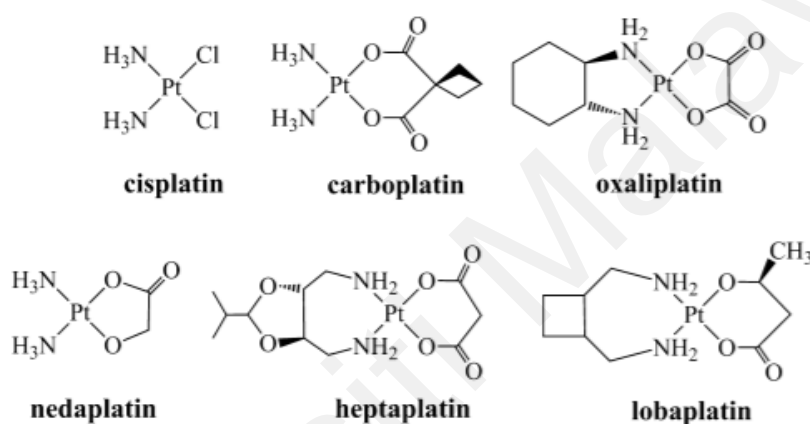


Figure 2.2 Structures of platinum-based anticancer drugs (Copyright permission from Johnstone et al., 2013).

2.3.1 Modifications in the structures of cisplatin

The usual structure-activity relationship proposed years ago required the drug to have charge neutrality, a square planar coordination geometry, the presence of a pair of inert ligands *cis* to one another in the coordination sphere and a pair of labile ligands in the remaining two sites (Kelland, 2007; Wheate et al., 2010). However, minor modifications in the structure of drugs rendered them less toxic and helped to overcome the drug resistance issue. In 2013, Johnstone and co-workers (2013) investigated some monofunctional platinum(II) compounds that lead to the discovery of potential anticancer

drug. **Figure 2.3** shows the structures of the monofunctional platinum complexes. Two types of monofunctional platinum(II) complexes that were prepared by this group are monofunctional compounds containing exocyclic nitrogen-donor ligands and monofunctional compounds containing endocyclic nitrogen-donor ligands. Although it was later discovered that these monofunctional platinum complexes lacked clinical significance, their discovery led to the search of platinum complexes with structures that deviates from the structure of cisplatin because even cisplatin was found to be inactive towards several types of cancers. Hence, all is not lost (Johnstone et al., 2013).

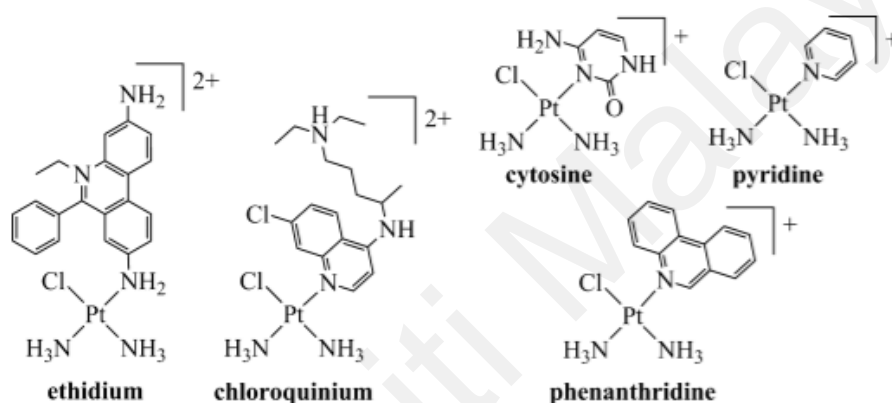


Figure 2.3 Monofunctional platinum complexes (Copyright permission from Johnstone et al., 2013).

Another approach of modification in the structure of cisplatin was introduced by Martin and co-workers (2001). They synthesised platinum complexes from [PtCl₂(en)] (en) ethane-1,2-diamine) by replacing the chloro leaving groups with novel acridinylthioureas. In this study, the Pt-S bond being highly stable, prevents the thiourea from being displaced by the DNA nucleophiles. The synthesised platinum-acridine conjugate was found to be cytotoxic at micromolar concentrations. It was also believed to be able to address the problem of drug resistance. Hence, the study revealed several platinum-acridine complexes as potential drugs for clinical use (Martins et al., 2001).

A similar study by Ackley and co-workers (2004) used PT-ACRAMTU, a novel platinum–intercalator conjugate $\{[\text{Pt}(\text{en})\text{Cl}(\text{ACRAMTU-S})](\text{NO}_3)_2$, ACRAMTU=1-[2-(acridin-9-ylamino)ethyl]-1,3-dimethylthiourea and its derivatives instead. **Figure 2.4** shows the synthesis of acridinylthioureas and their platinum conjugates. They postulated that replacement of the chloro leaving group by the thiourea non-leaving group managed to regulate biological activities of the newly synthesised compounds. The complexes showed promising cytotoxicity. However, their study suggested that drastic structural changes in the structure will be needed to produce a lead compound with greater activity (Ackley et al., 2004).

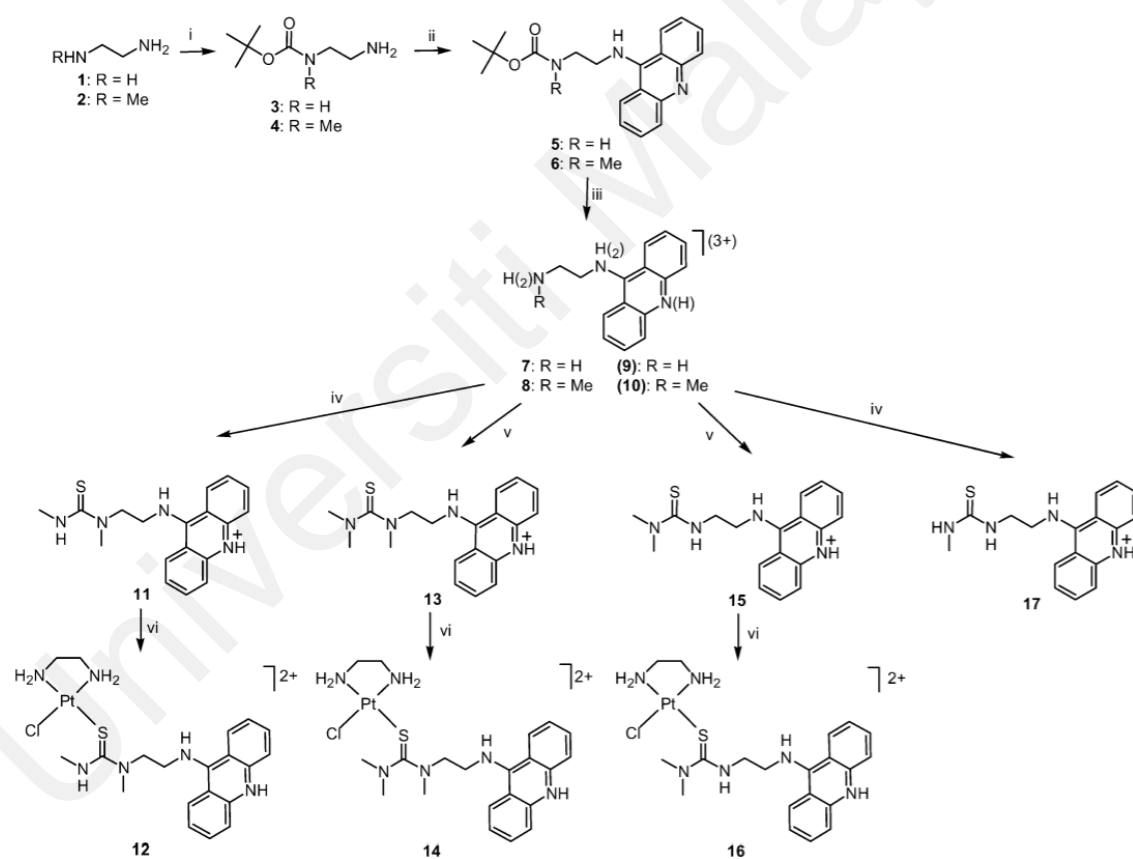


Figure 2.4 Synthesis of the acridinylthioureas and their platinum conjugates (Copyright permission from Ackley et al., 2004).

There is another approach in the modification of the structure of cisplatin, which is the formulation and analysis of nanoformulation of cisplatin (Cis) with C_{60} fullerene ($\text{C}_{60}+\text{Cis}$

complex) discovered by Prylutska and co-workers (2017). **Figure 2.5** shows the molecular docking of the FC60 to P-gp and MRP-1. The study proved that the C₆₀+Cis complex induced tumour cell growth *in vivo* and *in vitro*, showed higher toxicity than Cis alone and overcame drug resistance by the capability of C₆₀ to interfere with P-gp, MRP-1, and MRP-2 molecules. Therefore, the C₆₀+Cis complex is able to tackle the toxicity and drug resistance issues of cisplatin, rendering it a potential candidate in chemotherapeutic studies (Prylutska et al., 2017).

Universiti Malaya

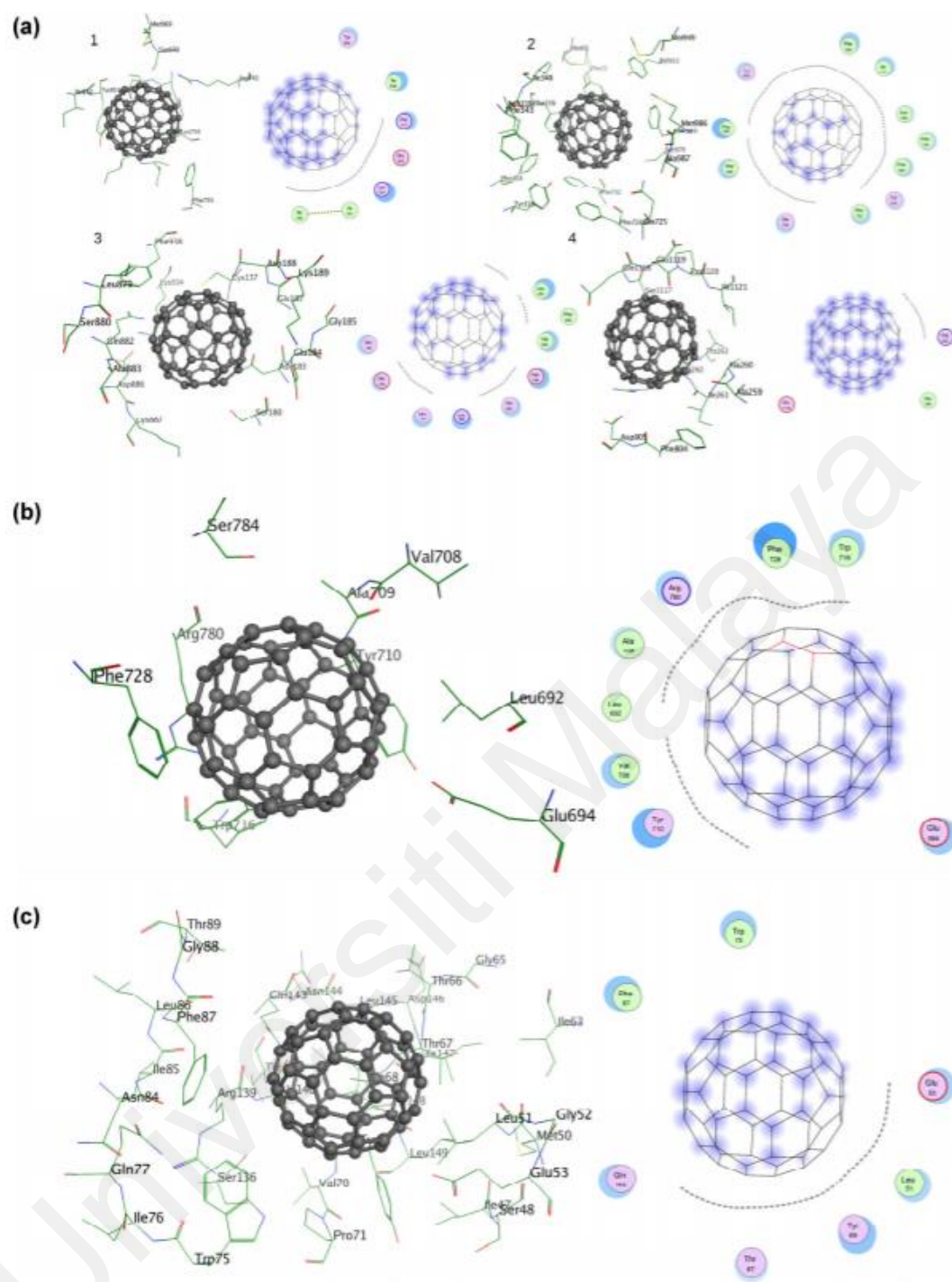


Figure 2.5 Molecular docking of the FC60 to P-gp and MRP-1. (a) Hypothetical geometric image of the FC60 binding to P-gp in four potential positions: 1, 2, 3, and 4; (b) potential binding site for FC60 binding to MRP-1; (c) potential binding site for FC60 binding to MRP-2 (Copyright permission from Prylutska et al., 2017).

2.3.2 Use of prodrug as a delivery strategy

Apart from modifying the structure of cisplatin, using prodrug to deliver the drug to targeted areas is another strategy that should be considered. Johnstone and co-workers (2013) studied six-coordinate Pt(IV) complexes that bear an octahedral geometry as prodrug and incorporated them into various nano-delivery devices (Gabano et al., 2009; Harper et al., 2010; Lovejoy & Lippard, 2009). The two prominent methods that were used by them are synthesising Pt(IV) complexes with biologically active axial ligands and using several nanoparticle delivery techniques. In the first method, the platinum complexes were synthesised with either carboxylate ligands or ligands attached by amide bond. Whereas in the second method, the platinum complexes were delivered to targeted area in four different ways which are by attaching them to single walled nanotubes or gold nanoparticles and encapsulating them with polymer nanoparticle to deliver both hydrophobic and polymer-conjugated Pt(IV) prodrug. Hence, these targeted delivery methods make these complexes less toxic than cisplatin, overcoming inherent and acquired resistance simultaneously (Johnstone et al., 2013).

Another study on targeting and delivery of platinum-based anticancer drug emphasised two main methods for drug delivery which are the active and passive methods. The active method comprises the conjugation of platinum drugs with selective targeting moieties or encapsulation of platinum drugs by bioactive substances such as hormones, carbohydrates, peptides and proteins (Bruijninx & Sadler, 2008; MacDiarmid et al., 2007). Whilst, the passive method includes the conjugation of platinum drugs with fabricated polymers or nanoparticles. The passive method uses polymeric micelles, liposomes, nanotubes and nanoparticles for encapsulation purposes. Targeted therapy using the mentioned delivery methods were able to circumvent normal tissues from damage and curb drug resistance (Wang & Guo, 2013).

Previous study by Butler and co-worker (2013) addressed the use of carbon nanotubes (CNTs) and nanorods, hollow Prussian blue (HPB), magnetic iron oxide and gold nanoparticles, liposomes, nanogels and polymers, as well as active targeting by conjugation to biodegradable proteins and peptides as methods of targeted delivery. Their findings suggested that new targeting and delivery modes could produce superior complexes with state-of-the-art mechanisms to eradicate tumour cells (Butler & Sadler, 2013).

2.3.3 Non-platinum anticancer drugs

The search for non-platinum anticancer drug continues as platinum based anticancer drugs suffer from side effects and drug resistance. It is noteworthy that metals like titanium, ruthenium and gallium were assessed in phase I and phase II trials whereas metals like iron, cobalt and gold were found to show promising outcome in preclinical trials. The results demonstrate that development of new metal complexes with up to date mode of actions and mechanisms is possible. This study by Ott and co-workers (2007) reports on the anticancer activity of metal complexes of iron, cobalt and gold. It was postulated that the unsubstituted ferrocene is inactive but salts of ferrocenium picrate and ferrocenium trichloroacetate showed improved cytotoxic activity due to their ability to form reactive active species (ROS) which could damage the structure of the DNA. Besides, ferrocene derivatives of the anti-estrogen tamoxifene or ferrocene pyrazole conjugates with various transition metals were found to exhibit antiproliferative activity recently. In addition, compounds with iron carbonyl moiety and iron(II) complexes containing pentadentate pyridyl ligands showed greater cytotoxicity and induced apoptosis (Ott & Gust, 2007).

As for cobalt, its alkyne complexes displayed potential antitumor activity in murine leukemia cells. Soon after, discovery of hexacarbonyldicobalt complexes with antiproliferative activity in different tumour cells led to further examination of the compounds as anticancer agents. The mode of action of revealed an efficient binding of these complexes to DNA. On the other hand, the hypoxia selective property of cobalt(III) complexes, enabling it to function as an anticancer agent was studied by this group. These complexes incorporated with nitrogen mustard ligands manifested hypoxic selectivity against tumour cells by ionising radiation and releasing potent cytotoxins. The pH of tumour cells which are slightly acidic activates cobalt(III) complexes to generate free radicals responsible for causing a structural change in DNA. Cobalt salen complexes are another group of antitumor agent worth mentioning. The kind of substituent attached to the aromatic ring, not its position affected cytotoxicity of this group of compounds Hence, DNA damage *via* oxidation is not one of its mode of action.

Studies on gold complexes were also reported by this group. Earlier studies on the well-known gold(I) phosphine complex, auranofin proved that it could be used to treat rheumatoid arthritis and in the meantime inhibit growth of tumour cells *in vitro* (Mirabelli et al., 1985; Simon et al., 1979; Sutton et al., 1972). Replacement of the thiosugar moiety by chlorine in the chloro(triethylphosphine)gold (I) which is an analog to auranofin displayed potent cytotoxicity. Subsequent evolution of gold(I) complexes with bis(diphenylphosphino)ethane ligands proved to develop crosslinks between DNA and protein, resulting in DNA strand breaks. The complexes also hindered the synthesis of protein, DNA and RNA. Hence, this class of compounds are cytotoxic towards tumour cells. In addition, gold(III) complexes were also found to exhibit potential antitumor activity (Ott et al., 2007).

As mentioned earlier, complexes of ruthenium, titanium and gallium are some examples of metal complexes under clinical trial. Chloro-ammine complexes were the

first ruthenium complexes to be studied. Although earlier studies on ruthenium complexes failed due to the insolubility of ruthenium complexes for pharmaceutical uses, incorporation of imidazole and indazole ligands into ruthenium complexes by Keppler were known to be particularly active against platinum-resistant colorectal autochthonous tumours (Keller, 1993). Moreover, activity against metastasizing tumours in mice by imidazole-dimethylsulfoxide ruthenium(III) complex was disclosed by Alessio and Sava (Sava et al., 1999). In 1992, Tocher and co-workers (1992) introduced the usage of arene ruthenium complexes as anticancer agents. Their cytotoxic ability was enhanced when the anticancer agent metronidazole was coordinated to a benzene ruthenium dichloro fragment (Dale et al., 1992). Soon after, this research led Dyson and Sadler to pioneer the field of antitumoural and antimetastatic arene ruthenium complexes, resulting in the discovery of $(\eta^6\text{-p-MeC}_6\text{H}_4\text{Pri})\text{Ru}(\text{P-pta})\text{Cl}_2$ (pta = 1,3,5-triaza-7-phospha-tricyclo-[3.3.1.1]decane), termed RAPTA-C (Dougan & Sadler, 2007; Dyson, 2007). Some of the recent advances in ruthenium arene complexes are synthesis of mononuclear arene ruthenium complexes containing P- or N-donor ligands, mononuclear arene ruthenium complexes with N,N-, N,O- or O,O-chelating ligands and multinuclear arene ruthenium complexes and clusters. The amphiphilic properties of arene ruthenium unit and its synthetic diversity plays vital role in chemotherapy, not to forget their low toxicity and high selectivity as well (Süss-Fink, 2010). Another study on macromolecular ruthenium complexes as anticancer agents explored the routes in which a water-soluble macromolecular drug with enhanced permeation and retention effect could be created by attaching RAPTA-C to polymer moieties (Blunden et al., 2012).

On the other hand, previous study revealed the antitumor activity of titanium complexes in mouse model with cervical cancer. To date, derivatives of titanocene dichloride (Cp_2TiCl_2) or diketonato complexes are the main classes of titanium complexes that has been studied. However, a vivid drawback of these classes is their

ability to hydrolyse quickly under normal conditions. Thus, salen complexes of titanium is chosen in this study due to its stability under physiological conditions. Interestingly, a slight deviation in the substitution pattern of the complexes could result in changes in its biological properties. In general, halogen substituted complexes have proven to display greater activity against diverse human cancer cell lines and induce cell death by apoptosis. Most importantly, the chlorine substituted complex exhibited high antitumor activity with low toxicity (Immel et al., 2011). In addition, reports on salan based titanium complexes appeared to be active towards cisplatin-resistant human ovarian cell lines and multi-drug resistant mouse lymphoma cell lines HU-1 and HU-2, suggesting that the complexes are unaffected by various drug resistance mechanisms (Cini et al., 2017).

The ability of gallium tartrate to treat syphilis led to the discovery of the therapeutic properties of gallium. Besides, gallium nitrate was used to treat hypercalcaemia. In addition, gallium complexes were found to be successful in treating infectious diseases, autoimmune disorders, accelerated bone resorption and cancer over the years. The *fac* and *mer* isomers of gallium maltolate that could readily interconvert in solution were found to have entered clinical trial. **Figure 2.6** shows the *fac* and *mer* isomers of octahedral gallium(III) complexes. The orally administered *mer* isomer of this compound proved to treat mammary gland cancer in mice. The compound showed similar activity as cisplatin *in vitro* and displayed a restraint in the drug resistance mechanism. Early studies on the mode of action of gallium complexes suggested that they target ribonucleotide reductase. However, studies on gallium maltolate indicated that it attacks the mitochondria instead and generate ROS as a way of inhibiting cell proliferation, leading to apoptosis of cell. On the other hand, octahedral gallium complexes showed high toxicity towards cisplatin-resistant human neuroblastoma, their mode of action revealed that they target the proteasome in prostate cancer cell lines. Hence, the study of

compounds containing gallium for cancer treatment persists as an essential area of research (Dabrowiak, 2017).

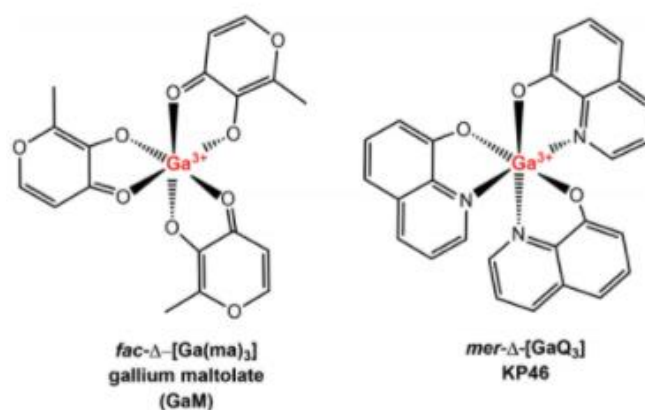


Figure 2.6 Structures of octahedral gallium(III) complexes (Copyright permission from Dabrowiak, 2017).

The role of gallium(III) complexes as antineoplastic drug against lymphoma and cancer of the bladder have been proven. Their molecular target is the proteasome. According to the study conducted by Chen and co-workers (2007), complex 5 which is gallium-iodo-amine inhibited proteasome greatly and induced apoptosis in prostate cancer cells. In addition, complex 5 inhibited the growth of PC-3 xenograft in mice *in vivo* by inhibiting proteasome and inducing apoptosis. Thus, prospective anticancer drugs can be developed from gallium complexes which act as potent proteasome e inhibitors (Chen et al., 2007).

2.4 Evolution of drugs for malaria

Malaria is a vector-borne endemic contagious ailment that is brought about by parasitic protozoa of the genus *Plasmodium*. The four significant species that cause malaria in humans are the *P. falciparum*, *P. vivax*, *P. ovale*, and *P. malariae*. The severe form, however, is caused by the former (Koram et al., 2007). The female *Anopheles* mosquito

requires a climate with high temperatures to transmit this vector-borne endemic to humans. Besides, the malaria parasites require a warm environment during their development in the mosquito to complete their growth cycle before being passed on to humans (Suwonkerd et al., 2013). The World Health Organisation (WHO) estimates that 300–500 million cases are reported each year with roughly one million deaths and these incidents are prevalent in emerging nations (Ramdzan et al., 2020). According to the World Malaria report 2019, 228 million cases of the disease and 405,000 of global malaria deaths were reported in 2018, while most of the reported mortality are among the young children (a child dies of malaria in every two minutes).

2.4.1 Chronological order of drug development for malaria

Factually, chloroquine (CQ), a 4-aminoquinoline drug, has been the most established antimalarial drug due to its satisfactory potency, low toxicity, and low cost (Boudhar et al., 2016). However, the *P. falciparum* has become resistant to CQ (Aguiar et al., 2018; Hyde, 2005), along with other antimalarial drugs such as sulfadoxine–pyrimethamine (SU-PY), mefloquine (MQ), and artemisinin (Naß & Efferth, 2019). Hence, discoveries of chloroquine followed by artemisinin were able to ward off malarial infection for some time until the parasite acquired resistance towards these drugs. Soon after, the therapeutic potential of ferroquine (FQ), which was once considered the most potent organometallic antimalarial drug explored. FQ was found to be exceedingly active *in vitro* against both CQ-resistant and CQ-susceptible *P. falciparum* and *P. vivax* isolates from different endemic areas (Biot et al., 2009; Held et al., 2015). Unfortunately, treatment with FQ was found to result in gastrointestinal side effects and central nervous disorders (Mombongoma et al., 2011). Hence, the discoveries of new drugs are crucial to address the issue of resistance and adverse effects.

2.4.2 Targets of antimalarial drugs

In general, antimalarial drugs function to inhibit the formation of hemozoin either by inhibiting proteases or forming iron chelators. Parasites biocrystallise heme into hemozoin to prevent the toxic effects from heme. Whereas, protease is needed to rupture the erythrocyte cytoskeleton and allow the merozoite-stage parasite to invade the red blood cells. Protease also assist the parasite with degradation of hemoglobin, eventually forming hemozoin. Hence, any substance that inhibits protease will lead to the inhibition of hemozoin formation and cause death to the parasite by toxicity of free heme. A study conducted by Rosenthal and co-workers (1998) revealed that various cysteine protease inhibitors were successful in inhibiting the development of *P. falciparum* and the degradation of hemoglobin (Coronado et al., 2014; Rosenthal, 1998).

Furthermore, a review by Padmanaban and co-workers (2007) addresses several potential antimalarial drug targets such as apicoplast, mitochondria, aqueous component of cytoplasm and food vacuole. It is believed that new strategies to battle malaria can be developed by discovering new targets. However, factors such as efficiency, toxicity, pharmacokinetic compatibility of drug and its side effects have to be taken into consideration (Padmanaban et al., 2007).

In addition, the parasites' ability to suit itself with two extremely different environments such as the vertebrate one and mosquito vector is fascinating. Its sophisticated life demands for development of new drugs that functions against new targets. Several other drug targets that were discovered later are N-myristoyltransferase, ubiquitin proteasome and dihydroorotate dehydrogenase which hinders the biosynthesis of pyrimidine (Hoelz et al., 2018; Pereira et al., 2018; Tate et al., 2014). Further studies have shown that cladosporin actively inhibits blood and liver stage *P. falciparum* by

inhibiting lysyl-tRNA synthetase, making the latter an important drug target (Baragaña et al., 2019).

2.4.3 Transition metal complexes for malaria

Quinoline based drugs have always exhibited antimalarial activity. One such example is chloroquine (CQ). However, the use of CQ have been halted lately due to drug resistance. Hence, new antimalarial drugs with transition metal ions are being synthesised. Studies have proved that metal complexation improved antimalarial activity because it inhibits hemozoin formation. A study by Sekhon and co-workers (2012) suggested several antimalarial drugs from metals such as iron, gold, ruthenium, cobalt, rhodium, iridium, copper, nickel, cobalt, zinc, osmium and palladium. Their findings revealed that the iron complexes were the most active. Interestingly, complexes of ruthenium are attracting more attention due to their low toxicity (Sekhon & Bimal, 2012). Hence, further studies should be conducted on ruthenium-based compounds to combat chloroquine-resistant parasites.

Another study conducted on the ruthenium(II) and osmium(II) arene complexes showed that these complexes exhibited different levels of antimalarial activity when tested against chloroquine-sensitive and chloroquine-resistant *P. falciparum*, where the ruthenium complexes displayed higher activity than the osmium complexes. Although metal complexation did not improve antimalarial activity, the ruthenium complexes showed higher resistance indices than the osmium complexes and free ligands. In fact, the resistance indices of ruthenium complexes were better than chloroquine's (Ekengard et al., 2015).

In addition, recent studies on one cationic and five neutral complexes of quinoline-triazole iridium(III) half sandwich shows that neutral, thermodynamic products are much

preferred than kinetic products. Besides, complexation of ligands with iridium(III) resulted in improved antiplasmodial activity. Unlike neutral complexes, the single cationic complex exhibited greatest activity, emphasizing the importance of different mechanism of action and location of metal coordination (Melis et al., 2020).

On the other hand, nickel(II), palladium(II) and copper(II) complexes of 2-hydroxy-benzaldehyde-ferrocenyl-sulfonylhydrazon showed moderate activity when tested against chloroquine-sensitive *P. falciparum* (Almendras et al., 2019). In a nutshell, transition metal complexes elevate the antimalarial activity of parent ligand by a certain degree.

2.5 Thiosemicarbazones as a whole

Thiosemicarbazones resulted from the Schiff base condensation reaction between a carbonyl group and thiosemicarbazide. They are uniquely named by placing the carbonyl group first followed by the thiosemicarbazone. The chemical properties and biological activities of thiosemicarbazones are rendered by the =NNH(CS)NH- moiety found in its structure. Hence, thiosemicarbazones are widely used in various fields such as industrial and analytical due to its extensive range of biological activities (Casas et al., 2000; West et al., 1993).

The ability of thiosemicarbazones to function as a metal chelator makes it important to researchers. Besides, their potential in the formation of metal complexes either monodentate, bidentate or tridentate makes them prominent in the field of coordination chemistry (Padhye & Kauffman, 1985). They can coordinate to metal as neutral molecules or as anionic ligands and can adopt a variety of different coordination. Thiosemicarbazones bind through their sulphur and hydrazine nitrogen atom with transition metal ion, makes them good chelating agents. Hence, thiosemicarbazones were

selected as ligands for complexation because they have better coordination tendency, form stable complexes, have better selectivity towards metals and form macrocyclic ligands (Chandra et al., 2013). In addition, they have great tendency to form coloured compounds from metal complexation, enabling them to be widely used in the analytical field to prepare metal ions. Apart from being cost effective, they can be easily synthesised.

Hydrazine carbothioamide is another way to address thiosemicarbazone. Being a sulphur analogy of semicarbazone, they display better biological activities. Previous studies have proved that thiosemicarbazones possess various biological activities including antimicrobial, antitumor and antimalarial (Tittal et al., 2020; Yu et al., 2009). Complexation of metal with a thiosemicarbazone ligand enhances the lipophilicity of the newly synthesised complex. Lipophilicity is needed to enable permeation of the complexes into cells that are being studied (Farrell, 2002). This can be done by either binding the thiosemicarbazones to a metal *in vivo* or using the metal as a vehicle to activate the ligand as cytotoxic agents (Afrasiabi et al., 2005).

Some examples of thiosemicarbazones and their metal complexes were explored on the surface as follows. A study on antibacterial activity of steroidal thiosemicarbazones was carried out by Khan and co-workers (2009) to determine the minimum inhibitory concentration (MIC) of the compounds by conducting the disk diffusion assay against gram-positive and gram-negative bacteria. It was found that the growth of both types of bacteria was inhibited more by thiosemicarbazones with acetoxy and chloro groups. An extension of this study by the same group using Pd(II) metal complexes showed that the complexes were better at inhibiting the growth of bacteria than the free thiosemicarbazone (Khan et al., 2008; Khan & Yusuf, 2009).

Another study conducted on the antifungal activity of heterocyclic thiosemicarbazone and their metal complexes indicated that among the four thiosemicarbazones prepared, 2-

acetylpyridine thiosemicarbazone was the most active. However, thiosemicarbazones that were complexed with copper(II) was found to have improved activity than the free thiosemicarbazones. Whereas, nickel(II) complexes of thiosemicarbazone did show appreciable amount of antifungal activity (Liberta & West, 1992). Besides, Alomar and co-workers (2013) performed a study on the antifungal activity of thiophene-2,3-dicarboxaldehyde bis(thiosemicarbazone) and its nickel(II), copper(II) and cadmium(II) complexes using broth microdilution method. Their findings suggested that the cadmium(II) complexes displayed the highest activity (Alomar et al., 2013). Evidently, incorporation of metal into thiosemicarbazone helps to improve its antifungal activity a great deal.

2.5.1 Thiosemicarbazones and their metal complexes for cancer treatment

Anticancer properties of thiosemicarbazones become significant when they are complexed with transition metal. Interestingly, ligands with NNS, ONS and ONO systems show increased potential as carcinostatic agents. Besides, the presence of substituent at N3 position was found to enhance the biological activities of thiosemicarbazones. In addition, thiosemicarbazones display cytotoxicity in mammalian cells by inhibiting ribonucleotide reductase, a vital enzyme for the synthesis of DNA precursor. The antileukemic activity of 2-formylpyridine thiosemicarbazone was reported by Brockman and co-workers in 1956 (Brockman et al., 1956).

In light of these interesting finding, further research was conducted on this class of compound and its metal complex. Latest findings by Silva and co-workers (2020) on silver(I) complexes of 2-formylpyridine thiosemicarbazones and 1,10-phenanthroline revealed that metal complexation resulted in compounds that were more cytotoxic than the free ligands. The cytotoxic activity of complexes was better than cisplatin.

Furthermore, 2-formylpyridine thiosemicarbazone and its derivatives displayed potent cytotoxicity by inhibiting ribonucleotide reductase. However, their silver(I) complexes induced apoptosis by generating ROS species and altering mitochondrial membrane potential, indicating that the mechanism of action of complexes differ moderately from the ligands. In addition, silver(I) complex of 2-formylpyridine thiosemicarbazone proved to be highly selective towards tumour cells by exhibiting lowest toxicity towards normal cells (MCF-10A) (Silva et al., 2020).

The 3-aminopyridine-2-carboxaldehyde thiosemicarbazone, better known as Triapine is an α -N-heterocyclic thiosemicarbazone which inhibits ribonucleotide reductase, an essential enzyme for the repair and synthesis of DNA. It has been proven to inhibit leukemia cells *in vitro*, rendering it a potential antineoplastic agent (Finch et al., 1999). On the other hand, complexation of Triapine with several metal ions such as zinc(II), gallium(III), copper(II) and iron(III) resulted in the two former complexes having higher cytotoxicity than the latter complexes. Hence, the mode of action of a cytotoxic ligand is strongly modulated by the selection of metal ion (Popović-Bijelić et al., 2011).

Another method thiosemicarbazones and its metal complexes induce apoptosis of cancerous cells is by acting as proteasome inhibitors. One such example is the synthesis of copper complexes of quinoline-2-carboxaldehyde to inhibit proteasome in human prostate cancer cells. It was noted that the antitumor activity of the parent ligand was greatly improved by the introduction of a cytotoxic thiocarbonyl side chain (Adsule et al., 2006). Among the complexes synthesised, copper complex of quinoline-2-carboxaldehyde with a thiocarbonyl substituent proved to be the most cytotoxic, where it inhibits proteasome and induce apoptosis in prostate cancer cells.

A study on copper(II) complexes of thiosemicarbazones by Sirbu and co-workers (2017) emphasised on the ability of copper complexes to generate ROS species which in

turn stimulates nrf2-mediated oxidative response pathway in breast cancer cells (Sîrbu et al., 2017). In another study conducted by Zeglis and co-workers (2011), copper(II) complexes were found to hinder topoisomerase-II α and impede the growth of breast cancer cells as well (Zeglis et al., 2011). Hence, thiosemicarbazones and its metal complexes were seen to inhibit proliferation of cancer cells through several different mechanisms such as inhibiting ribonucleotide reductase, inhibiting proteasome inhibitor, producing antioxidant response by generating ROS species and inhibiting topoisomerase II.

However, latest findings suggest that copper complexes of thiosemicarbazone induce apoptosis by inhibiting protein disulfide isomerase (PDI), an enzyme in endoplasmic reticulum (ER). Hence, cell death is mediated *via* a non-oxidative stress pathway. Evidently, the PDI serves as the current target for treating cancer. Besides, salicylaldehyde derivatives were discovered as fascinating candidates as anticancer drugs (Carcelli et al., 2020). Thus, thiosemicarbazone and their metal complexes play a great role in cancer treatment.

2.5.2 Antimalarial properties of thiosemicarbazones and their metal complexes

The wide range of biological activity thiosemicarbazones possess is of no doubt. Thiosemicarbazone of 2-acetylpyridine which was monosubstituted at the N4 position was found to show antimalarial activity. In 1979, Klayman and co-workers (1979) figured that 2-acetylpyridine-4-phenyl-3-thiosemicarbazone possessed outstanding antimalarial activity when tested against *Plasmodium berghei* in mice. Their findings suggested that modifying the compound with different substituent at the N4 position such as benzyl, phenethyl or cyclohexyl functional groups resulted in new compounds with antimalarial

activity as well (Klayman et al., 1979). Interestingly, compounds with phenyl and cyclohexyl substituent were the most effective.

The same group later reported on N^4, N^4 -disubstituted 2-acetylpyridine thiosemicarbazone. According to their findings, compounds that were disubstituted with alkyl or cycloalkyl at the N^4 position showed better antimalarial activity than the monosubstituted compounds. However, the activity was greatly enhanced when the N^4 position was incorporated into a monocyclic or bicyclic system such as piperidine, piperazine, or azabicyclo[3.2.2]nonane. Hence, the antimalarial activity of 2-acetylpyridine thiosemicarbazone is strongly dependent on the nature of molecular configuration about the N^4 position (Klayman et al., 1979).

Early studies by Scovill and co-workers (1982) proposed that complexation of metals such as Ni(II), Cu(II) and Fe(III) did not improve antimalarial activity of the free N^4, N^4 -disubstituted 2-acetylpyridine thiosemicarbazone ligands. The free ligands were seen to possess higher antimalarial activity (Scovill et al., 1982). However, subsequent study on gold(I) thiosemicarbazone complexes by Khanye and co-workers (2010) proved that metal complexation enhances the efficacy of the complex as antimalarial agent. Gold(I) complexes of thiosemicarbazones were found to display improved activity than their free ligands (Khanye et al., 2010).

Further studies on antimalarial activity of metal complexes of thiosemicarbazone revealed that Au(I) and Pd(II) complexes of thiosemicarbazone displayed greatest potency among other tested compounds. It is noteworthy that compounds containing 4-amino-7-chloroquinoline moieties showed improved activity (Summers, 2019). Thus, coordination of transition metal complexes to thiosemicarbazones improve its biological efficacies.

2.5.3 Fluorene-2-carboxaldehyde and polyhydroxybenzaldehyde thiosemicarbazones

Earlier research identified salicylaldehyde as potential anticancer agents. However, very little has been reported on the efficacies of fluorene-2-carboxaldehyde and polyhydroxybenzaldehyde to function as anticancer drugs. Derivatives of fluorene were found to display carcinogenetic and mutagenetic characteristics. Previous work has reported on the use of fluorene-2-carboxaldehyde as model drug in cancer treatment (Oliveira et al., 2017; Pearce et al., 2014). In addition, it is believed that planar, aromatic and heterocyclic ligands intercalate the duplex DNA and cause DNA damage. Hence, such compounds are prominent candidates in cancer research (Zhang et al., 2013).

Kumar and co-workers (2018) reported on the antibacterial, antifungal and anti-oxidant activities of Pd(II), Ni(II)dppm and [Cu(II)bipy/phen] complexes of 2,4-dihydroxybenzaldehyde-4-phenyl-3-thiosemicarbazone. Although the antibacterial and antifungal activities of Cu(II) and Pd(II) were at moderate levels, the Pd(II) complex was seen to exhibit improved anti-oxidant activity (Kumar et al., 2018).

On the other hand, Shawish and co-workers (2014) demonstrated the anti-inflammatory activity of Ni(II) complexes of polyhydroxybenzaldehyde N4-Thiosemicarbazone. Their findings suggested that Ni(II) complex of 2,3-dihydroxybenzaldehyde thiosemicarbazone actively inhibited NF- κ B transactivation and displayed potent anti-inflammatory activity (Shawish et al., 2014). Another study by this group reported on the antimicrobial activity of Ni(II) complexes of polyhydroxybenzaldehyde thiosemicarbazone, where complexes of 2,3-dihydroxybenzaldehyde-4-ethyl-3-thiosemicarbazone and 2,3-dihydroxybenzaldehyde-4-phenyl-thiosemicarbazone proved to be the most active against *Salmonella enterica* (Shawish et al., 2014). However, not much have been discussed on the antimalarial

activity of metal complexes of fluorene-2-carboxaldehyde and polyhydroxybenzaldehyde thiosemicarbazones.

2.5.4 Nickel complexes of thiosemicarbazones

The fact that nickel is an essential trace element for humans cannot be denied. Nickel compounds can act as antifungal, antibacterial, antimicrobial, and anticancer drugs. Besides, nickel(II) complexes bind and cleave DNA to exert its biological properties. Nickel complexes were also seen to interfere with proteins and enzymes responsible for DNA replication to hinder DNA repair (Anjomshoa et al., 2015). In general, transition metal complexes show biological activities. However, transition metal complexes with thiosemicarbazone-derived ligands proved to exhibit improved activities. For instance, a study by Sobiesiak and co-workers (2016) proved the ability of nickel(II) complex of thiosemicarbazones to actively inhibit human leukemia cells (U937) and induce apoptosis. In addition, this complex also displayed anticancer activity against human breast cancer cells (MCF7) (Sobiesiak et al., 2016).

A study on nickel(II) bis(thiosemicarbazone) complexes demonstrated the ability of the complexes to cleave DNA naturally and interfere with DNA and protein. Besides, the findings also revealed the remarkable cytotoxic activity of the complexes against human breast cancer cells (MCF7) and human lung cancer cells (A549) (Haribabu et al., 2015). Another study by the same group proved that nickel(II) complexes of bis(isatin thiosemicarbazone) induced apoptosis of human myeloma cancer cell (IM-9) *via* mitochondria-mediated pathway and arrested the cells in G₀/G₁ phase (Balachandran et al., 2018).

Recently, a study on bis(citronellalthiosemicarbazonato)nickel(II) [Ni(S-tcitr)₂] revealed the use of genetic tools and involvement of an intricate mechanism of action to

obtain genome-wide understandings on its target. It was found that the cytotoxicity of Ni(S-tcitr)₂ was not instigated by the generation of ROS. Instead, it was due to the interference with iron homeostasis (Baruffini et al., 2020). Hence, nickel complexes of thiosemicarbazones have been proven to display significant biological activity as anticancer agents.

Not much have been reported on the antimalarial activity of nickel complexes of thiosemicarbazones. Hence, the study focuses and reports results on the antimalarial activities of these complexes.

Universiti Malaysia

CHAPTER 3: METHODOLOGY

3.1 Materials and solutions

The chemicals for synthesis (thiosemicarbazides, fluorene-2-carboxaldehyde, 2,3,4-trihydroxybenzaldehyde, 2,5-dihydroxybenzaldehyde, nickel(II) acetate, nickel(II) chloride hexahydrate and chloroquine phosphate were purchased from Sigma Aldrich, Germany and Alfa Aesar, England. Solvents were purchased from Merck, Germany.

3.2 Physical measurements

The FT-IR spectra of all the ligands and metal complexes were recorded as KBr pellets using a Perkin-Elmer Spectrum RX-1 spectrometer. The NMR spectra was determined in a DMSO-d₆ with a JEOL ECX 400 spectrometer at 400 MHz. A Thermo Finnigan Eager 300 CHN elemental analyser was used to determine the percentage of carbon, hydrogen and nitrogen. Any crystals collected from recrystallisation were subjected to X-RAY using a Rigaku Oxford (formerly Agilent Technologies) Super Nova Dual diffractometer with Cu K α ($\lambda = 1.54184 \text{ \AA}$) radiation at 160–170 K.

3.3 Syntheses

3.3.1 Synthesis of fluorene-2-carboxaldehyde thiosemicarbazone (L1)

The ligand was prepared by following a published procedure with minor changes (Lu et al., 2011). The ethanolic solution containing the fluorene-2-carboxaldehyde (0.1951 g, 1 mmol) and thiosemicarbazide (0.0910 g, 1 mmol) was refluxed for 4 hours. The yellow precipitate was then filtered off and washed with ethanol. The dried yellow precipitate was collected and recrystallized with hot chloroform.

Yield: 0.2658 g, 92.90 %. Melting point: 186-188 °C. Anal. Calc. for C₁₅H₁₃N₃S: C, 67.39; H, 4.90; N, 15.72. Found: C, 66.82; H, 5.17; N, 14.90 %. IR (KBr disc, cm⁻¹): 3341 s, 3160 s, 1588 s, 1360 s, 841 m (s, strong; m, medium; w, weak).

¹H NMR signals (DMSO-d₆, TMS, ppm): 11.43 (s, 1H, N(2)H), 8.19 (s, 1H, N(3)H), 8.13 (s, 1H, N(3)H), 8.06 (s, 1H, CH=N), 8.04 (s, 1H, aromatic), 7.93 (d, 1H, aromatic, J= 3.66 Hz), 7.91 (d, 1H, aromatic, J=3.66 Hz), 7.78 (d, 1H, aromatic, J= 8.24 Hz), 7.60 (d, 1H, aromatic, J= 7.33 Hz), 7.39 (t, 1H, aromatic, J= 15.11 Hz), 7.33 (t, 1H, aromatic, J= 14.65 Hz), 3.94 (s, 2H, CH₂). ¹³C NMR signals (DMSO-d₆, TMS, ppm): 193.36 (C=S), 178.26 (C=N), 143.95, 143.20, 141.05, 133.32, 127.65, 127.30, 126.39, 125.78, 124.14, 12,92, 120.99, 120.69 (C-aromatic), 36.80 (CH₂).

3.3.2 Synthesis of fluorene-2-carboxaldehyde-4-methyl-3-thiosemicarbazone (L2)

Similar as the preparation of (L1) by using 4-methyl-3-thiosemicarbazide (0.1071 g, 1 mmol).

Yield: 0.2172 g, 72.15 %. Melting point: 184-188 °C. Anal. Calc. for C₁₆H₁₅N₃S: C, 68.30; H, 5.37; N, 14.93. Found: C, 67.73; H, 4.89; N, 14.82 %. IR (KBr disc, cm⁻¹): 3300 m, 3108 m, 1546 s, 1396 m, 821 m (s, strong; m, medium; w, weak).

¹H NMR signals (DMSO-d₆, TMS, ppm): 11.44 (s, 1H, N(2)H), 8.51 (q, 1H, N(3)H, J= 4.58 Hz), 8.09 (s, 1H, CH=N), 8.02 (s, 1H, aromatic), 7.89 (d, 1H, aromatic, J= 7.79 Hz), 7.87 (d, 1H, aromatic, J= 7.79 Hz), 7.73 (d, 1H, aromatic, J= 7.79 Hz), 7.57 (d, 1H, aromatic, J= 7.33 Hz), 7.35 (t, 1H, aromatic, J= 13.74 Hz), 7.29 (d, 1H, aromatic, J= 14.65 Hz), 3.91 (s, 2H, CH₂), 3.01 (d, 3H, CH₃, J= 4.58 Hz). ¹³C NMR signals (DMSO-d₆, TMS, ppm): 193.39 (C=S), 178.05 (C=N), 144.13, 142.69, 133.40, 129.85, 128.94, 127.84, 127.25, 126.39, 125.78, 123.94, 121.91, 120.98 (C-aromatic), 36.81 (CH₂), 31.33 (CH₃).

3.3.3 Synthesis of fluorene-2-carboxaldehyde-4-ethyl-3-thiosemicarbazone (L3)

Similar as the preparation of (L1) by using 4-ethyl-3-thiosemicarbazide (0.1201 g, 1 mmol).

Yield: 0.2853 g, 90.65 %. Melting point: 196-200 °C. Anal. Calc. for C₁₇H₁₇N₃S: C, 69.12; H, 5.80; N, 14.22. Found: C, 68.60; H, 5.84; N, 14.04 %. IR (KBr disc, cm⁻¹): 3370 m, 3158 m, 1538 s, 1379 m, 832 m (s, strong; m, medium; w, weak).

¹H NMR signals (DMSO-d₆, TMS, ppm): 11.36 (s, 1H, N(2)H), 8.54 (t, 1H, N(3)H, J= 11.91 Hz), 8.09 (s, 1H, CH=N), 8.01 (s, 1H, aromatic), 7.88 (d, 1H, aromatic, J= 7.79 Hz), 7.86 (d, 1H, aromatic, J= 7.79 Hz), 7.73 (d, 1H, aromatic, J= 7.79 Hz), 7.56 (d, 1H, aromatic, J= 6.87 Hz), 7.34 (t, 1H, aromatic, J= 13.74 Hz), 7.29 (t, 1H, aromatic, J= 14.65 Hz), 3.97 (s, 2H, CH₂), 3.58 (q, 2H, CH₂, J= 12.82 Hz), 1.12 (t, 3H, CH₃, J= 14.20 Hz).
¹³C NMR signals (DMSO-d₆, TMS, ppm): 193.34 (C=S), 177.03 (C=N), 144.13, 143.25, 142.82, 141.03, 133.36, 127.84, 127.63, 127.30, 125.93, 123.96, 120.97, 120.67 (C-aromatic), 38.82 (CH₂), 36.83 (CH₂), 15.21 (CH₃).

3.3.4 Synthesis of bis(fluorene-2-carboxaldehyde thiosemicarbazonato)nickel (II) complex [Ni(L1)₂], (1)

About 10 ml chloroform solution containing ligand (L1) (0.1842 g, 1 mmol) was added to about 10 ml ethanolic solution containing nickel(II) acetate (0.0884 g, 0.5 mmol). The mixture was refluxed for 4 hours. The brown precipitate formed was collected using filtration and washed with chloroform and distilled water. The precipitate was then recrystallized using DMF.

Yield: 0.1366 g, 50.11 %. Melting point: 276-280 °C. Anal. Calc. for C₃₀H₂₄N₆NiS₂: C, 59.65; H, 4.70; N, 14.76. Found: C, 60.12; H, 4.05; N, 14.12%. IR (KBr disc, cm⁻¹): 3283 m, 3180 m, 1509 s, 1327 s, 764 m, 561 m, 441 m (s, strong; m, medium; w, weak).

¹H NMR signals (DMSO-d₆, TMS, ppm): 8.50 (s, 1H, N(3)H), 8.10 (s, 1H, CH=N), 7.17 (s, 1H, N(3)H), 7.93 (d, 1H, aromatic, J= 10.07 Hz), 7.90 (d, 1H, aromatic, J= 10.07 Hz), 7.61 (d, 1H, aromatic), 7.42 (d, 1H, aromatic, J= 13.74 Hz), 7.39 (t, 1H, aromatic, J= 13.28 Hz), 7.37 (t, 1H, aromatic, J= 13.28 Hz), 7.17 (s, 1H, aromatic), 3.92 (s, 2H, CH₂).
¹³C NMR signals (DMSO-d₆, TMS, ppm): 176.63 (C=N), 154.15 (C=N), 144.78, 144.03, 143.45, 140.74, 131.93, 131.67, 129.08, 128.24, 127.48, 125.74, 121.20, 120.11 (C-aromatic), 37.05 (CH₂).

3.3.5 Synthesis of bis(fluorene-2-carboxaldehyde-4-methyl-3-thiosemicarbazonato)nickel(II) complex [Ni(L2)₂], (2)

Similar as the preparation of (1) by using ligand (L2) (0.2074 g, 1 mmol).

Yield: 0.1474 g, 49.83%. Melting point: 260-264 °C. Anal. Calc. for C₃₂H₃₀N₆NiS₂: C, 62.05; H, 4.56; N, 13.57. Found: C, 61.60; H, 4.46; N, 13.44%. IR (KBr disc, cm⁻¹): 3355 m, 3108 m, 1520 s, 1389 s, 732 m, 563 w, 485 w (s, strong; m, medium; w, weak).

¹H NMR signals (DMSO-d₆, TMS, ppm): 8.46 (s, 1H, N(3)H), 8.13 (d, 1H, CH=N, J= 7.33 Hz), 7.93 (d, 1H, aromatic, J= 8.24 Hz), 7.91 (d, 1H, aromatic, J= 8.24 Hz), 7.59 (d, 1H, aromatic, J= 6.87 Hz), 7.57 (d, 1H, aromatic, J= 6.87 Hz), 7.50 (s, 1H, aromatic), 7.37 (t, 1H, aromatic, J= 16.49 Hz), 7.37 (t, 1H, aromatic, J= 16.49 Hz), 3.91 (s, 2H, CH₂), 2.88 (t, 3H, CH₃, J= 7.79 Hz). ¹³C NMR signals (DMSO-d₆, TMS, ppm): 175.65 (C=N), 154.23 (C=N), 144.78, 143.97, 143.41, 140.80, 131.74, 128.97, 128.21, 127.47, 125.72, 121.21, 120.16 (C-aromatic), 37.03 (CH₂), 32.27 (CH₃).

3.3.6 Synthesis of bis(flourene-2-carboxaldehyde-4-ethyl-3-thiosemicarbazonato)nickel (II) complex [Ni(L3)₂], (3)

Similar as the preparation of (1) by using ligand (L3) (0.2954 g, 1 mmol).

Yield: 0.1519 g, 39.57%. Melting point: 220-224 °C. Anal. Calc. for C₃₄H₃₂N₆NiS₂: C, 63.07; H, 4.98; N, 12.98. Found: C, 62.64; H, 5.10; N, 12.86%. IR (KBr disc, cm⁻¹): 3411 s, 3108 m, 1521 m, 1349 s, 763 m, 561 w, 447 w (s, strong; m, medium; w, weak).

¹H NMR signals (DMSO-d₆, TMS, ppm): 8.44 (s, 1H, N(3)H), 8.09 (d, 1H, CH=N, J= 7.79 Hz), 7.90 (s, 1H, aromatic), 7.88 (d, 1H, aromatic, J= 2.29 Hz), 7.59 (d, 1H, aromatic, J= 7.33 Hz), 7.57 (d, 1H, aromatic, J= 7.33 Hz), 7.36 (d, 1H, aromatic, J= 6.87 Hz), 7.34 (t, 1H, aromatic, J= 3.66 Hz), 7.31 (t, 1H, aromatic, J= 13.28 Hz), 3.89 (s, 2H, CH₂), 3.28 (q, 2H, CH₂, J= 12.82 Hz), 1.14 (t, 3H, CH₃, J= 14.65 Hz). ¹³C NMR signals (DMSO-d₆, TMS, ppm): 174.90 (C=N), 154.05 (C=N), 144.76, 143.94, 143.40, 140.81, 131.73, 131.58, 128.82, 128.19, 127.47, 125.72, 121.21, 120.15 (C-aromatic), 37.01 (CH₂), 31.30 (CH₂), 14.89 (CH₃).

3.3.7 Synthesis of 2,3,4-trihydroxybenzaldehyde-4-methyl-3-thiosemicarbazone (L4)

The ligand was prepared by following a published procedure with slight changes (Shawish et al., 2010). The ethanolic solution containing 2,3,4-trihydroxybenzaldehyde and 4-methyl-3-thiosemicarbazide was refluxed for 4 hours. The brown powder formed from cooled solution was recrystallized with ethanol.

Yield: 0.27 g, 81 %. Melting point: 110-114 °C. Anal. Calc. for C₉H₁₁N₃O₃S: C, 44.80; H, 4.60; N, 17.42. Found: C, 44.13; H, 4.45; N, 16.86 %. IR (KBr disc, cm⁻¹): 3452 s, 3202 w, 3180 m, 1637 s, 1346 w, 1283 s, 823 s (s, strong; m, medium; w, weak).

¹H NMR signals (DMSO-d₆, TMS, ppm): 11.19 (s, 1H, N(2)H), 9.53 (s, 1H, OH), 8.96 (s, 1H, OH), 8.41 (s, 1H, N(3)H), 8.23 (d, 1H, OH, J= 4.58 Hz), 8.19 (s, 1H, CH=N), 7.12 (d, 1H, aromatic, J= 8.70 Hz), 6.32 (d, 1H, aromatic, J= 8.70 Hz), 2.95 (d, 3H, CH₃, J= 4.58 Hz). ¹³C NMR signals (DMSO-d₆, TMS, ppm): 177.51 (C=S), 141.87 (C=N), 148.62 (C-OH), 146.99 (C-OH), 133.20 (C-OH), 118.45, 113.15, 108.43 (C-aromatic), 31.33 (CH₃).

3.3.8 Synthesis of 2,3,4-trihydroxybenzaldehyde-4-ethyl-3-thiosemicarbazone (L5)

Similar as the preparation of (L4) by using 4-ethyl-3-thiosemicarbazide.

Yield: 0.31 g, 91 %. Melting point: 108-110 °C. Anal. Calc. for C₁₀H₁₅N₃O₄S: C, 43.95; H, 5.53; N, 15.37. Found: C, 44.58; H, 5.32; N, 15.50 %. IR (KBr disc, cm⁻¹): 3439 s, 3349 w, 3170 m, 1632 s, 1348 w, 1251 s, 798 m (s, strong; m, medium; w, weak).

¹H NMR signals (DMSO-d₆, TMS, ppm): 11.12 (s, 1H, N(2)H), 9.53 (s, 1H, OH), 8.99 (s, 1H, OH), 8.43 (s, 1H, OH), 8.26 (t, 1H, N(3)H, J= 11.45 Hz), 8.19 (s, 1H, CH=N), 7.11 (d, 1H, aromatic, J= 8.24 Hz), 6.32 (d, 1H, aromatic, J= 8.70 Hz), 3.53 (q, 2H, CH₂, J= 20.61 Hz), 1.08 (t, 3H, CH₃, J= 14.20 Hz). ¹³C NMR signals (DMSO-d₆, TMS, ppm): 176.44 (C=S), 142.01 (C=N), 148.64 (C-OH), 146.96 (C-OH), 133.20 (C-OH), 118.55, 113.10, 108.16 (C-aromatic), 38.76 (CH₂), 15.23 (CH₃).

3.3.9 Synthesis of 2,3,4-trihydroxybenzaldehyde-4-phenyl-3-thiosemicarbazone (L6)

Similar as the preparation of (L4) by using 4-phenyl-3-thiosemicarbazide.

Yield: 0.29 g, 89 %. Melting point: 124-128 °C. Anal. Calc. for C₁₄H₁₃N₃O₃S: C, 55.43; H, 4.32; N, 13.85. Found: C, 55.34; H, 3.79; N, 13.67 %. IR (KBr disc, cm⁻¹): 3531, 3441 s, 3149 w, 1612 s, 1345 w, 1261 s, 804 m (s, strong; m, medium; w, weak).

¹H NMR signals (DMSO-d₆, TMS, ppm): 11.56 (s, 1H, N(2)H), 9.89 (s, 1H, OH), 9.58 (s, 1H, OH), 8.46 (s, 1H, N(3)H), 8.31 (s, 1H, CH=N), 6.34 (d, 1H, OH, J= 8.70 Hz), 7.54 (d, 2H, aromatic, J= 7.79 Hz), 7.31 (t, 3H, aromatic, J= 15.57 Hz), 7.13 (t, 2H, aromatic, J=14.65 Hz). ¹³C NMR signals (DMSO-d₆, TMS, ppm): 175.54 (C=S), 147.19 (C=N), 153.76 (C-OH), 151.42 (C-OH), 148.90 (C-OH), 142.80, 139.68, 133.19, 129.59, 128.50, 125.80, 125.45, 118.93, 112.93, 108.19 (C-aromatic).

3.3.10 Synthesis of 2,3,4-trihydroxybenzaldehyde-4-(4-ethylphenyl)-3-thiosemicarbazone (L7)

Similar as the preparation of (L4) by using 4-(4-ethylphenyl)-3-thiosemicarbazide.

Yield: 0.25 g, 81 %. Melting point: 104-108 °C. Anal. Calc. for C₁₆H₁₇N₃O₃S: C, 57.99; H, 5.17; N, 12.68. Found: C, 57.52; H, 4.98; N, 12.25 %. IR (KBr disc, cm⁻¹): 3352, 3341, 3140 s, 1634 s, 1378 w, 1271 s, 833 m (s, strong; m, medium; w, weak).

¹H NMR signals (DMSO-d₆, TMS, ppm): 11.51 (s, 1H, N(2)H), 9.84 (d, 1H, OH, J= 16.72 Hz), 9.65 (s, 1H, N(3)H), 8.33 (s, 1H, CH=N), 6.49 (d, 1H, OH, J= 8.24 Hz), 6.37 (d, 1H, OH, J= 8.70 Hz), 7.44 (d, 2H, aromatic, J= 8.24 Hz), 7.18 (d, 2H, aromatic, J= 8.24 Hz), 7.10 (d, 2H, aromatic, J= 8.24 Hz), 2.59 (q, 2H, CH₂, J= 22.90 Hz), 1.17 (t, 3H, CH₃, 15.11 Hz). ¹³C NMR signals (DMSO-d₆, TMS, ppm): 175.59 (C=S), 147.16 (C=N),

153.76 (C-OH), 151.42 (C-OH), 148.85 (C-OH), 140.99, 137.30, 132.68, 127.78, 125.85, 118.90, 115.91, 112.95, 108.18 (C-aromatic).

Melting point: 104-108 °C

3.3.11 Synthesis of (2,3,4-trihydroxybenzaldehyde-4-methyl-3-thiosemicarbazonato)-(triphenylphosphine)ni(II) [Ni(L4)PPh₃]Cl, (4)

The ethanolic solution containing the ligand (L4), triphenylphosphine and nickel(II) chloride hexahydrate was refluxed for 6 hours. The solution was left aside for slow evaporation. Brown precipitate formed was then recrystallized with either ethanol or a mixture of DMF and acetonitrile in a 1:2 ratio to promote crystal growth.

Yield: 0.18 g, 63 %. Melting point: 180-184 °C. Anal. Calc. for C₂₇H₂₅ClN₃NiO₃PS.H₂O: C, 54.35; H, 4.22; N, 7.04. Found: C, 54.99; H, 4.74; N, 6.63 %. IR (KBr disc, cm⁻¹): 3427, 3310 s, 3169 m, 1616 s, 1434 s, 1380 m, 1273 s, 1084 s, 788 m, 689 s, 533 m, 509 s, 488 m (s, strong; m, medium; w, weak).

¹H NMR signals (DMSO-d₆, TMS, ppm): 11.17 (s, 1H, N(2)H), 8.23 (s, 1H, N(3)H), 8.19 (s, 1H, CH=N), 6.44 (d, 1H, OH, J= 8.24 Hz), 6.32 (d, 1H, OH, J= 8.24 Hz), 7.58 (d, 3H, aromatic, J= 7.33 Hz), 7.39 (s, 12H, aromatic), 7.12 (d, 1H, aromatic, J= 8.24 Hz), 7.04 (d, 1H, aromatic, J= 8.24 Hz), 2.93 (d, 3H, CH₃, J= 3.66 Hz). ¹³C NMR signals (DMSO-d₆, TMS, ppm): 177.29 (C=S), 141.65 (C=N), 148.59 (C-OH), 146.91 (C-OH), 134.08 (C-O-Ni), 133.15, 130.73, 129.33, 118.26, 112.93, 108.26 (C-aromatic).

3.3.12 Synthesis of (2,3,4-trihydroxybenzaldehyde-4-ethyl-3-thiosemicarbazonato)-(triphenylphosphine)ni(II) [Ni(L5)PPh₃]Cl, (5)

Similar as the preparation of (4) by using ligand (L5).

Yield: 0.22 g, 71 %. Melting point: 140-144 °C. Anal. Calc. for C₂₈H₂₆ClN₃NiO₃PS.H₂O: C, 55.07; H, 4.46; N, 6.88. Found: C, 55.41; H, 5.06; N, 6.23 %. IR (KBr disc, cm⁻¹): 3454, 3218 s, 3161 s, 1610 s, 1435 s, 1320 m, 1292 s, 1091 s, 779 m, 691 s, 528 m, 503 s, 494 m (s, strong; m, medium; w, weak).

¹H NMR signals (DMSO-d₆, TMS, ppm): 11.10 (s, 1H, N(2)H), 8.27 (s, 1H, N(3)H), 8.18 (s, 1H, CH=N), 6.33 (d, 1H, OH, J= 8.24 Hz), 6.05 (s, 1H, OH), 7.42 (s, 16H, aromatic), 7.11 (d, 1H, aromatic, J= 8.70 Hz), 1.27 (s, 2H, CH₂), 1.06 (t, 3H, CH₃, J= 13.74 Hz). ¹³C NMR signals (DMSO-d₆, TMS, ppm): 176.35 (C=S), 141.45 (C=N), 148.60 (C-OH), 146.91 (C-OH), 134.04 (C-O-Ni), 133.14, 132.59, 132.22, 132.12, 131.99, 131.91, 129.32, 118.03, 113.12, 108.23 (C-aromatic), 38.78 (CH₂), 15.22 (CH₃).

3.3.13 Synthesis of (2,3,4-trihydroxybenzaldehyde-4-phenyl-3-thiosemicarbazonato)-(triphenylphosphine)ni(II) [Ni(L6)PPh₃], (6)

Similar as the preparation of (4) by using ligand (L6).

Yield: 0.22 g, 71 %. Melting point: 264-268 °C. Anal. Calc. for C₃₂H₂₇N₃NiO₃PS: C, 61.66; H, 4.37; N, 6.74. Found: C, 61.35; H, 5.08; N, 6.41 %. IR (KBr disc, cm⁻¹): 3448, 3370, 1562 s, 1436 s, 1318 m, 1239 s, 1093 s, 765 s, 690 s, 529 m, 507 s, 489 m (s, strong; m, medium; w, weak).

¹H NMR signals (DMSO-d₆, TMS, ppm): 9.25 (s, 1H, N(3)H), 9.25 (s, 1H, OH), 8.45 (d, 1H, CH=N, J= 8.70 Hz), 7.76 (t, 6H, aromatic, J= 17.86 Hz), 7.62 (d, 3H, aromatic, J= 8.24 Hz), 7.54 (t, 9H, aromatic, J= 13.28 Hz), 7.18 (t, 2H, aromatic, J= 15.57 Hz), 6.85 (t, 2H, aromatic, J= 16.03 Hz), 6.21 (d, 1H, OH, J= 8.70 Hz), 4.70 (s, 1H, SH). ¹³C NMR

signals (DMSO-d₆, TMS, ppm): 164.87 (C=N), 164.70 (C=N), 153.42 (C-O-Ni), 150.25 (C-OH), 146.48 (C-OH), 141.92, 134.43, 134.33, 133.70, 131.83, 129.55, 129.45, 128.97, 123.26, 121.51, 118.44, 110.79, 107.86 (C-aromatic).

3.3.14 Synthesis of (2,3,4-trihydroxybenzaldehyde-4-(4-ethylphenyl)-3-thiosemicarbazonato)-(triphenylphosphine)ni(II) [Ni(L7)PPh₃], (7)

Similar as the preparation of (4) by using ligand (L7).

Yield: 0.22 g, 71 %. Melting point: 156-160 °C. Anal. Calc. for C₃₇H₄₂N₄NiO₆PS: C, 58.44; H, 5.57; N, 7.37. Found: C, 58.98; H, 5.57; N, 7.83 %. IR (KBr disc, cm⁻¹): 3441, 3296, 3187, 1654 s, 1436 s, 1315 m, 1277 s, 1095 s, 782 s, 693, 531 m, 510 s, 493 m (s, strong; m, medium; w, weak).

¹H NMR signals (DMSO-d₆, TMS, ppm): 9.21 (s, 1H, OH), 9.14 (s, 1H, N(3)H), 8.40 (d, 1H, CH=N, J= 8.70 Hz), 7.74 (t, 6H, aromatic, J= 17.86 Hz), 7.52 (t, 9H, aromatic, J= 18.72 Hz), 7.01 (d, 4H, aromatic, J= 8.70 Hz), 6.82 (d, 2H, aromatic, J= 8.70 Hz), 6.17 (d, 1H, OH, J= 8.70 Hz), 4.68 (s, 1H, SH), 2.45 (q, 2H, CH₂, J= 5.50 Hz), 1.08 (t, 3H, CH₃, J= 15.11 Hz). ¹³C NMR signals (DMSO-d₆, TMS, ppm): 164.84 (C=N), 164.67 (C=N), 153.06 (C-O-Ni), 150.16 (C-OH), 146.39 (C-OH), 139.75, 136.88, 134.43, 134.33, 132.06, 131.96, 131.82, 129.54, 129.44, 129.01, 128.16, 123.18, 118.63, 110.83, 107.81 (C-aromatic), 28.04 (CH₂), 16.38 (CH₃).

3.3.15 Synthesis of 2,5-dihydroxybenzaldehyde thiosemicarbazone (L8)

The ligand was prepared following a published procedure with minor changes (Rogolino et al., 2015). The ethanolic solution containing 2,5-dihydroxybenzaldehyde and thiosemicarbazide was refluxed for 4 hours. The brown precipitate formed from the cooled solution was recrystallized with ethanol.

Yield: 0.27 g, 81 %. Melting point: 102-106 °C. Anal. Calc. for C₈H₉N₃O₂S: IR (KBr disc, cm⁻¹): 3428 s, 3328 w, 3135 m, 1625 s, 1341 m, 1286 s, 818 m (s, strong; m, medium; w, weak).

¹H NMR signals (DMSO-d₆, TMS, ppm): 11.32 (s, 1H, N(2)H), 9.20 (s, 1H, OH), 8.81 (s, 1H, OH), 8.25 (s, 1H, CH=N), 8.05 (s, 1H, N(3)H), 7.77 (s, 1H, N(3)H), 7.19 (s, 1H, aromatic), 6.64 (d, 2H, aromatic, J= 1.37 Hz). ¹³C NMR signals (DMSO-d₆, TMS, ppm): 178.04 (C=S), 140.72 (C=N), 150.41 (C-OH), 150.02 (C-OH), 121.06, 119.33, 117.38, 112.29 (C-aromatic).

3.3.16 Synthesis of 2,5-dihydroxybenzaldehyde-4-methyl-3-thiosemicarbazone (L9)

Similar as the preparation of (L8) by using 4-methyl-3-thiosemicarbazide.

Yield: 0.29 g, 85 %. Melting point: 112-114 °C. Anal. Calc. for C₉H₁₃N₃O₃S: C, 44.43; H, 5.39; N: 17.27. Found: C, 44.92; H, 5.36; N: 17.15 %. IR (KBr disc, cm⁻¹): 3366 s, 3257 w, 3135 m, 1557 s, 1333 w, 1246 s, 823 s (s, strong; m, medium; w, weak).

¹H NMR signals (DMSO-d₆, TMS, ppm): 11.33 (s, 1H, N(2)H), 9.19 (s, 1H, OH), 8.80 (s, 1H, OH), 8.34 (q, 1H, N(3)H, J= 4.58 Hz), 8.25 (s, 1H, CH=N), 7.24 (s, 1H, aromatic), 6.64 (d, 2H, aromatic, J=1.83 Hz), 2.95 (d, 3H, CH₃, J= 4.58 Hz). ¹³C NMR signals (DMSO-d₆, TMS, ppm): 177.95 (C=S), 140.01 (C=N), 150.43 (C-OH), 149.93 (C-OH), 121.31, 119.12, 117.26, 112.36 (C-aromatic), 31.35 (CH₃).

3.3.17 Synthesis of 2,5-dihydroxybenzaldehyde-4-ethyl-3-thiosemicarbazone (L10)

Similar as the preparation of (L8) by using 4-ethyl-3-thiosemicarbazide.

Yield: 0.29 g, 85 %. Melting point: 136-140 °C. Anal. Calc. for C₁₀H₁₅N₃O₃S: C, 46.68; H, 5.88; N: 16.33. Found: C, 46.79; H, 5.61; N: 16.39 %. IR (KBr disc, cm⁻¹): 3389 s, 3267 w, 3155 m, 1551 s, 1377 m, 1283 s, 804 s (s, strong; m, medium; w, weak).

¹H NMR signals (DMSO-d₆, TMS, ppm): 11.30 (s, 1H, N(2)H), 9.22 (s, 1H, OH), 8.84 (s, 1H, OH), 8.39 (q, 1H, N(3)H, J= 11.45 Hz), 8.29 (s, 1H, CH=N), 7.27 (s, 1H, aromatic), 6.67 (d, 2H, aromatic, J= 0.92 Hz), 3.56 (q, 2H, CH₂, J= 20.15), 1.13 (t, 3H, CH₃, J= 14.20 Hz). ¹³C NMR signals (DMSO-d₆, TMS, ppm): 176.91 (C=S), 140.05 (C=N), 150.42 (C-OH), 149.96 (C-OH), 121.28, 119.14, 117.27, 112.31 (C-aromatic), 38.78 (CH₂), 15.18 (CH₃).

3.3.18 Synthesis of 2,5-dihydroxybenzaldehyde-4-phenyl-3-thiosemicarbazone (L11)

Similar as the preparation of (L8) by using 4-phenyl-3-thiosemicarbazone.

Yield: 0.29 g, 85 %. Melting point: 108-112 °C. Anal. Calc. for C₁₄H₁₃N₃O₂S: C, 58.52; H, 4.56; N: 14.62. Found: C, 58.10; H, 4.16; N: 14.48 %. IR (KBr disc, cm⁻¹): 3318 s, 3155 m, 1542 s, 1330 m, 1269 s, 816 s (s, strong; m, medium; w, weak).

¹H NMR signals (DMSO-d₆, TMS, ppm): 11.69 (s, 1H, N(2)H), 9.97 (s, 1H, OH), 9.29 (s, 1H, OH), 8.82 (d, 1H, N(3)H, J= 1.37 Hz), 8.38 (s, 1H, CH=N), 7.54 (d, 2H, aromatic, J= 7.79 Hz), 7.32 (t, 3H, aromatic, J= 15.57 Hz), 7.15 (t, 1H, aromatic, J= 15.11 Hz) 6.67 (d, 2H, aromatic, J= 0.92 Hz). ¹³C NMR signals (DMSO-d₆, TMS, ppm): 176.14 (C=S), 140.98 (C=N), 150.46 (C-OH), 150.23 (C-OH), 139.66, 128.59, 128.33, 126.04, 125.68, 121.07, 119.52, 117.33, 112.60 (C-aromatic).

3.3.19 Synthesis of (2,5-dihydroxybenzaldehyde thiosemicarbazonato)-(triphenylphosphine)ni(II), [Ni(L8)PPh₃] (8)

The ethanolic solution containing the ligand (L8), triphenylphosphine and nickel(II)chloride hexahydrate was refluxed for 6 hours. The solution was left aside for

slow evaporation. Dark brown precipitate formed was then recrystallized with a mixture of DMF and acetonitrile in a 1:2 ratio.

Yield: 0.21 g, 75 %. Melting point: 110-114 °C. Anal. Calc. for C₂₆H₂₂N₃NiO₂PS: C, 49.82; H, 5.70; N, 7.04. Found: C, 48.97; H, 3.87; N, 6.51 %. IR (KBr disc, cm⁻¹): 3352, 3213 s, 3132 s, 1620 s, 1268 s, 758 w, 534 s, 511 s, 496 s (s, strong; m, medium; w, weak). ¹H NMR signals (DMSO-d₆, TMS, ppm): 8.55 (s, 1H, N(3)H), 8.10 (d, 1H, CH=N, J= 8.70 Hz), 7.67 (t, 6H, aromatic, J= 17.86 Hz), 7.50 (t, 9H, aromatic, J= 14.20 Hz), 6.64 (s, 1H, aromatic), 6.59 (d, 1H, aromatic, J= 8.70 Hz), 6.43 (s, 1H, OH), 6.14 (d, 1H, aromatic, J=8.70 Hz). ¹³C NMR signals (DMSO-d₆, TMS, ppm): 171.42 (C=N), 171.26 (C=N), 154.63 (C-OH), 149.79 (C-O), 146.94, 134.64, 134.55, 131.42, 129.82, 129.38, 129.07, 128.97, 122.28, 120.20, 117.66, 115.11 (C-aromatic).

3.3.20 Synthesis of (2,5-dihydroxybenzaldehyde-4-methyl-3-thiosemicarbazonato)-(triphenylphosphine)ni(II) [Ni(L9)PPh₃], (9)

Similar as the preparation of (8) by using ligand (L9).

Yield: 0.22 g, 79 %. Melting point: 122-124 °C. Anal. Calc. for C₂₇H₂₅N₃NiO₂PS.H₂O.C₃H₇NO: C, 56.71; H, 5.24; N, 8.82. Found: C, 56.98; H, 6.06; N, 8.33 %. IR (KBr disc, cm⁻¹): 3366, 3279 s, 1606 s, 1222 s, 828 w, 530 s, 518 s, 496 s (s, strong; m, medium; w, weak).

¹H NMR signals (DMSO-d₆, TMS, ppm): 8.53 (s, 1H, N(3)H), 8.22 (d, 1H, CH=N, J= 9.16 Hz), 7.64 (t, 8H, aromatic, J=17.40 Hz), 7.50 (t, 7H, aromatic, J= 13.74 Hz), 6.85 (d, 1H, aromatic, J= 4.58 Hz), 6.69 (d, 1H, aromatic, J= 2.75 Hz), 6.59 (d, 1H, aromatic, J= 2.75 Hz), 6.14 (d, 1H, OH, J= 9.16 Hz), 2.65 (d, 3H, CH₃, J= 4.58 Hz). ¹³C NMR signals (DMSO-d₆, TMS, ppm): 170.51 (C=N), 170.35 (C=N), 154.60 (C-OH), 150.54

(C-O), 146.96, 134.67, 134.57, 131.43, 129.80, 129.35, 129.07, 128.96, 122.33, 120.15, 117.78, 115.22 (C-aromatic), 32.27 (CH₃).

3.3.21 Synthesis of (2,5-dihydroxybenzaldehyde-4-ethyl-3-thiosemicarbazonato)-(triphenylphosphine)ni(II) [Ni(L10)PPh₃]Cl, (10)

Similar as the preparation of (8) by using ligand (L10).

Yield: 0.22 g, 79 %. Melting point: 190-194 °C. Anal. Calc. for C₂₈H₂₇ClN₃NiO₂PS.H₂O: C, 56.23; H, 5.19; N, 6.56. Found: C, 55.85; H, 4.82; N, 6.52 %. IR (KBr disc, cm⁻¹): 3286 m, 3145 s, 1634 s, 1337 m, 1266 s, 749 s, 528 s, 510 s, 498 s (s, strong; m, medium; w, weak).

¹H NMR signals (DMSO-d₆, TMS, ppm): 11.20 (s, 1H, N(2)H), 9.22 (s, 1H, OH), 8.31 (s, 1H, N(3)H), 8.17 (s, 1H, CH=N), 7.52 (d, 3H, aromatic, J= 6.87 Hz), 7.32 (s, 8H, aromatic), 7.16 (d, 2H, aromatic, J= 16.94 Hz), 6.57 (t, 4H, aromatic, J= 21.52 Hz), 6.04 (d, 1H, aromatic, J= 7.79 Hz), 1.00 (t, 2H, CH₂, J= 13.74 Hz), 0.93 (t, 3H, CH₃, J= 13.28 Hz). ¹³C NMR signals (DMSO-d₆, TMS, ppm): 176.72 (C=S), 139.92 (C=N), 150.33 (C-OH), 149.92 (C-O), 134.28, 129.10, 121.14, 119.08, 117.21, 112.12 (C-aromatic), 38.63 (CH₂), 15.15 (CH₃).

3.3.22 Synthesis of (2,5-dihydroxybenzaldehyde-4-phenyl-3-thiosemicarbazonato)-(triphenylphosphine)ni(II) [Ni(L11)PPh₃]Cl, (11)

Similar as the preparation of (8) by using ligand (L11).

Yield: 0.23 g, 80 %. Melting point: 114-118 °C. Anal. Calc. for C₃₈H₄₀N₅NiO₄PS: C, 60.65; H, 5.36; N, 9.31. Found: C, 60.26; H, 4.92; N, 9.34 %. IR (KBr disc, cm⁻¹): 3219 m, 1652 s, 1381 s, 1252 s, 744 s, 524 s, 502 s, 490 s (s, strong; m, medium; w, weak).

¹H NMR signals (DMSO-d₆, TMS, ppm): 9.31 (s, 1H, OH), 8.68 (s, 1H, N(3)H), 8.49 (d, 1H, CH=N, J= 8.70 Hz), 7.67 (t, 8H, aromatic, J= 18.32 Hz), 7.52 (t, 9H, aromatic, J= 12.82 Hz), 7.18 (t, 2H, aromatic, J= 15.57 Hz), 6.85 (t, 1H, aromatic, J=14.20 Hz), 6.78 (d, 1H, aromatic, J= 3.21 Hz), 6.65 (d, 1H, aromatic, J= 3.21 Hz), 6.22 (d, 1H, aromatic, J= 8.70 Hz). ¹³C NMR signals (DMSO-d₆, TMS, ppm): 166.19 (C=N), 166.02 (C=N), 155.42 (C-OH), 153.07 (C-O), 147.12, 141.86, 134.69, 134.60, 131.53, 129.69, 129.24, 129.15, 129.05, 128.98, 123.33, 121.63, 120.48, 118.57, 117.40, 115.22 (C-aromatic).

3.4 X-ray crystallography

In this research, all complexes were recrystallised from dimethylformamide (DMF). The complexes are all dark brown in colour. A Rigaku Oxford (formerly Agilent Technologies) Super Nova Dual diffractometer with Cu K α ($\lambda = 1.54184 \text{ \AA}$) radiation at 160–170 K was used to generate the unit cell parameter and intensity data. Atoms were labelled using OLEX2 (Dolomanov et al., 2009). Whereas, the Mercury CSD 2.0 (Macrae et al., 2008) was used for crystal structure visualization and analysis. In addition, the crystallographic information files were edited, validated and formatted using publCIF (Westrip, 2010).

3.5 Biological assays

3.5.1 MTT cytotoxicity assay

The three cell lines used in the current study i.e. human colorectal carcinoma HCT 116, prostate adenocarcinoma PC-3, and breast adenocarcinoma MCF7 were purchased from American Type Culture Collection (ATCC, USA). The cells were cultured in McCoy's 5A medium (HCT 116), RPMI medium (PC-3), and DMEM (MCF7),

supplemented with 10% fetal bovine serum and incubated at 37°C in a humidified atmosphere containing 5% CO₂.

The MTT assay was employed to test the ability of the synthesized compounds to inhibit cancer cell growth as outlined previously (Beekman et al., 1996). Briefly, the cells were seeded into 96-well microplate, incubated overnight, and treated with various concentrations of compound for 72 hours. Cisplatin was used as positive control. MTT was added into each well and incubated for another 3 hours before the addition of DMSO. The absorbance of each well was measured using Tecan M200 Infinite Pro Microplate Reader at 570 and 650 nm as reference wavelength. The IC₅₀ values were determined by plotting percentage of viability against the concentration of treatment on a logarithmic scale using GraphPad Prism 7 software (Graphpad software Inc., CA, USA).

3.5.2 Determination of antimalarial activity by testing on *Plasmodium falciparum* culture

The *P. falciparum* 3D7 strain was used in this experiment. Fifty µl of seven 5-fold serial dilutions of chloroquine (positive control) and the compounds in RPMI 1640 complete culture medium, with a maximum test concentration of 1 µM for chloroquine and 25 µM for the rest of the compounds were dispensed into 96-well plates. Then, 150 µl of blood media parasite mixture (BMPM) was added into the wells giving a final volume of 200 µL with final hematocrit of 2 % and 0.5 % ring stage parasite (Fatih et al., 2013). A gas chamber containing 5% CO₂, 5% O₂ and 90% N₂ at 37.5-38.0 °C was used to incubate the drug plates containing the BMPM. The drug plates were incubated for 36 to 42 hours until at least 50% of the ring stage parasites had matured to schizonts. The drug concentrations and drug free control was done in duplicate. After completing incubation, the plates were tilted at an approximate angle of 45° for about 30 minutes,

that is until the supernatant separates from the erythrocyte mixture. Thick blood smears were made for each concentration from the erythrocytes that remained in the fluid once the supernatants were removed. After thorough drying, they were stained with 10% Giemsa stain (Kosaisavee et al., 2006). Microscopic evaluation was done by counting the number of schizonts with five or more nuclei out of a total 200 asexual parasites in every thick film. Only schizonts with at least five well-defined chromatin dots were classified as schizonts. Free merozoites and gametocytes were not included in the count to ensure optimal maturity (Russell et al., 2008). The schizont counts were expressed as a proportion relative to the drug free control. Results were reported as mean (\pm SD) from two different experiments which were performed in duplicates each. IC₅₀ values were generated using GraphPad Prism 7 software (Graphpad software Inc., CA, USA).

CHAPTER 4: RESULTS AND DISCUSSION

4.1 Synthesis of ligands and metal complexes

4.1.1 Synthesis of fluorene-2-carboxaldehyde-N4 thiosemicarbazone ligands (L1-L3) and their metal complexes (1-3)

The proposed structures of all compounds and their methods of syntheses are shown in **Figure 4.1** and **Scheme 4.1**, respectively. All ligands and complexes were obtained in good yield with sharp melting points. Results from elemental analyses for all three complexes corroborated the proposed formulation from crystal data. Crystal data and results from elemental analysis prove the formation of ligand **L1** and **L3**. The ligands (**L1-L3**) were yellow in colour and the complexes (**1-3**) were dark brown in colour. The ligands were found to be coordinating in the thiolate form in all three complexes. Besides, all ligands are soluble in selected polar solvents such as ethanol, methanol, DMF, DMSO and chloroform. Whereas, the complexes are only soluble in DMF and DMSO.

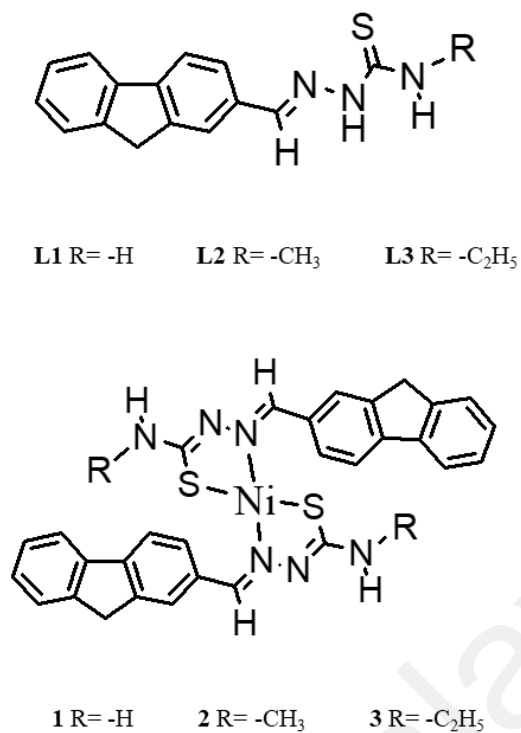
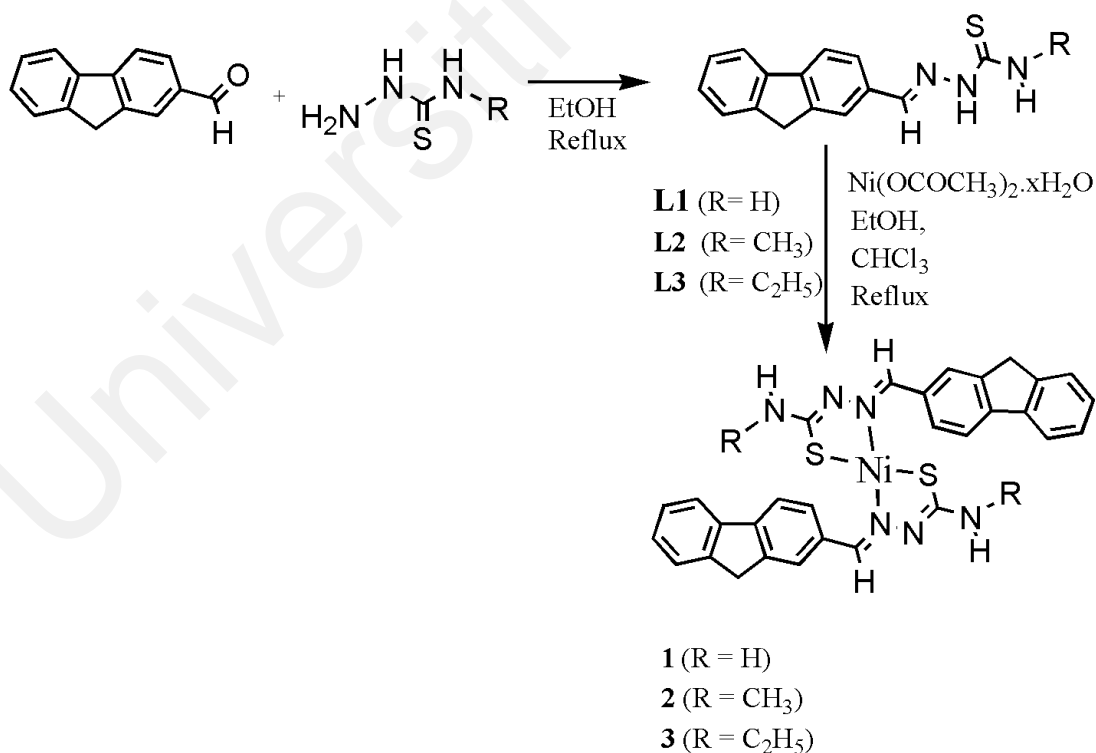


Figure 4.1 Proposed structures of ligands (L1-L3) and complexes (1-3).



Scheme 4.1 Schematic representation for the synthesis of ligands (L1-L3) and metal complexes (1-3).

4.1.2 Synthesis of 2,3,4-trihydroxybenzaldehyde-N4 thiosemicarbazone ligands (L4-L7) and their metal complexes (4-7)

The proposed structures of all compounds and their methods of syntheses are shown in **Figure 4.2** and **Scheme 4.2**, respectively. All ligands and complexes were obtained in good yield with sharp melting points. Besides, the proposed structures were in good agreement with the data obtained from various spectroscopic analysis. Results from elemental analyses for all compounds corroborated with the proposed formulation from crystal data. The ligands (**L4-L7**) were yellowish brown in colour and the complexes (**4-7**) were blackish brown in colour. Ligands (**L4-L5**) were found to be coordinating to the metal centre in the thione form whereas ligands (**L6-L7**) were found to be coordinating to the metal centre in the thiolate form. Besides, all ligands and complexes are soluble in selected polar solvents such as ethanol, methanol, DMF and DMSO.

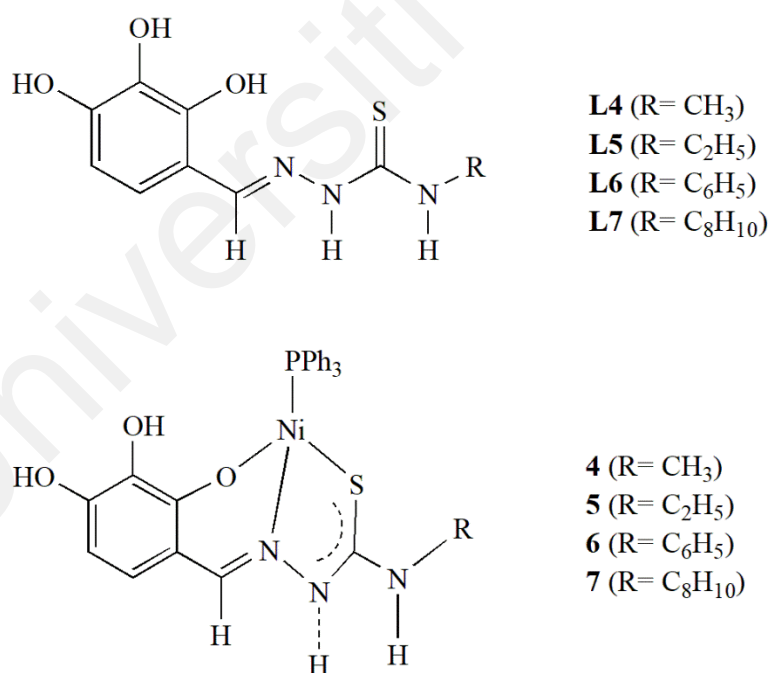
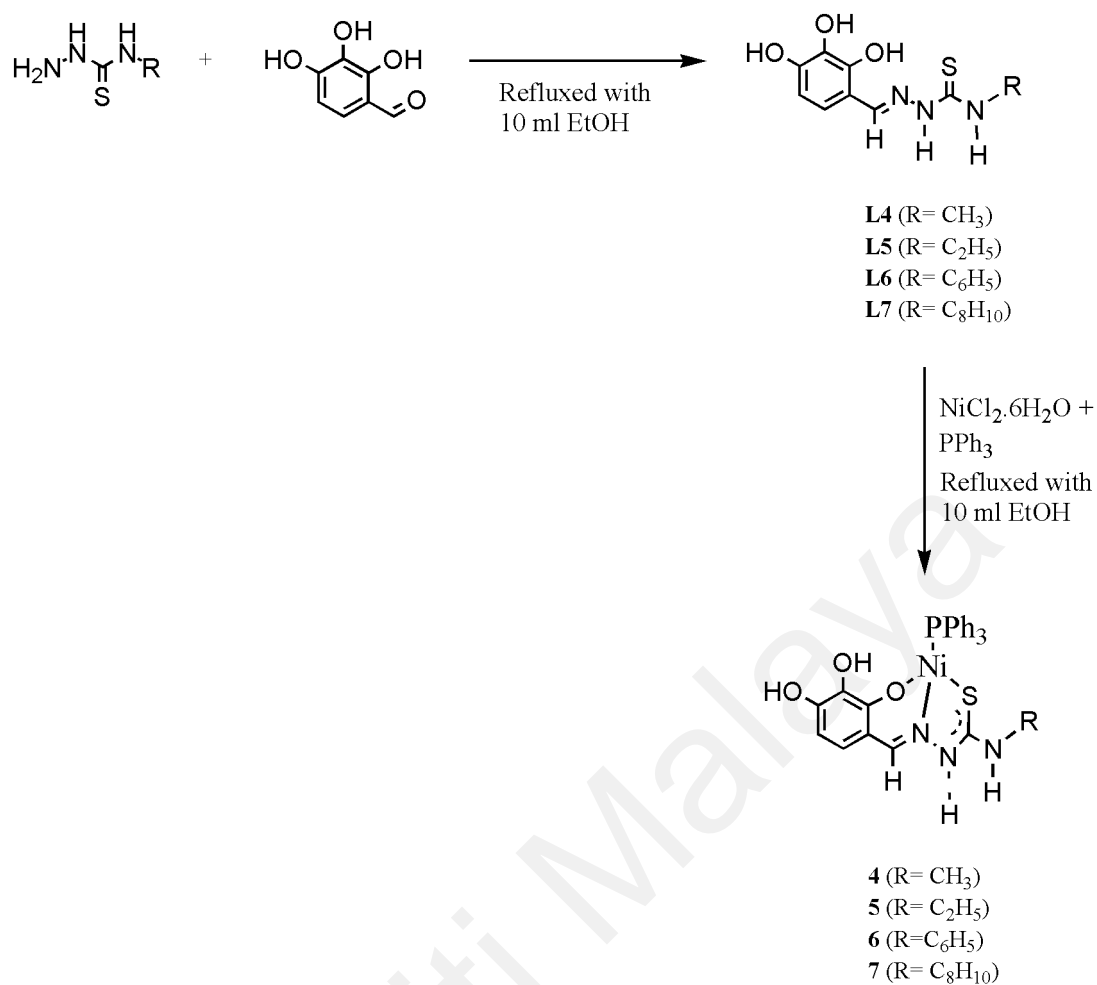


Figure 4.2 Proposed structures of ligands (L4-L7) and complexes (4-7).



Scheme 4.2 Schematic representation for the synthesis of ligands (L4-L7) and metal complexes (4-7).

4.1.3 Synthesis of 2,5-dihydroxybenzaldehyde-N⁴ thiosemicarbazone ligands (L8-L11) and their metal complexes (8-11)

The proposed structures of all compounds and their methods of syntheses are shown in **Figure 4.3** and **Scheme 4.3**, respectively. All ligands and complexes were obtained in good yield with sharp melting points. Besides, the proposed structures were in good agreement with the data obtained from various spectroscopic analysis. Results from elemental analyses for all compounds corroborated with the proposed formulation from crystal data. The ligands (**L8-L11**) were yellowish brown in colour and the complexes (**8-11**) were blackish brown in colour. Only ligand **L10** was found to be coordinating to the metal complex in its thione form. Whilst the other ligands were found to be coordinating in their tautomeric thiolate form.

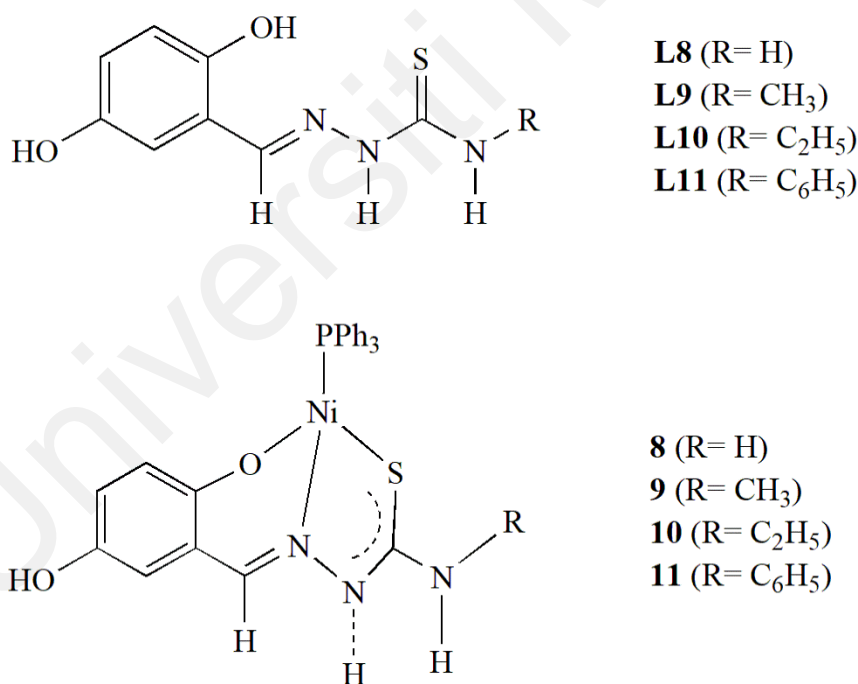
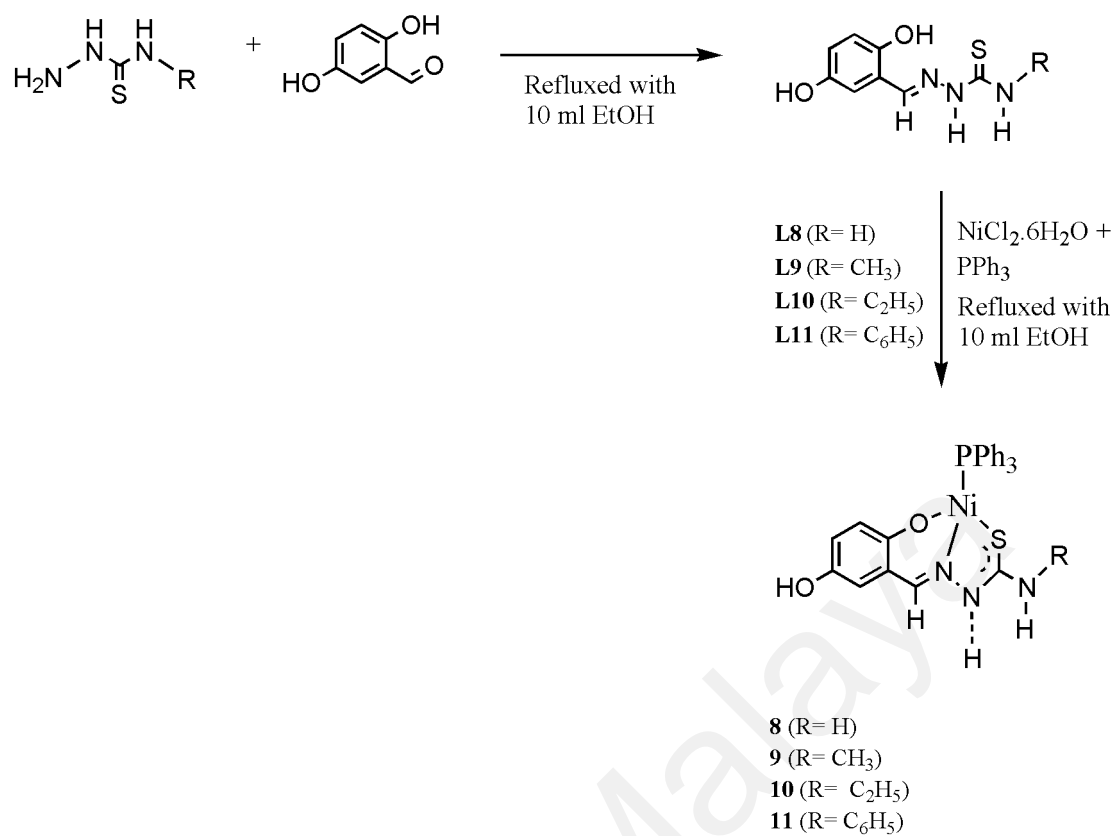


Figure 4.3 Proposed structures of ligands (L8-L11) and complexes (8-11).



Scheme 4.3 Schematic representation for the synthesis of ligands (L8-L11) and metal complexes (8-11).

4.2 Infrared spectra

4.2.1 Infrared spectra of fluorene-2-carboxaldehyde-N4 thiosemicarbazone ligands (L1-L3) and their metal complexes (1-3)

Sections 4.2.1.1 and 4.2.1.2 describe in detail the infrared spectra of ligands (L1-L3) and their metal complexes (1-3), respectively.

4.2.1.1 Infrared spectra of ligands (L1-L3)

Table 4.1 shows the infrared spectra of ligands and complexes. Meanwhile, Figure 4.4 and 4.5 show the infrared spectra of ligand L1 and complex 1, respectively. All ligands have the azomethine imine peak at a range of 1538-1588 cm^{-1} (Shawish et al., 2014). The thioamide $\nu(\text{NC}=\text{S})$ peaks for all ligands were observed at a range of 1360-1396 cm^{-1} (Shawish et al., 2014). Besides, the N-H stretching vibration at the N(3) position for all ligands were observed at a range of 3300-3370 cm^{-1} (Lobana et al., 2009). The absence of $\nu(\text{S-H})$ band at a range of 2600-2800 cm^{-1} and the presence of the $\nu(\text{N(2)H})$ band at a range of 3108-3160 cm^{-1} indicates that all ligands remain in their thione form (Jouad et al., 2001; Tan et al., 2012).

4.2.1.2 Infrared spectra of metal complexes (1-3)

As for metal complexes (1-3), the azomethine imine peaks were found to have shifted to lower wavenumbers. This confirms the coordination of all ligands to their respective metal complexes through the azomethine imine nitrogen atom (Ajani et al., 2009; Andiappan et al., 2018; Kotkar & Juneja, 2013). Besides, the emergence of new $\nu(\text{Ni-S})$ and $\nu(\text{Ni-N})$ bands at a range of 441-485 cm^{-1} and 561-563 cm^{-1} , respectively guarantees once again the coordination of ligands to metal through their bidentate N,S atoms. The

disappearance of the $\nu(\text{N}(2)\text{H})$ bands in complexes (**1-3**) presents convincing affirmation that the ligands are coordinated to their metal centres in the deprotonated form which is the thiolate form (Latheef et al., 2007; Reena & Kurup, 2010; Seena & Kurup, 2007; Seena & Kurup, 2008). Moreover, a decrease in frequency of the thioamide band from $1360\text{-}1396\text{ cm}^{-1}$ and $821\text{-}841\text{ cm}^{-1}$ to $1327\text{-}1389\text{ cm}^{-1}$ and $732\text{-}764\text{ cm}^{-1}$ suggests that the ligands are coordinated to the metal *via* the thiolate sulphur (Campbell, 1975), confirmed by a decrease in stretching frequency in the metal complex of the earlier mentioned bands which belonged to the $\nu(\text{C}=\text{S})$ and $\nu(\text{C}-\text{S})$ vibrations. This is due to a change in bond order and strong electron delocalisation (John et al., 2004; Sreekanth et al., 2006).

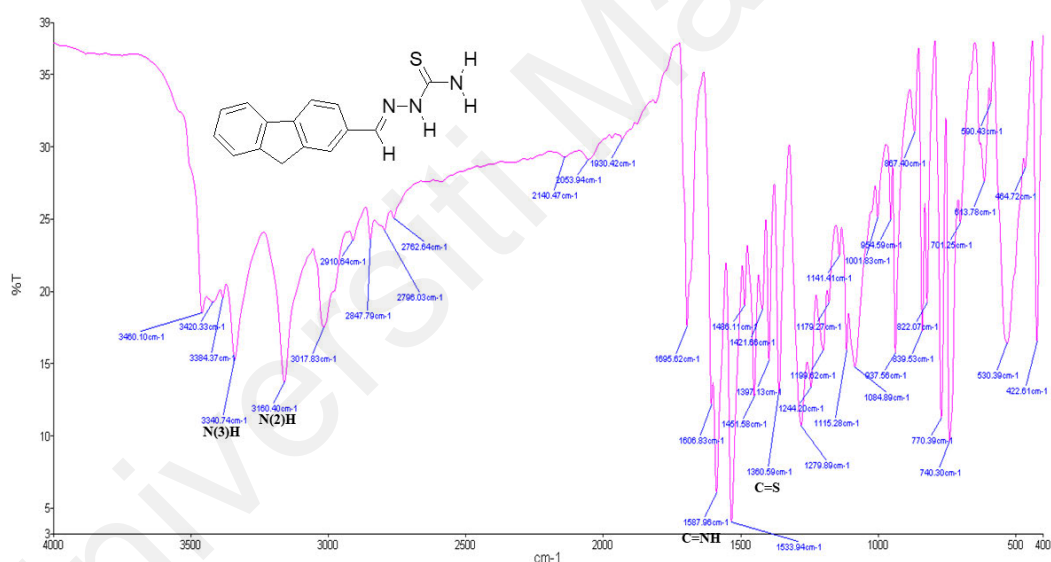


Figure 4.4 Infrared spectra of ligand L1.

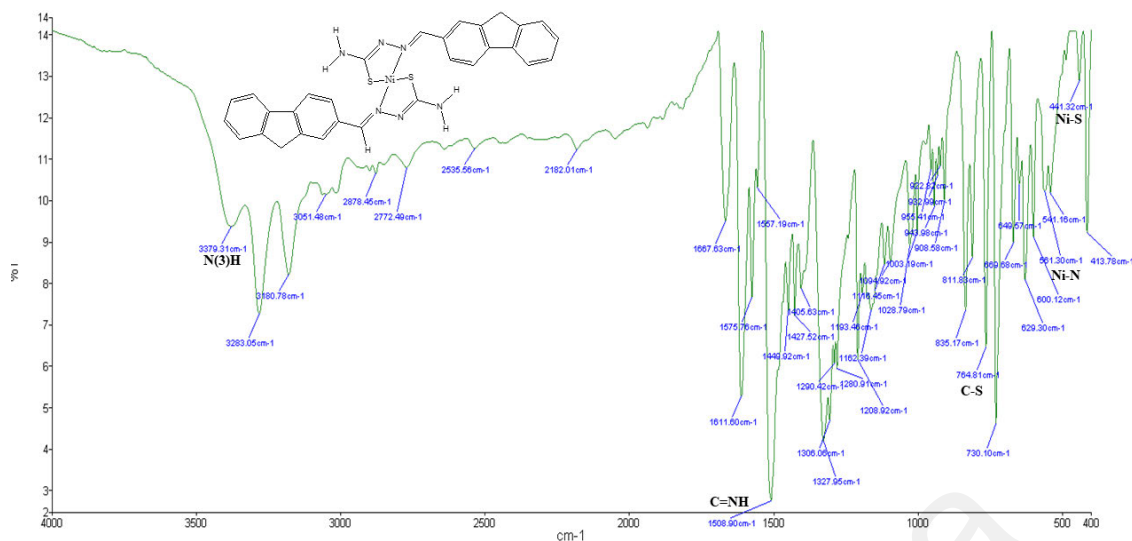


Figure 4.5 Infrared spectra of complex 1.

Table 4.1 Infrared spectra of ligands (L1-L3) and complexes (1-3).

Compound	$\nu(\text{cm}^{-1})$						
	CH=N	NC=S	C-S	N(2)H	N(3)H	Ni-S	Ni-N
L1	1588	1360	841	3160	3341	-	-
L2	1546	1396	821	3108	3300	-	-
L3	1538	1379	832	3158	3370	-	-
1	1509	1327	764	-	3283	441	561
2	1520	1389	732	-	3355	485	563
3	1521	1349	763	-	3411	447	561

4.2.2 Infrared spectra of 2,3,4-trihydroxybenzaldehyde-N4 thiosemicarbazone ligands (L4-L7) and their metal complexes (4-7)

Sections 4.2.2.1 and 4.2.2.2 describe in detail the infrared spectra of ligands (L4-L7) and their metal complexes (4-7), respectively.

4.2.2.1 Infrared spectra of ligands (L4-L7)

Table 4.2 shows the infrared spectra of ligands and complexes. Meanwhile, Figure 4.6 and 4.7 show the infrared spectra of ligand L4 and complex 4, respectively. All ligands have the azomethine imine peak at a range of $1612-1637\text{ cm}^{-1}$ (Arutyunyan et al., 2018). The thioamide $\nu(\text{NC}=\text{S})$ peaks for all ligands were observed at a range of $1345-1378\text{ cm}^{-1}$ (Shawish et al., 2014). Besides, the hydrazinic proton $\nu(\text{N}(3)\text{H})$ for all ligands were observed at a range of $3202-3441\text{ cm}^{-1}$ (Marchewka et al., 2003; Munakata et al., 2001). The absence of $\nu(\text{S-H})$ band at 2570 cm^{-1} and the presence of the $\nu(\text{N}(2)\text{H})$ band at a range of $3140-3180\text{ cm}^{-1}$ indicates that all ligands are in their thione form (Jouad et al., 2001; Tan et al., 2012). The $\nu(\text{OH})$ peaks for these ligands were observed at a range of $3352-3531\text{ cm}^{-1}$ (Liu et al., 2013; Weckler & Lutz, 1996). Whereas the peaks belonging to $\nu(\text{C-O})$ were observed at a range of $1251-1283\text{ cm}^{-1}$ (Shawish et al., 2014).

4.2.2.2 Infrared spectra of metal complexes (4-7)

In most cases, the azomethine imine peaks $\nu(\text{CH}=\text{N})$ of metal complexes would be found to have shifted to lower wavenumbers as is the case in complexes (4-6) (Kotkar et al., 2013). However, the mentioned peak was found to have shifted to higher wavenumber in complex 7. Hence, addition of metal salt can also cause a shift to higher wavenumbers (Andiappan et al., 2018). This confirms the coordination of all ligands to their metal

centre through the azomethine imine nitrogen atom. The hydrazinic proton $\nu(\text{N}(3)\text{H})$ in all complexes were found to have shifted to higher wavenumbers and be at a range of $3310\text{-}3454\text{ cm}^{-1}$, indicating that complexation has occurred through the azomethine imine nitrogen atom. However only complexes **4** and **5** showed the presence of $\nu(\text{N}(2)\text{H})$ peak at a range of $3161\text{-}3169\text{ cm}^{-1}$, indicating that ligands **L4** and **L5** are coordinated to the metal centre in their initial thione form (Lobana et al., 2009). The disappearance of the $\nu(\text{N}(2)\text{H})$ bands in complexes **6** and **7** presents convincing affirmation that ligands **L6** and **L7** are coordinated to their metal centres in the deprotonated thiolate form. Besides, the emergence of new $\nu(\text{Ni-S})$, $\nu(\text{Ni-N})$ and $\nu(\text{Ni-O})$ at a range of $488\text{-}494\text{ cm}^{-1}$, $528\text{-}533\text{ cm}^{-1}$ and $503\text{-}510\text{ cm}^{-1}$, respectively guarantees once again the coordination of ligands to metal centre through their O,N,S tridentate binding sites (Latheef et al., 2007; Reena et al., 2010; Seena et al., 2007). The $\nu(\text{OH})$ peak for all complexes were observed at a range of $3218\text{-}3448\text{ cm}^{-1}$, suggesting that only one phenolic OH group was involved in metal complexation. The $\nu(\text{C-O})$ peaks in metal complexes were found to be at similar ranges as their free ligands. The bands due to triphenylphosphine after metal complexation for all complexes were found to be at ranges of $1434\text{-}1436\text{ cm}^{-1}$, $1084\text{-}1095\text{ cm}^{-1}$ and $689\text{-}693\text{ cm}^{-1}$ (Shawish et al., 2014).

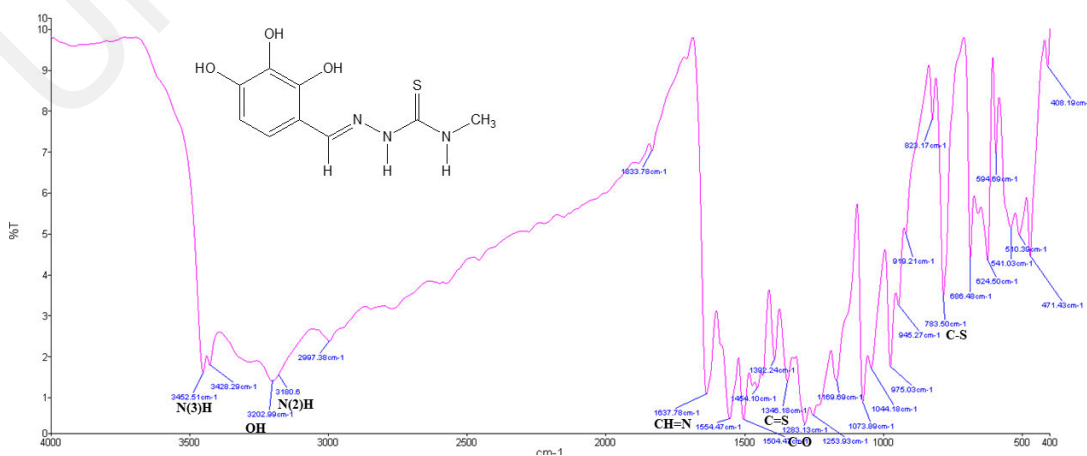


Figure 4.6 Infrared spectra of ligand L4.

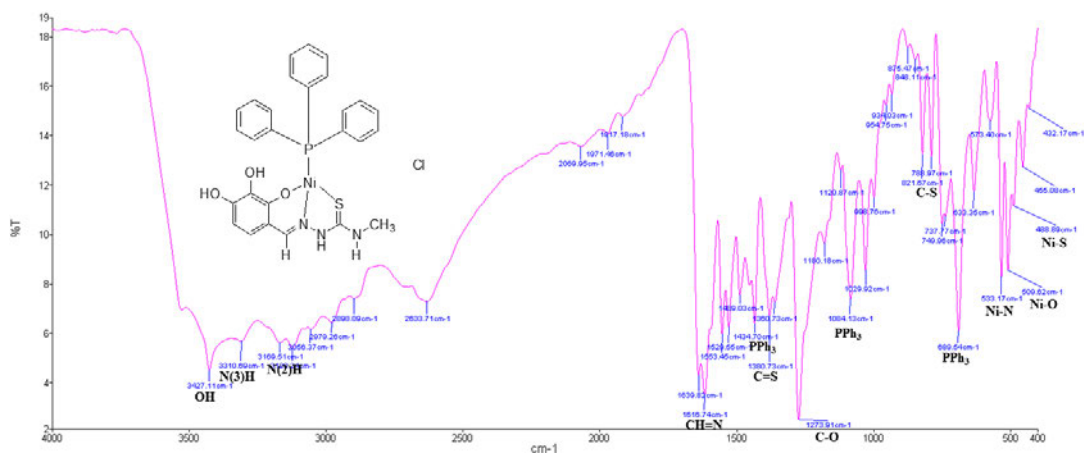


Figure 4.7 Infrared spectra of complex 4.

Table 4.2 Infrared spectra of ligands (L4-L7) and complexes (4-7).

Compd.	$\nu(\text{cm}^{-1})$								
	CH=N	C=S /C-S	N(2)H	N(3)H	OH	Ni-S	Ni-N	Ni-O	PPh ₃
L4	1637	1346 /823	3180	3202	3452	-	-	-	-
L5	1632	1348 /798	3170	3349	3439	-	-	-	-
L6	1612	1345 /804	3149	3441	3531	-	-	-	-
L7	1634	1378 /833	3140	3341	3352	-	-	-	-
4	1616	1380 /788	3169	3310	3427	488	533	509	1434 1084 689
5	1610	1320 /779	3161	3454	3218	494	528	503	1435 1091 691
6	1562	1318 /765	-	3370	3448	489	529	507	1436 1093 690
7	1654	1315 /782	-	3439	3534	493	531	510	1436 1095 693

4.2.3 Infrared spectra of 2,5-dihydroxybenzaldehyde-N4 thiosemicarbazone ligands (L8-L11) and their metal complexes (8-11)

Sections 4.2.3.1 and 4.2.3.2 describe in detail the infrared spectra of ligands (L8-L11) and their metal complexes (8-11), respectively.

4.2.3.1 Infrared spectra of ligands (L8-L11)

Table 4.3 shows the infrared spectra of ligands and complexes. Meanwhile, Figure 4.8 and 4.9 show the infrared spectra of ligand L8 and complex 8, respectively. The azomethine imine $\nu(\text{CH}=\text{N})$ peaks of all ligands were found at a range of 1532-1625 cm^{-1} (Sutradhar et al., 2007; Yıldız et al., 1998). Whereas, the thioamide $\nu(\text{NC}=\text{S})$ peaks for all ligands were found at a range of 1311-1340 cm^{-1} (Esteves-Souza et al., 2006; Vandresen et al., 2014). (Esteves-Souza et al., 2006; Vandresen et al., 2014). Whilst, the hydrazinic proton N(2)H peaks were observed to be at 3017-3159 cm^{-1} indicating that the ligands are in the thione form (Ferrari et al., 2002). The absence of any peak around 2500 cm^{-1} belonging to the $\nu(\text{SH})$ group once again confirms the state of all ligands in their thione form (Singh & Dikshit, 1995). Besides, the hydrazinic proton N(3)H peaks were found to be at a range of 3156-3328 cm^{-1} (Fatondji et al., 2013). As for the vibrations caused by $\nu(\text{OH})$ peak, they were found to be at a range of 3366-3428 cm^{-1} (Rosu et al., 2010; Tan et al., 2012).

4.2.3.2 Infrared spectra of metal complexes (8-11)

The azomethine imine $\nu(\text{CH}=\text{N})$ peak in complex 8 was seen to shift to a lower wavenumber than its free ligand as is in most cases. However, the mentioned peak was found to shift to higher wavenumbers in complexes 9, 10 and 11. The $\nu(\text{C}=\text{S})$ peak for

complex **10** was observed at 1337 cm^{-1} , suggesting that ligand **L10** was coordinated to the metal ion in its initial thione form. However, complexes **8**, **9** and **11** display a loss of double bond character upon deprotonation of the NH group resulting in the disappearance of the thioamide $\nu(\text{C}=\text{S})$ peak (Amoedo et al., 2006). The emergence of new peaks at $744\text{--}828\text{ cm}^{-1}$ due to $\nu(\text{C}-\text{S})$ suggests coordination of sulfur atom after enolization followed by deprotonation (Kalaivani et al., 2012). In addition, complex **10** was seen to exhibit a peak at 3054 cm^{-1} belonging to the hydrazinic proton N(2)H. This peak was not found in other complexes, indicating that ligands **L8**, **L9** and **L10** were coordinated to the metal ion in their thiolate form. On the other hand, the hydrazinic proton N(3)H were found to be at a range of $3193\text{--}3286\text{ cm}^{-1}$. The peak due to $\nu(\text{OH})$ were seen at a range of $3284\text{--}3393\text{ cm}^{-1}$ stipulating the presence of free OH group in the metal complex, indicating that only one OH group was involved in metal complexation. Emergence of new peaks at a range of $495\text{--}498\text{ cm}^{-1}$, $524\text{--}535\text{ cm}^{-1}$ and $502\text{--}511\text{ cm}^{-1}$ belonging to $\nu(\text{Ni}-\text{S})$, $\nu(\text{Ni}-\text{N})$ and $\nu(\text{Ni}-\text{O})$, respectively were observed. Whereas, bands due to triphenylphosphine $\nu(\text{PPh}_3)$ were observed at a range of $1433\text{--}1435\text{ cm}^{-1}$, $1096\text{--}1098\text{ cm}^{-1}$ and $689\text{--}694\text{ cm}^{-1}$ (Prabhakaran et al., 2013).

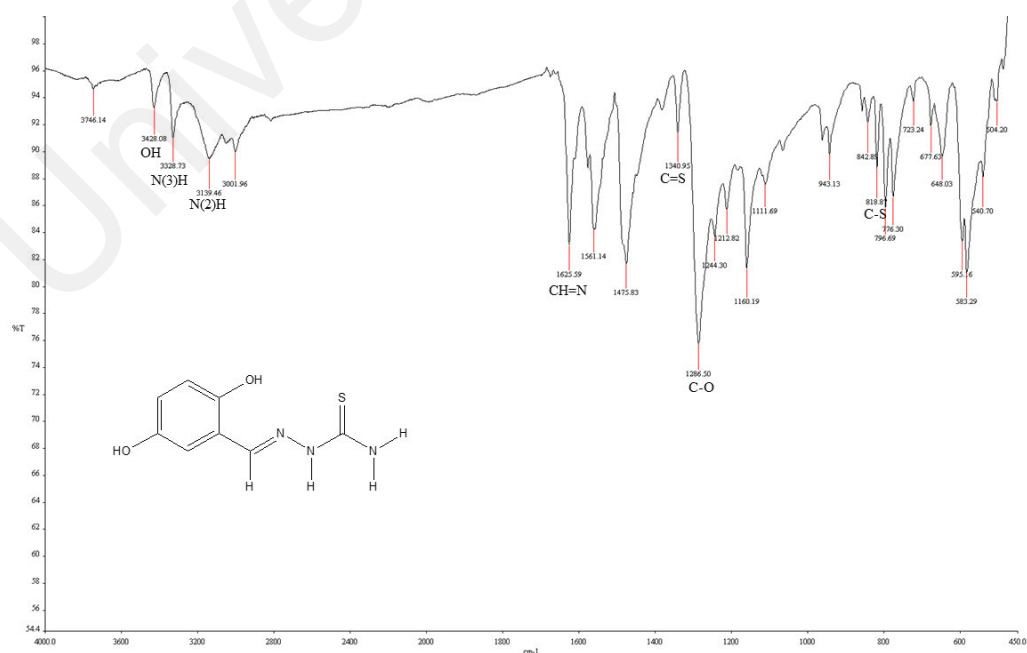


Figure 4.8 Infrared spectra of ligand **L8**.

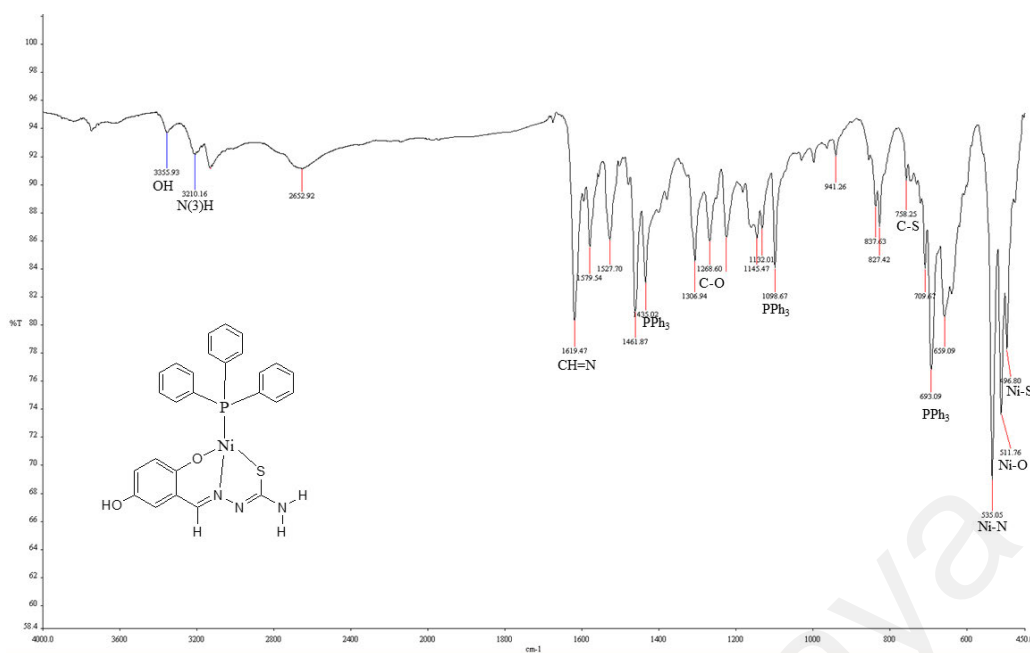


Figure 4.9 Infrared spectra of complex 8.

Table 4.3 Infrared spectra of ligands (L8-L11) and complexes (8-11).

Compd.	$\nu(\text{cm}^{-1})$								
	CH=N	C=S /C-S	N(2)H	N(3)H	OH	Ni-S	Ni-N	Ni-O	PPh ₃
L8	1625	1340 /818	3139	3328	3428	-	-	-	-
L9	1557	1333 /823	3040	3259	3366	-	-	-	-
L10	1532	1311 /803	3017	3156	3389	-	-	-	-
L11	1539	1330 /816	3159	3235	3391	-	-	-	-
8	1619	758	-	3210	3355	496	535	511	1435 1098 693
9	1606	828	-	3211	3355	496	530	507	1434 1096 689
10	1634	1337 /749	3054	3286	3286	498	528	510	1433 1096 694
11	1653	744	-	3193	3284	495	524	502	1434 1097 690

4.3 ^1H NMR and ^{13}C NMR spectra

4.3.1 ^1H NMR and ^{13}C NMR spectra of fluorene-2-carboxaldehyde-N4 thiosemicarbazone ligands (L1-L3) and their metal complexes (1-3)

Sections 4.3.1.1 and 4.3.1.2 describe in detail the ^1H NMR and ^{13}C NMR spectra of ligands (L1-L3) and their metal complexes (1-3), respectively.

4.3.1.1 ^1H NMR and ^{13}C NMR spectra of ligands (L1-L3)

The proton and carbon resonance signals of ligands and complexes are shown in **Table 4.4** and **4.5**, respectively. **Figure 4.10** and **4.11** show the ^1H NMR and ^{13}C NMR spectra of ligand **L1**, respectively. Whilst the ^1H NMR and ^{13}C NMR spectra of complex **1** are shown in **Figure 4.12** and **4.13**, respectively. Ligands were seen to have a singlet proton resonance signal at 8.06-8.09 ppm which belonged to the azomethine imine group, (CH=N) (Çukurovali et al., 2002). An absence in resonance signal at 4 ppm which belonged to the (S-H) indicates that the ligands are in the thioamide form. Besides, a singlet at 11.36-11.44 ppm confirms the presence of thiohydrazinic (N(2)H) proton, stipulating that the ligands are in the thioamide form (Afrasiabi et al., 2004). Whereas, the (N(3)H) resonance signal was found to be at 8.13-8.54 ppm and the shift in resonance signal is highly dependent on the substituent group attached to it (Ackerman et al., 1999). The aromatic ring proton resonance signals for all ligands were found to be at around 7.06-8.02 ppm (Lewis et al., 2012).

Carbon resonance signal was shown by all ligands at 193.34-193.39 ppm due to (C=S) (King et al., 2011). Meanwhile, resonance signals of azomethine carbon at around 177.05-178.26 ppm confirms the formation of Schiff base (Raman et al., 2004). The aromatic carbons produce resonance signals at 120.67-144.13 ppm (Fatondji et al., 2013).

Whereas, the CH₂ and CH₃ resonance signals for the ligands were assigned at around 36.80-38.82 ppm and 15.21-31.33 ppm, respectively (Isab & Al-Arfaj, 1991; Shawish & Bashir, 2014). The proposed structures were in tandem with the total number of carbon resonance signals in the spectra of all ligands.

4.3.1.2 ¹H NMR and ¹³C NMR spectra of metal complexes (1-3)

The proton for azomethine imine group (CH=N) was found to have shifted slightly downfield in the complexes. This shows that the ligands have been coordinated to the metal *via* the azomethine nitrogen atom (Lopez-Garriga et al., 1986). However, the azomethine proton of complexes **2** and **3** were found as a doublet due to coupling of the imine proton with the metal ion (Udhayakumari et al., 2015). Ligands (**L1-L3**) are coordinated to metal in the thiolate form rather than the usual thioamide form. This is proven by the absence of any attributable resonance signal at 11.36-11.44 ppm. The resonance signal of (N(3)H) protons for complex **1** was seen to have shifted downfield. This could be due to the lowering of bond order as an outcome of thione to thiol tautomerization in the complex (Rodríguez-Argüelles et al., 1999). However, the (N(3)H) resonance signals of complexes **2** and **3** were seen to shift slightly upfield although in usual case it shifts downfield. Occasional change in trend is common. Metal complexation was seen to not affect the aromatic ring proton as they were found to resonate at similar frequencies as their ligands.

As for the complexes, the carbon resonance signals due to (C=S) were not found. This is because the complexes are no longer in the initial thioamide form as their ligands, instead they have undergone tautomerization and were found to be in the thiolate form. Hence, emergence of a new resonance signal at 154.05-154.23 ppm belonging to the azomethine carbon was discovered. On the other hand, the azomethine carbons that were

found in the ligands were seen to have shifted upfield due to metal complexation *via* the azomethine imine nitrogen atom (Lobana et al., 2009). Besides, there were no significant changes in the resonance signals produced by the aromatic and aliphatic carbons. Once again, the total number of carbon resonance signals in the spectra of all complexes were in tandem with their proposed structures.

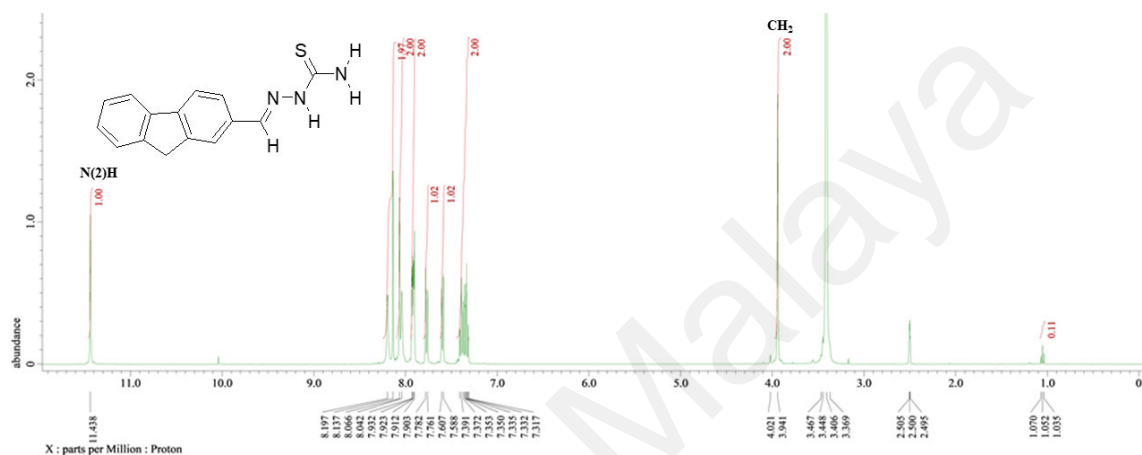


Figure 4.10 ^1H NMR spectra of ligand L1.

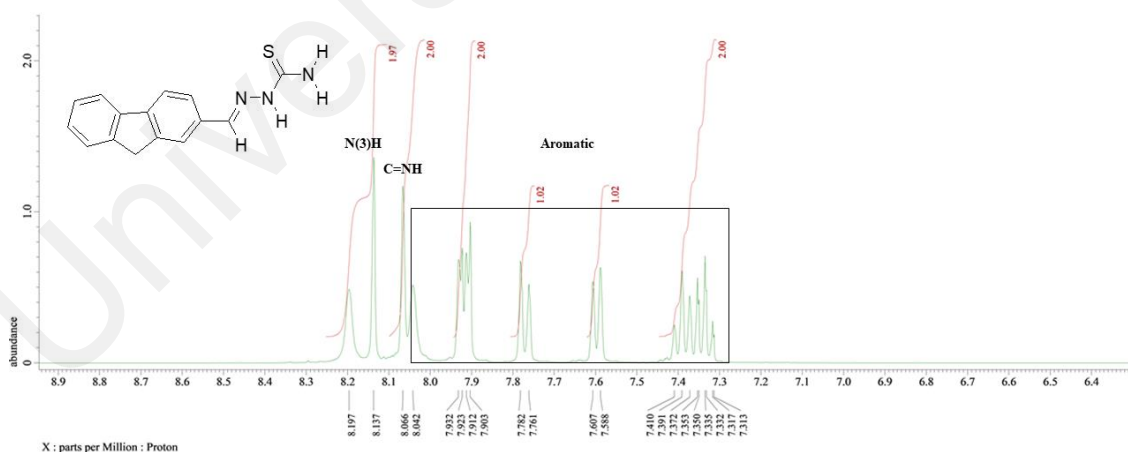


Figure 4.10, continued.

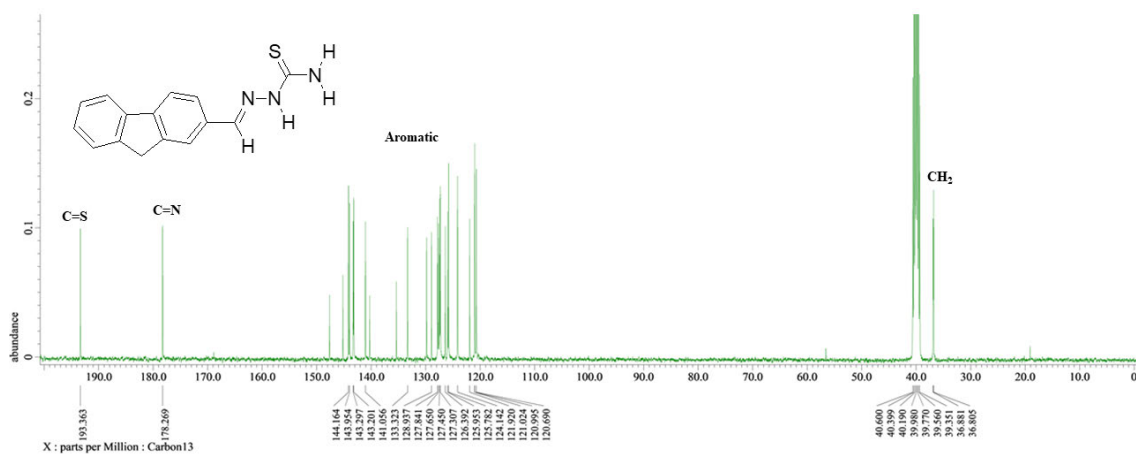


Figure 4.11 ^{13}C NMR spectra of ligand L1.

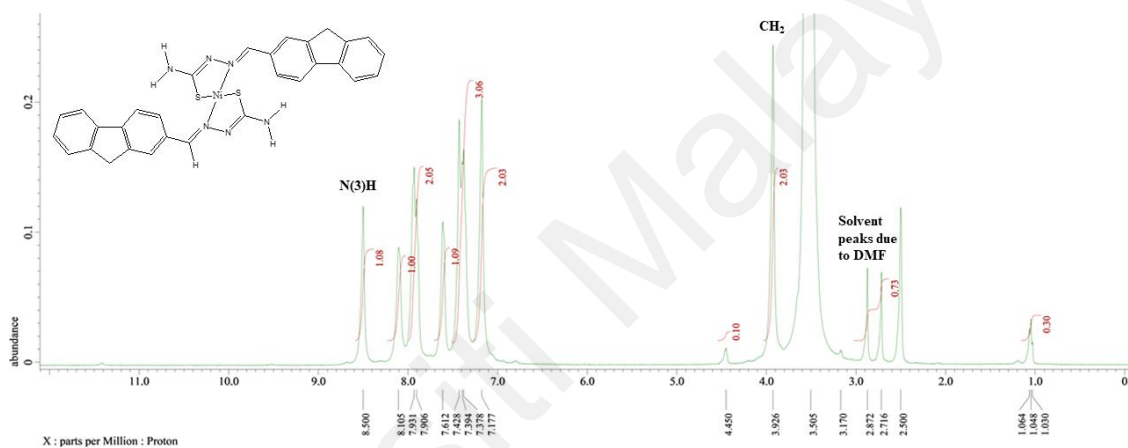


Figure 4.12 ^1H NMR spectra of complex 1.

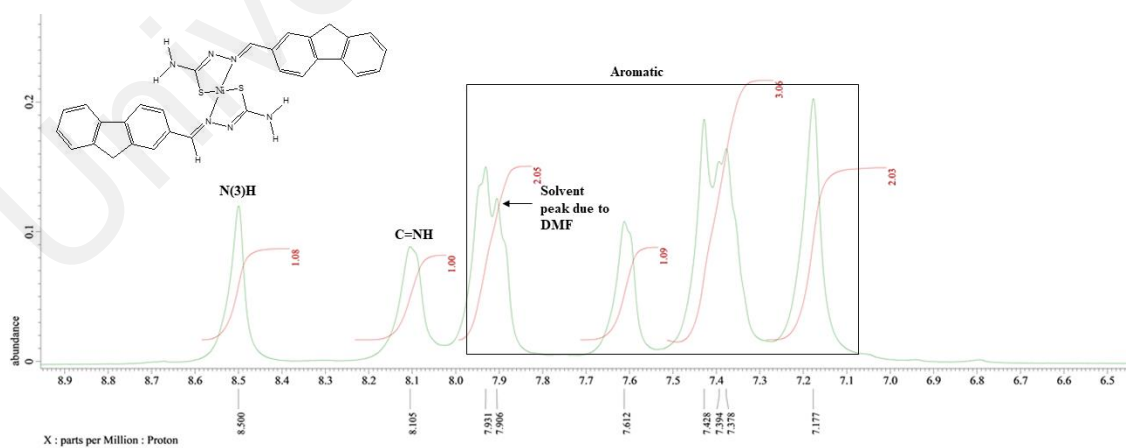


Figure 4.12, continued.

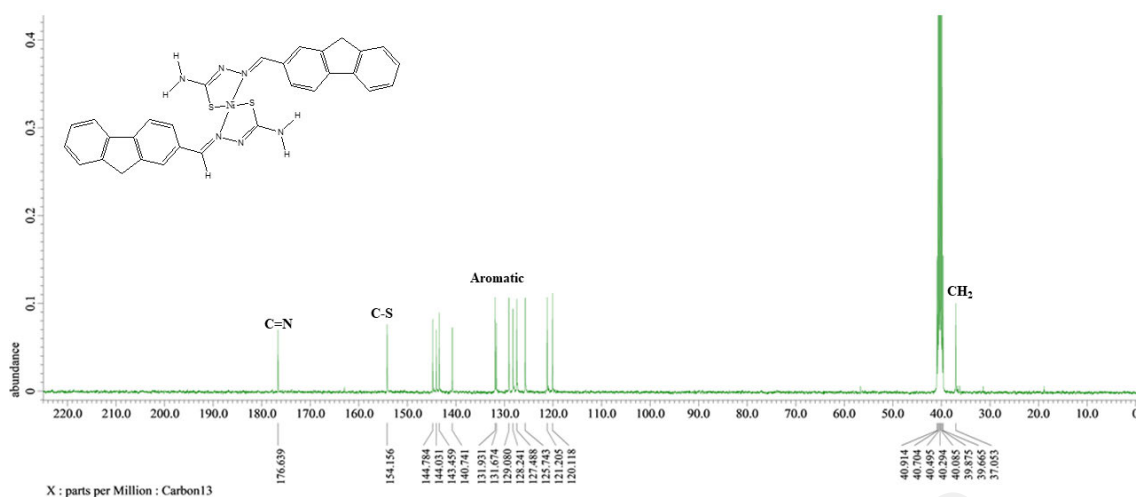


Figure 4.13 ^{13}C NMR spectra of complex 1.

Table 4.4 ^1H NMR spectra of ligands (L1-L3) and complexes (1-3).

Compd.	$\delta(\text{ppm})$				
	CH=N	N(2)H	N(3)H	Aromatic	Aliphatic
L1	8.06 (s, 1H)	11.43 (s, 1H)	8.19 (s, 1H)	7.06-7.93	3.94 (s, 2H)
L2	8.09 (s, 1H)	11.44 (s, 1H)	8.13 (s, 1H)	7.29-8.02	3.91 (s, 2H) 3.01 (d, 3H)
L3	8.09 (s, 1H)	11.36 (s, 1H)	8.54 (t, 1H)	7.29-8.01	3.97 (s, 2H) 3.58 (q, 2H) 1.12 (t, 3H)
1	8.10 (s, 1H)	-	8.50 (s, 1H)	7.17-7.93	3.92 (s, 2H)
2	8.13 (d, 1H)	-	8.17 (s, 1H)	7.39-7.93	3.91 (s, 2H) 2.88 (d, 3H)
3	8.09 (d, 1H)	-	8.44 (s, 1H)	7.31-7.90	3.89 (s, 2H) 3.28 (q, 2H) 1.14 (t, 2H)

Table 4.5 ^{13}C NMR spectra of ligands (L1-L3) and complexes (1-3).

Compd.	$\delta(\text{ppm})$			
	C=N	C=S	Aromatic	Aliphatic
L1	178.26	193.36	120.69-143.95	36.80 (CH ₂)
L2	178.05	193.39	120.98-144.13	36.81 (CH ₂) 31.33 (CH ₃)
L3	177.05	193.34	120.67-144.13	38.82 (CH ₂) 36.83 (CH ₂) 15.21 (CH ₃)
1	176.63 154.15	-	120.11-144.78	37.05 (CH ₂)
2	175.65 154.23	-	120.16-144.78	37.03 (CH ₂) 32.27 (CH ₃)
3	174.90 154.05	-	120.15-144.76	37.01 (CH ₂) 31.80 (CH ₂) 14.89 (CH ₃)

4.3.2 ^1H NMR and ^{13}C NMR spectra of 2,3,4-trihydroxybenzaldehyde-N4 thiosemicarbazone ligands (L4-L7) and their metal complexes (4-7)

Sections 4.3.2.1 and 4.3.2.2 describe in detail the ^1H NMR and ^{13}C NMR spectra of ligands (L4-L7) and their metal complexes (4-7), respectively.

4.3.2.1 ^1H NMR and ^{13}C NMR spectra of ligands (L4-L7)

Table 4.6 shows the proton resonance signals of all ligands and complexes whereas the carbon resonance signals are shown in **Table 4.7**. The **Figure 4.14** and **4.15** show the ^1H NMR and ^{13}C NMR spectra of ligand **L4**, respectively. Whilst the ^1H NMR and ^{13}C NMR spectra of complex **4** are shown in **Figure 4.16** and **4.17**, respectively. The singlet proton resonance signal belonging to the azomethine imine group ($\text{CH}=\text{N}$) was seen to be at a range of 8.19-8.33 ppm for all ligands (Amato et al., 2007). The fact that all ligands are in their thioamide form is proved by the absence of resonance signal at around 4 ppm which belongs to the (S-H) group (Tan et al., 2012). The presence of all ligands in their thioamide form is further confirmed by the appearance of singlet proton resonance signal at a range of 11.12-11.56 ppm which belongs to the thiohydrazinic proton (N(2)H) (Afrasiabi et al., 2004; Chellaian & Johnson, 2014; Raj & Kurup, 2007). The hydrazinic (N(3)H) proton resonance signal for all ligands were found to be at a range of 8.26-9.65 ppm and the shift in resonance signal is highly dependent on the substituent group attached to it (Ackerman et al., 1999; Bayrak et al., 2009). The resonance signal for aromatic ring which appeared as multiplets were observed at a range of 6.32-9.89 ppm for all ligands (Çukurovali et al., 2002). Also, the phenolic OH resonance signal was observed at a range of 6.34- 9.89 ppm (Afzal et al., 2014; Tunçel & Serin, 2005). Whilst, the aliphatic proton resonance signals due to $-\text{CH}_2$ and $-\text{CH}_3$ groups were seen to be at a range of 2.95-3.53 ppm and 1.08-2.95 ppm for all ligands (Mazzei et al., 2001).

Carbon resonance signals showed by azomethine imine nitrogen (C=N) for all ligands were observed at a range of 141.87-147.19 ppm. The resonance signal for thioamide (C=S) were found to be at a range of 175.54-177.51 for all ligands, stipulating that the ligands are in their thione form (Beckford et al., 2009). Besides, the resonance signal for phenolic OH were detected at a range of 133.20-153.76 ppm. Whilst, the resonance signals caused by aromatic carbons were observed at 108.14-142.80 ppm (Tomma, 2017). Whereas, resonance signals due to aliphatic carbons caused by -CH₂ group and -CH₃ group were spotted at 28.18-38.76 ppm and 15.23-31.38 ppm, respectively (Barnholtz et al., 2001; Prasad et al., 2009; Shawish et al., 2014). The total number of carbon resonance signals from the spectra were in tandem with the proposed structures of all ligands.

4.3.2.2 ¹H NMR and ¹³C NMR spectra of metal complexes (4-7)

The azomethine imine nitrogen (CH=N) resonance signal was found to have shifted slightly downfield and resonate at a range of 8.18-8.45 ppm, proving that the ligands are coordinated to the metal centre *via* their azomethine imine nitrogen atom. The azomethine resonance signal for complexes **6** and **7** were observed as doublets due to coupling with phosphorus atom of triphenylphosphine (Prabhakaran et al., 2013). Complexes **4** and **5** show resonance signals due to thiohydrazinic proton (N(2)H) at 11.17 ppm and 11.10 ppm, respectively. Hence, ligands **L4** and **L5** were found to have coordinated to the metal centre in their thioamide form. However, resonance signal at this range was absent in complexes **6** and **7**, indicating that ligands **L6** and **L7** were coordinated to the metal centre in their thiolate form. This is further confirmed by the emergence of a new resonance signal belonging to the (S-H) group at 4.70 ppm and 4.68 ppm for complexes **6** and **7**, respectively. The hydrazinic proton resonance signal (N(3)H) was seen to have shifted downfield in complexes **5** and **6** as a result of decrease in electron density due to the

electron withdrawal by metal centre, sulphur, and deprotonated phenolic OH (Mostafa et al., 2000). However, complexes **4** and **7** were seen to not follow this trend as occasional change in trend is common. The resonance signal due to phenolic OH in all complexes were observed at a range of 6.05-9.25 ppm, similar as their ligands, suggesting that only one phenolic OH group was involved in metal complexation. Resonance signals of aromatic protons in all complexes were found to resonate at similar resonances as their ligands because aromatic protons were not affected by metal complexation. There is not much variation in the resonance signals produced by aliphatic protons in all complexes from their respective ligands because aliphatic protons are not involved in metal complexation as well.

Since the azomethine imine nitrogen (C=N) is involved in metal complexation, their resonance signals were observed at 141.65 ppm and 141.45 ppm for complexes **4** and **5**, respectively. Their thioamide carbon resonance signals (C=S) were spotted at 177.29 ppm and 176.35 ppm, indicating that ligands **L4** and **L5** were coordinated to the metal centre in their initial thione form. Furthermore, a slight upfield shift in the thioamide resonance signal observed in complexes **4** and **5** is due to lowering of C-S bond order as a result of metal complexation (Prabhu & Ramesh, 2013). However, complexes **6** and **7** produced resonance signals at a range of 164.67-164.87 ppm which belongs to the azomethine imine nitrogen (C=N). This downfield shift of the mentioned group reaffirms the coordination of ligands **L6** and **L7** to the metal centre *via* their azomethine imine nitrogen atom. Besides, the resonance signal due to thioamide carbon was absent in these complexes, confirming that ligands **L6** and **L7** were coordinated to the metal centre in the thiolate form. The resonance signal caused by phenolic OH was spotted at a range of 146.39-150.25 ppm, denoting that only one of the phenolic OH was involved in metal complexation. Significant changes were not observed in the resonance signals produced

by aromatic and aliphatic carbon atoms. Once again, the number of carbon atoms from the spectra were in tandem with the proposed structures for all complexes.

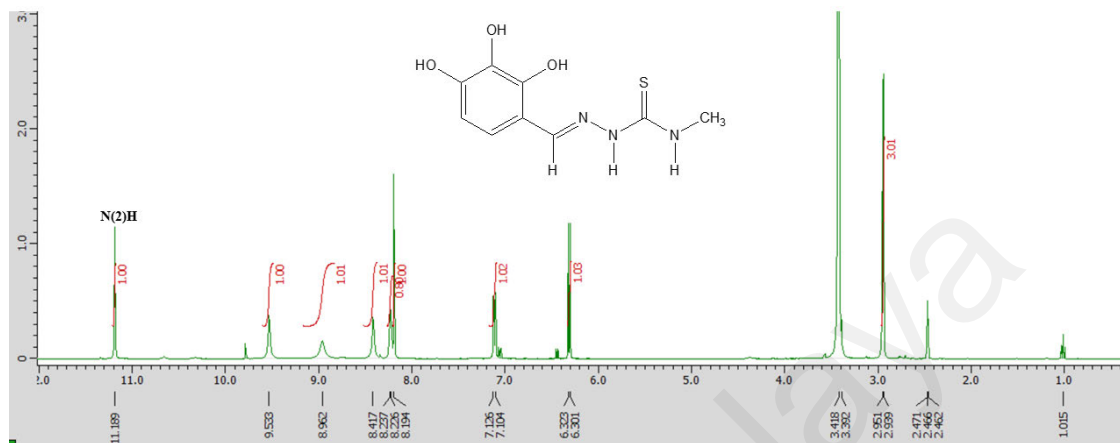


Figure 4.14 ^1H NMR spectra of ligand L4.

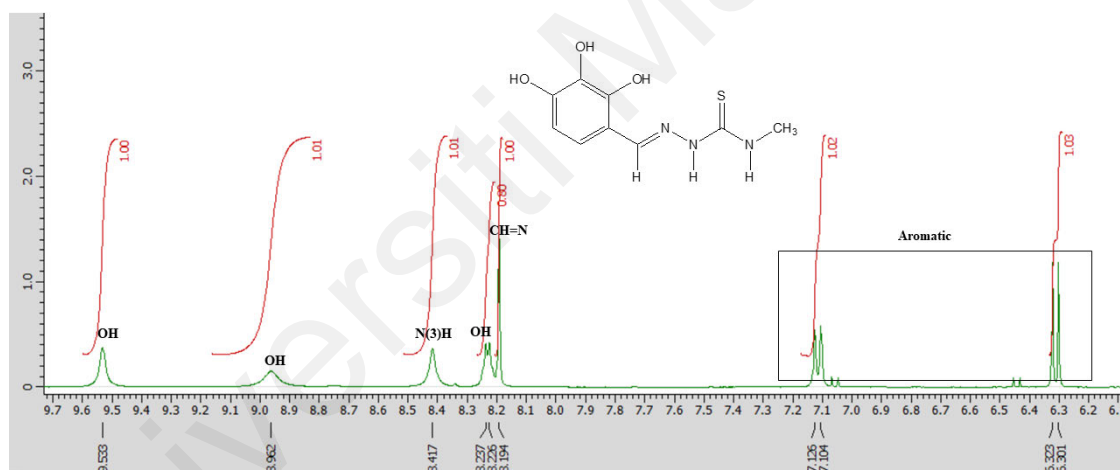


Figure 4.14, continued.

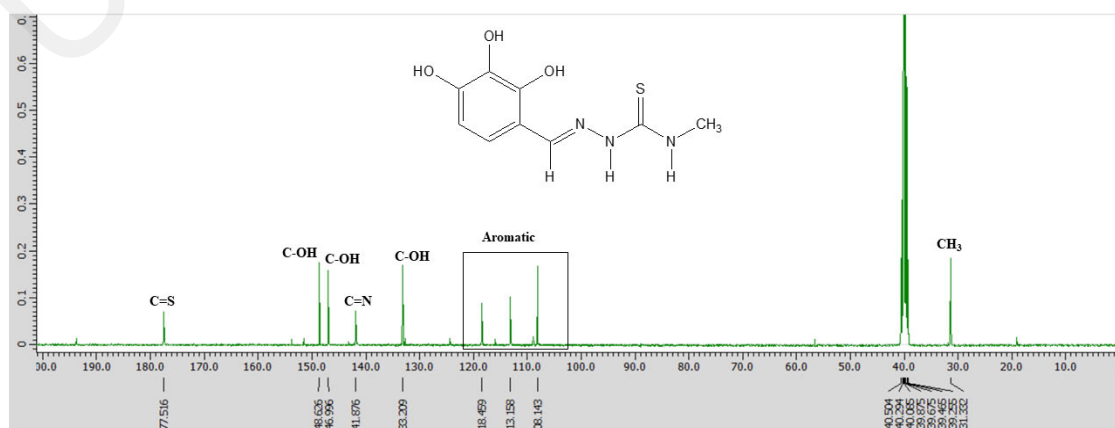


Figure 4.15 ^{13}C NMR spectra of ligand L4.

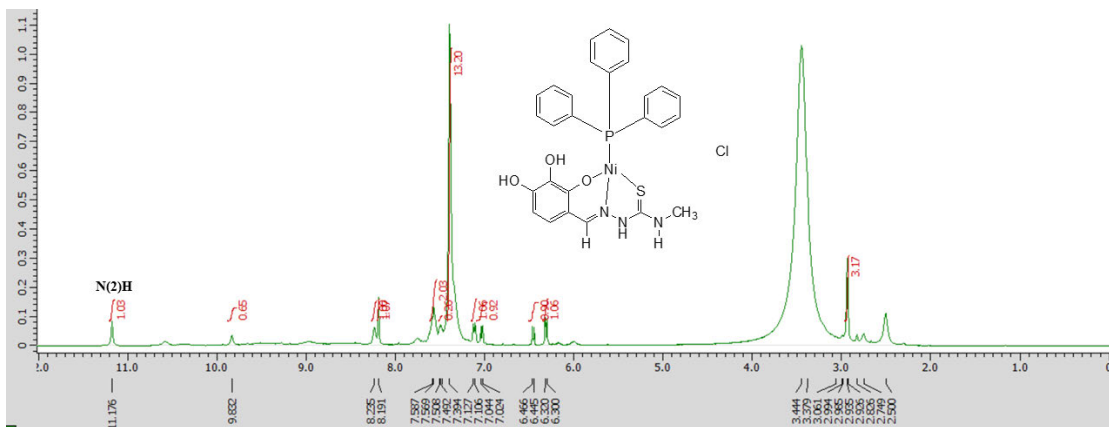


Figure 4.16 ^1H NMR spectra of complex 4.

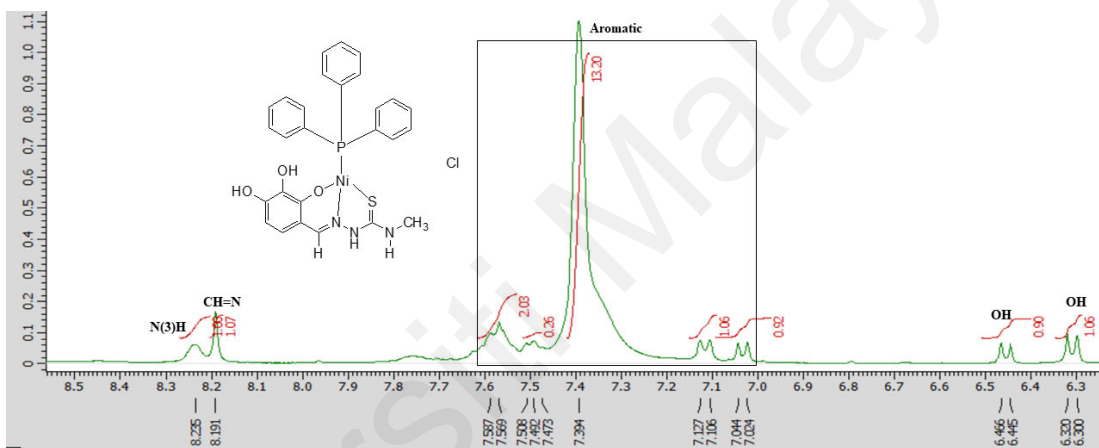


Figure 4.16, continued.

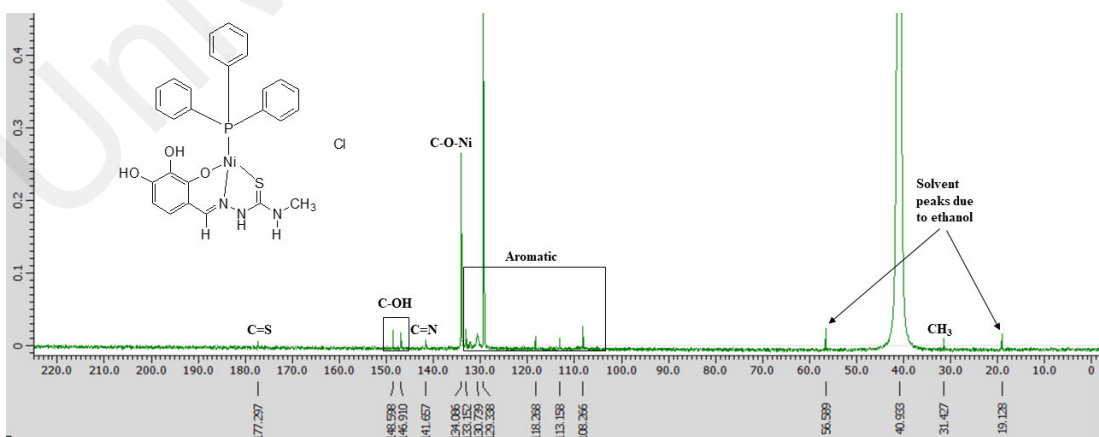


Figure 4.17 ^{13}C NMR spectra of complex 4.

Table 4.6 ¹H NMR spectra of ligands (L4-L7) and complexes (4-7).

Compd.	$\delta(\text{ppm})$					
	CH=N	N(2)H	N(3)H	OH	Aromatic	Aliphatic
L4	8.19 (s, 1H)	11.19 (s, 1H)	8.41 (s, 1H)	9.53 (s, 1H) 8.96 (s, 1H) 8.23 (d, 1H)	6.32-7.12	2.95 (d, CH ₃)
L5	8.19 (s, 1H)	11.20 (s, 1H)	8.26 (t, 1H)	9.55 (s, 1H) 8.99 (s, 1H) 8.43 (s, 1H)	6.32-7.11	3.53 (q, CH ₂) 1.08 (t, CH ₃)
L6	8.31 (s, 1H)	11.56 (s, 1H)	8.46 (s, 1H)	9.89 (s, 1H) 9.58 (s, 1H) 6.34 (d, 1H)	7.13-7.54	-
L7	8.33 (s, 1H)	11.51 (s, 1H)	9.65 (s, 1H)	9.84 (d, 1H) 6.49 (d, 1H) 6.37 (d, 1H)	7.10-7.44	2.59 (q, CH ₂) 1.17 (t, CH ₃)
4	8.19 (s, 1H)	11.17 (s, 1H)	8.23 (s, 1H)	6.46 (d, 1H) 6.32 (d, 1H)	7.04-7.58	2.93 (d, CH ₃)
5	8.18 (s, 1H)	11.10 (s, 1H)	8.27 (s, 1H)	6.33 (d, 1H) 6.05 (s, 1H)	7.11-7.42	1.27 (q, CH ₂) 1.06 (t, CH ₃)
6	8.45 (d, 1H)	-	9.25 (s, 1H)	9.25 (s, 1H) 6.21 (d, 1H)	6.85-7.76	-
7	8.40 (d, 1H)	-	9.14 (s, 1H)	9.21 (s, 1H) 6.17 (d, 1H)	6.82-7.74	2.45 (q, CH ₂) 1.08 (t, CH ₃)

Table 4.7 ¹³C NMR spectra of ligands (L4-L7) and complexes (4-7).

Compd.	$\delta(\text{ppm})$				
	C=N	C=S	C-O	Aromatic	Aliphatic
L4	141.87	177.51	133.20-148.62	108.43-118.45	31.33 (CH ₃)
L5	142.01	176.44	133.20-148.64	108.16-118.54	38.76 (CH ₂) 15.23 (CH ₃)
L6	147.19	175.54	148.90-153.76	108.19-142.80	-
L7	147.16	175.59	148.85-153.76	108.18-140.99	28.18 (CH ₂) 16.17 (CH ₃)
4	141.65	177.29	134.08-148.59	108.26-133.15	31.42 (CH ₃)
5	141.45	176.35	134.04-148.60	108.23-133.42	38.78 (CH ₂) 15.22 (CH ₃)
6	164.87 164.70	-	146.48-153.06	107.86-141.92	-
7	164.84 164.67	-	146.39-153.06	107.81-139.75	28.04 (CH ₂) 16.38 (CH ₃)

4.3.3 ^1H NMR and ^{13}C NMR spectra of 2,5-dihydroxybenzaldehyde-N4 thiosemicarbazone ligands (L8-L11) and their metal complexes (8-11)

Sections 4.3.3.1 and 4.3.3.2 describe in detail the ^1H NMR and ^{13}C NMR spectra of ligands (L8-L11) and their metal complexes (8-11), respectively.

4.3.3.1 ^1H NMR and ^{13}C NMR spectra of ligands (L8-L11)

Table 4.8 shows the proton resonance signals of all ligands and complexes whereas the carbon resonance signals are shown in **Table 4.9**. The **Figure 4.18** and **4.19** show the ^1H NMR and ^{13}C NMR spectra of ligand **L8**, respectively. Whilst the ^1H NMR and ^{13}C NMR spectra of complex **8** are shown in **Figure 4.20** and **4.21**, respectively. The azomethine imine group ($\text{CH}=\text{N}$) showed a singlet proton resonance signal at a range of 8.25-8.38 ppm for all ligands (Eğlence-Bakır et al., 2019; Singh et al., 2004). Whereas, the singlet proton resonance signals for (N(2)H) were observed at a range of 11.30-11.69 ppm, indicating that all ligands are in their thione form (Singh et al., 2008). Proton resonance signals at a range of 7.77-8.82 ppm belonging to N(3)H were also observed (Kalaivani et al., 2012). Besides, the singlet proton resonance signal due to the phenolic oxygen were found to be at a range of 8.80-9.97 ppm (Shawish et al., 2016). As for the aromatic group, their resonance signals were seen to be at a range of 6.64-7.54 ppm. The aliphatic resonance signals belonging to the CH_2 and CH_3 groups were observed to be at 3.56 ppm and 1.13-2.95 ppm, respectively (Salam et al., 2018).

All ligands showed carbon resonance signals for azomethine imine nitrogen ($\text{C}=\text{N}$) at 140.01-140.98 ppm. Whereas, the carbon resonance signals for thioamide ($\text{C}=\text{S}$) were found to be at 176.14-178.04 ppm, signifying the presence of all ligands in their thione form (Alekseyev et al., 2010). In addition, the carbon resonance signal due to the phenolic OH group were observed at 149.93-150.46 ppm (Abdul Halim et al., 2019). Whilst,

aromatic carbon resonance signals were recorded at a range of 112.29-139.66 ppm. As for the aliphatic carbons, resonance signals due to CH₂ and CH₃ were observed at 31.35 ppm and 15.18-38.78 ppm, respectively (Fang et al., 2018).

4.3.3.2 ¹H NMR and ¹³C NMR spectra of metal complexes (8-11)

In general, the azomethine imine (CH=N) resonance signal in complexes were found to have shifted slightly downfield and resonate at a range of 8.10-8.49 ppm, suggesting the involvement of the azomethine imine nitrogen in metal complexation. Evidently, coordination with phosphorus atom of triphenylphosphine has cause the azomethine imine resonance signals of complexes **8**, **9** and **11** to appear as a doublet (Prabhakaran et al., 2013). Interestingly, complex **10** shows a singlet resonance signal at 11.20 ppm belonging to the thioamide proton (N(2)H), indicating that ligand **L10** has been coordinated to the metal centre in its actual thione form. However, the disappearance of resonance signal around this range in complexes **8**, **9** and **11** strongly stipulate that ligands **L8**, **L9** and **L11** were coordinated to the metal centre in the anionic form after deprotonation at N(2) (Kalaivani et al., 2012). The singlet hydrazinic proton (N(3)H) recorded slight deviation from their ligands and were found to resonate at 8.31-8.68 ppm. Furthermore, the resonance signals due to OH group were observed at 6.14-9.31 ppm, suggesting the non-participation of phenolic oxygen from coordination and confirming the involvement of a single OH group in metal complexation (Đilović et al., 2008; Muthukumar & Viswanathamurthi, 2010). Complex multiplets were observed at 6.04-7.67 ppm due to aromatic protons of ligands and triphenylphosphine. Resonance signals of aliphatic protons in all complexes were found to resonate at a similar resonance as their ligands because aliphatic protons were not affected by metal complexation.

The disappearance of carbon resonance signal belonging to the thioamide (C=S) group in complexes **8**, **9** and **11** indicates that ligands **L8**, **L9** and **L11** were coordinated to the metal centre in their tautomerized thiol form. As a result, emergence of new resonance signals at 166.02-171.42 ppm was observed due to azomethine imine nitrogen (C=N) (Chellan et al., 2010). In this case, the (C=N) resonance signals were seen to have shifted downfield, suggesting once again the complexation of metal through the azomethine imine nitrogen atom and thiolate sulfur. However, the thioamide (C=S) resonance signal for complex **10** was found to resonate at 176.72 ppm, confirming that ligand **L10** was coordinated to the metal in its usual thione form. Hence, the azomethine imine (C=N) resonance signal for complex **10** was observed at 139.92 ppm, a similar range as its ligand. On the other hand, new resonance signals at 150.33-155.42 ppm belonging to (C-O) were observed. The carbon resonance signals caused by phenolic OH were spotted at 149.79-153.07 ppm, signifying the participation of only one OH group in metal complexation. Since the aromatic and aliphatic carbons of the complexes were not involved directly in metal complexation, hence they were found to resonate at similar frequencies as their ligands.

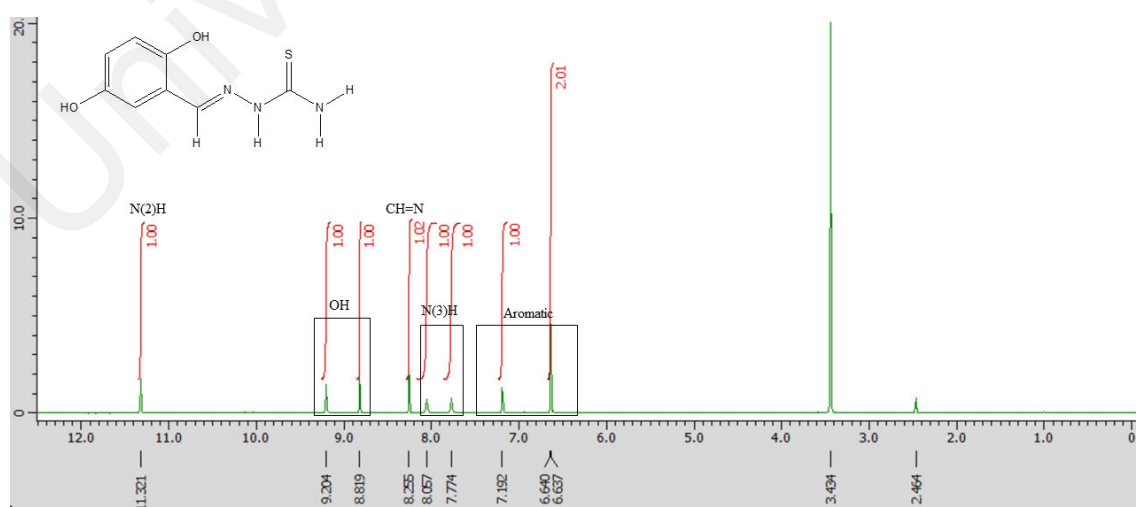


Figure 4.18 ¹H NMR spectra of ligand L8.

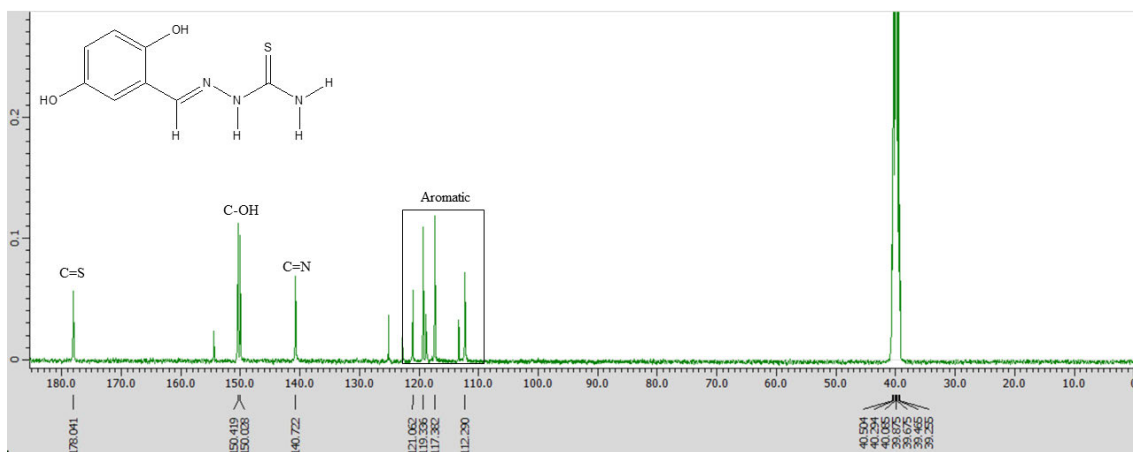


Figure 4.19 ^{13}C NMR spectra of ligand L8.

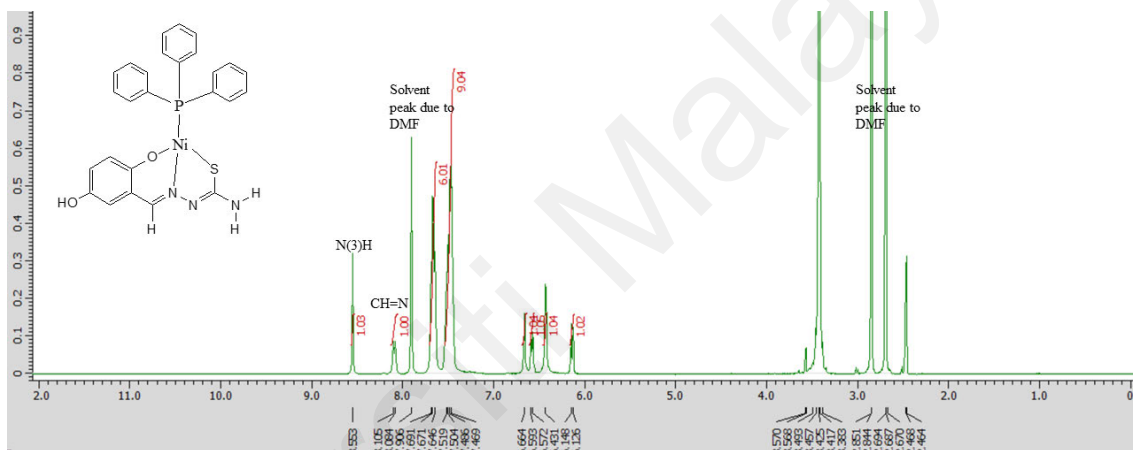


Figure 4.20 ^1H NMR spectra of complex 8.

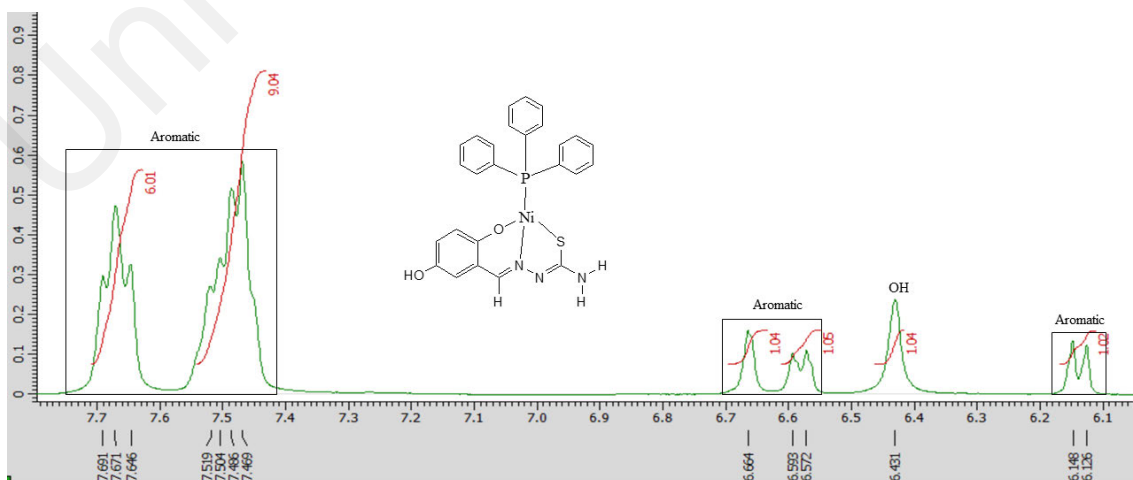


Figure 4.20, continued.

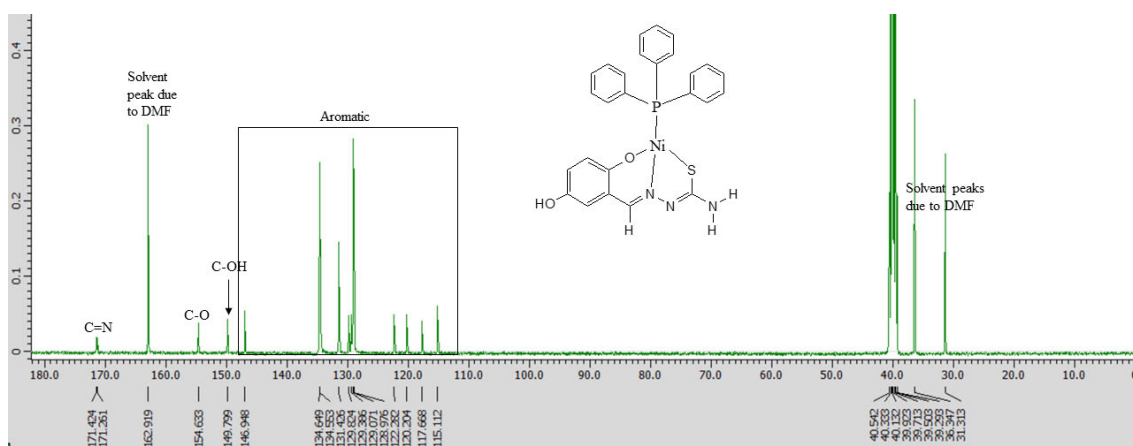


Figure 4.21 ^{13}C NMR spectra of complex 8.

Universiti Malaysia

Table 4.8 ¹H NMR spectra of ligands (L8-L11) and complexes (8-11).

Compd.	$\delta(\text{ppm})$					
	C=NH	N(2)H	N(3)H	OH	Aromatic	Aliphatic
L8	8.25 (s, 1H)	11.32 (s, 1H)	8.05 (s, 1H) 7.77 (s, 1H)	9.20 (s, 1H) 8.81 (s, 1H)	6.64-7.19	-
L9	8.25 (s, 1H)	11.33 (s, 1H)	8.34 (q, 1H)	9.19 (s, 1H) 8.80 (s, 1H)	6.64-7.24	2.95 (d, CH ₃)
L10	8.29 (s, 1H)	11.30 (s, 1H)	8.39 (q, 1H)	9.22 (s, 1H) 8.84 (s, 1H)	6.67-7.27	3.56 (q, CH ₂) 1.13 (t, CH ₃)
L11	8.38 (s, 1H)	11.69 (s, 1H)	8.82 (d, 1H)	9.97 (s, 1H) 9.29 (s, 1H)	6.67-7.54	-
8	8.10 (d, 1H)	-	8.55 (s, 1H)	6.43 (s, 1H)	6.14-7.67	-
9	8.22 (d, 1H)	-	8.53 (s, 1H)	6.14 (d, 1H)	6.59-7.64	2.65 (d, CH ₃)
10	8.17 (s, 1H)	11.20 (s, 1H)	8.31 (s, 1H)	9.22 (s, 1H)	6.04-7.52	1.00 (t, CH ₂) 0.93 (t, CH ₃)
11	8.49 (d, 1H)	-	8.68 (s, 1H)	9.31 (s, 1H)	6.22-7.67	-

Table 4.9 ¹³C NMR spectra of ligands (L8-L11) and complexes (8-11).

Compd.	$\delta(\text{ppm})$				
	C=N	C=S	C-O	Aromatic	Aliphatic
L8	140.72	178.04	150.02-150.41	112.290-121.06	-
L9	140.01	177.95	149.93-150.43	112.36-121.31	31.351 (CH ₃)
L10	140.05	176.91	149.96-150.42	112.31-121.28	38.78 (CH ₂) 15.18 (CH ₃)
L11	140.98	176.14	150.23-150.46	112.60-139.66	-
8	171.42 171.26	-	149.79-154.63	115.11-146.94	-
9	170.51 170.35	-	150.54-154.60	115.22-146.96	32.27 (CH ₃)
10	139.92	176.72	149.92-150.33	112.12-134.28	38.63 (CH ₂) 15.15 (CH ₃)
11	166.19 166.07	-	153.07-155.42	115.22-147.12	-

4.4 Crystal structures

4.4.1 Crystal structures of fluorene-2-carboxaldehyde-N4 thiosemicarbazone ligands (L1-L3) and their metal complexes (1-3)

The crystal data and structure refinement parameters of ligands **L1** and **L3** are shown in **Table 4.10** and **4.12**, respectively. **Table 4.14**, **4.16** and **4.18** show the crystal data and structure refinement parameters of complexes **1**, **2** and **3**, respectively. Whereas, the selected bond lengths and bond angles of ligands **L1** and **L3** and are shown in **Table 4.11** and **4.13**, respectively. As for complexes **1**, **2** and **3**, their selected bond lengths and bond angles are shown in **Table 4.15**, **4.17** and **4.19**, respectively. Meanwhile, the crystal structures of ligands **L1** and **L3** are shown in **Figure 4.22** and **4.24**. Whereas, the crystal structures of complexes **1**, **2** and **3** are shown in **Figure 4.26**, **4.28** and **4.30**, respectively. The unit cell packing of ligand **L1** and **L3** are shown in **Figure 4.23** and **4.25**, respectively. Whilst, the unit cell packing of complexes **1**, **2** and **3** are shown in **Figure 4.27**, **4.29** and **4.31**, respectively.

4.4.1.1 Crystal structures of ligands L1 and L3

Ligands **L1** and **L3** were found to have crystallised into a monoclinic lattice with two different space groups which are $I2/a$ and $P2_1$, respectively. The C15-S1 bond lengths were seen at 1.6953 (19) and 1.685 (13) Å for ligands **L1** and **L3**, respectively. Whereas, the C15-N2 bond lengths for ligands **L1** and **L3** were found to be at 1.348 (2) and 1.369 (17) Å, respectively. The bond lengths are similar as those observed in other thiosemicarbazone indicating that the ligands are in the thioamide form (Teoh et al., 1999; Tran Buu et al., 2019). As for ligand **L1**, vivid hydrogen bonding interactions O-H--S and N-H--O are observed. The water molecules were seen to bridge the adjacent ligands. On the other hand, hydrogen bonding interaction N-H--S is observed in ligand **L3**.

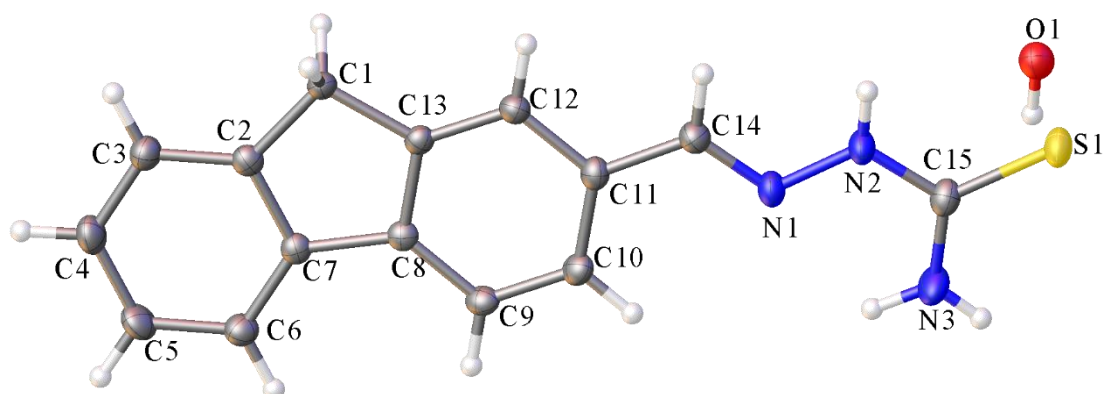


Figure 4.22 Ellipsoid plot of ligand L1 drawn at 50 % probability level.

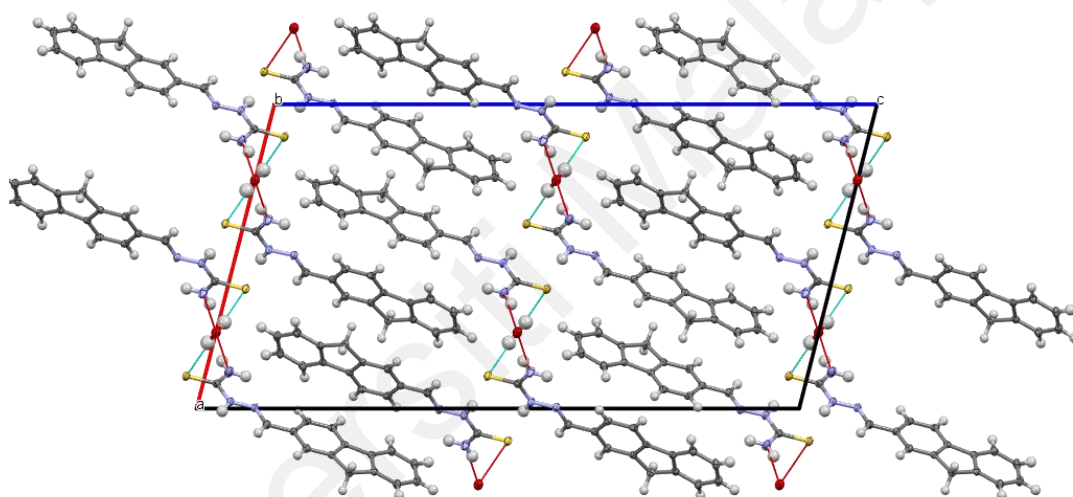


Figure 4.23 Unit cell packing diagram of ligand L1 viewed along axis b. Water molecules bridge the adjacent ligands forming O-H--S and N-H--O hydrogen bonding interactions.

Table 4.10 Crystallographic data summary for ligand L1.

Compound	L1
Empirical formula	C ₁₅ H ₁₃ N ₃ S.H ₂ O
Formula weight	184.23
Crystal system	Monoclinic
Space group	I2/a
Unit cell dimensions	
a (Å)	16.2682(17)
b (Å)	5.4578(6)
c (Å)	31.269(4)
β (°)	104.387(13)
V (Å³)	2689.3(6)
Z	12
F(000)	1160
D_{calc} (mg m⁻³)	1.365
Absorption coefficient, μ (mm⁻¹)	0.23
T (K)	100
Crystal size (mm)	0.34 × 0.16 × 0.13
Reflections collected	13093
Independent reflections (R_{int})	3719 (0.043)
Data/restraints/parameters	3719/0/193
R[F² > 2σ(F²)]	0.049
wR(F²)	0.131
S	1.04
Largest difference peak and hole (e Å⁻³)	0.46 and -0.32

Table 4.11 Selected bond lengths (Å) and bond angles (°) for ligand L1.

Bond lengths		Bond angles	
N1—N2	1.374 (2)	C14—N1—N2	116.55 (16)
N1—C14	1.276 (2)	C15—N2—N1	119.05 (16)
C5—C6	1.389 (3)	N2—C15—S1	120.37 (15)
C5—C4	1.392 (3)	N3—C15—N2	116.56 (17)
N2—C15	1.348 (2)	N3—C15—S1	123.05 (14)
N3—C15	1.325 (3)	N1—C14—C11	121.27 (16)
C15—S1	1.6953 (19)		

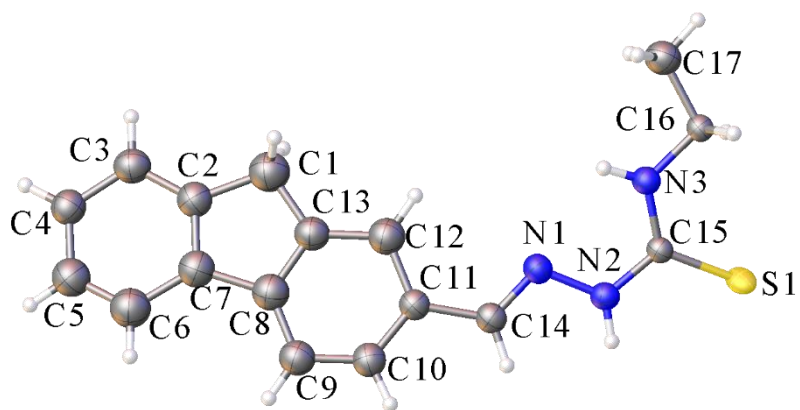


Figure 4.24 Ellipsoid plot of ligand L3 drawn at 50 % probability level.

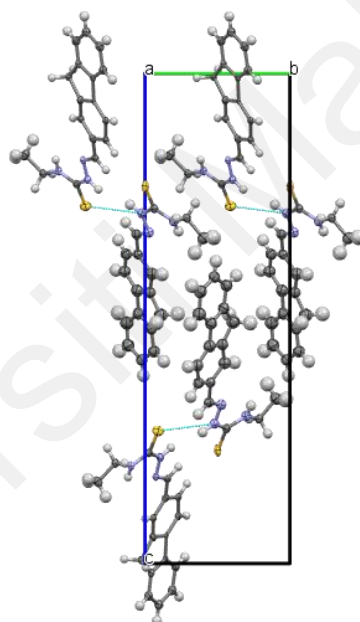


Figure 4.25 Unit cell packing diagram of ligand L3 viewed along axis a. Vivid N-H...S hydrogen bonding interaction is observed.

Table 4.12 Crystallographic data summary for ligand L3.

Compound	L3
Empirical formula	C ₁₇ H ₁₇ N ₃ S
Formula weight	295.39
Crystal system	Monoclinic
Space group	<i>P</i> 2 ₁
Unit cell dimensions	
a (Å)	6.3670(12)
b (Å)	8.3970(11)
c (Å)	28.484(5)
β (°)	96.095(19)
V (Å ³)	1514.3(4)
Z	4
F(000)	624
D _{calc} (mg m ⁻³)	1.296
Absorption coefficient, μ (mm ⁻¹)	0.21
T (K)	100
Crystal size (mm)	0.34 × 0.16 × 0.13
Reflections collected	11815
Independent reflections (R _{int})	6517 (0.068)
Data/restraints/parameters	6517/241/80
R[F ² > 2σ(F ²)]	0.131
wR(F ²)	0.355
S	1.01
Largest difference peak and hole (e Å ⁻³)	1.23 and -0.84

Table 4.13 Selected bond lengths (Å) and bond angles (°) for ligand L3.

Bond lengths		Bond angles	
S1—C15	1.685 (13)	C14—N1—N2	111.4 (12)
S2—C32	1.697 (12)	C15—N2—N1	117.7 (12)
N1—C14	1.295 (19)	C15—N3—C16	121.5 (11)
N1—N2	1.393 (16)	C31—N4—N5	115.7 (10)
N2—C15	1.369 (17)	C32—N5—N4	122.2 (11)
N3—C15	1.383 (18)	C32—N6—C33	126.2 (10)
N3—C16	1.435 (17)	C31—N4—N5	115.7 (10)
N4—C31	1.292 (15)	C32—N5—N4	122.2 (11)
N4—N5	1.376 (13)	C32—N6—C33	126.2 (10)
N5—C32	1.319 (15)	N2—C15—S1	118.9 (11)
N6—C32	1.309 (16)	N3—C15—S1	123.0 (10)
N6—C33	1.487 (15)	N6—C32—S2	123.3 (9)
		N5—C32—S2	119.9 (10)
		N3—C16—C17	106.0 (12)
		N1—C14—C11	123.8 (14)
		N2—C15—N3	118.0 (11)
		N4—C31—C28	123.4 (11)
		N6—C32—N5	116.8 (11)

4.4.1.2 Crystal structures of complexes (1-3)

Complexes (**1-3**) were found to have crystallised into monoclinic and triclinic lattices with $P2_1/c$, and $P1$ space groups, respectively. The C15-S1 bond lengths were seen at 1.737 (6), 1.734 (5) and 1.743 (3) Å for complexes **1**, **2** and **3**, respectively. Whereas the C15-N2 bond lengths for complexes **1**, **2** and **3** were seen at 1.323 (9), 1.299 (7) and 1.297 (3) Å, respectively. This indicates that the C15-S1 bond is a single bond since it is considerably longer than the usual C=S bond and the C15-N2 bond which is shorter than the usual C-N is a double bond (Anjum et al., 2019). Coordination results in an increase of the single-bond character for C-S bond (Mathew & Palenik, 1969). Hence, ligands (**1-3**) are coordinated to the metal in the thiolate form through their bidentate N,S atoms. In addition, complexes (**4-6**) display a square planar geometry. This is because the bite angle around the metal, S1-Ni1-N1 are approximately at 90° although there is slight deviation. The deviation may be due to the restricted bite angle caused by the ligand (Elmagbari et al., 2019). Also, the N1ⁱ-Ni1-N1 and S1-Ni1-S1ⁱ bonds interact at 180° signifying that the complexes are in a square planar geometry. Complexes were seen to adopt the trans conformation unlike the ligands which adopt the cis conformation.

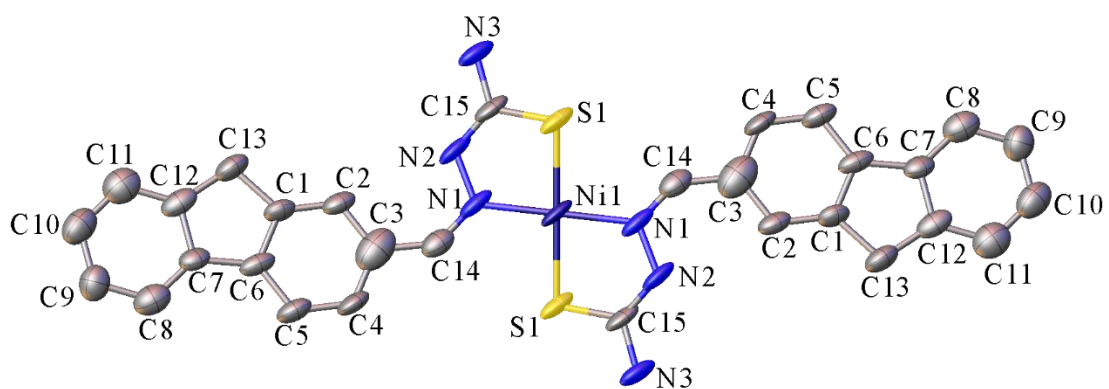


Figure 4.26 Ellipsoid plot of complex 1 drawn at 50 % probability level.

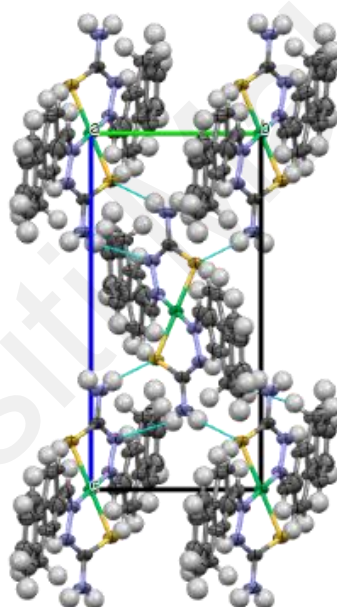


Figure 4.27 Unit cell packing diagram of complex 1 viewed along axis a. N-H...S hydrogen bonding interaction is observed.

Table 4.14 Crystallographic data summary for complex 1.

Compound	1
Empirical formula	C ₃₀ H ₂₄ N ₆ NiS ₂
Formula weight	603.39
Crystal system	Monoclinic
Space group	P2 ₁ /c
Unit cell dimensions	
a (Å)	12.1280(19)
b (Å)	7.1116 (5)
c (Å)	15.7781(12)
β (°)	109.669(12)
V (Å ³)	1281.5 (3)
Z	2
F(000)	624
D _{calc} (mg m ⁻³)	1.564
Absorption coefficient, μ (mm ⁻¹)	2.89
T (K)	100
Crystal size (mm)	0.10×0.10×0.05
Reflections collected	4972
Independent reflections (R _{int})	2520 (0.085)
Data/restraints/parameters	2520/9/169
R[F ² > 2σ(F ²)]	0.094
wR(F ²)	0.278
S	1.01
Largest difference peak and hole (e Å ⁻³)	0.70 and -1.07

Table 4.15 Selected bond lengths (Å) and bond angles (°) for complex 1.

Bond lengths		Bond angles	
Ni1—N1 ⁱ	1.923 (5)	N1 ⁱ —Ni1—N1	180.0 (2)
Ni1—N1	1.923 (5)	N1 ⁱ —Ni1—S1	94.35 (15)
Ni1—S1	2.1891 (13)	N1—Ni1—S1	85.65 (15)
Ni1—S1 ⁱ	2.1891 (13)	N1 ⁱ —Ni1—S1 ⁱ	85.65 (15)
S1—C15	1.737 (6)	N1—Ni1—S1 ⁱ	94.35 (15)
N1—C14	1.283 (10)	S1—Ni1—S1 ⁱ	180.00 (6)
N1—N2	1.395 (6)	C15—S1—Ni1	93.95 (19)
N2—C15	1.323 (9)	C14—N1—N2	116.4 (5)
N3—C15	1.351 (7)	C14—N1—Ni1	124.6 (4)
		N2—N1—Ni1	118.7 (5)
		C15—N2—N1	111.3 (5)
		N2—C15—N3	118.0 (5)
		N2—C15—S1	123.8 (4)
		N3—C15—S1	118.2 (5)

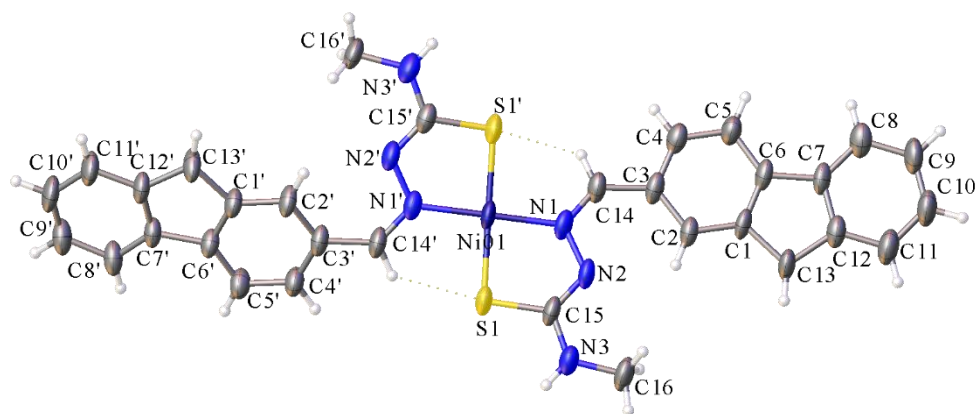


Figure 4.28 Ellipsoid plot of complex 2 drawn at 50 % probability level.

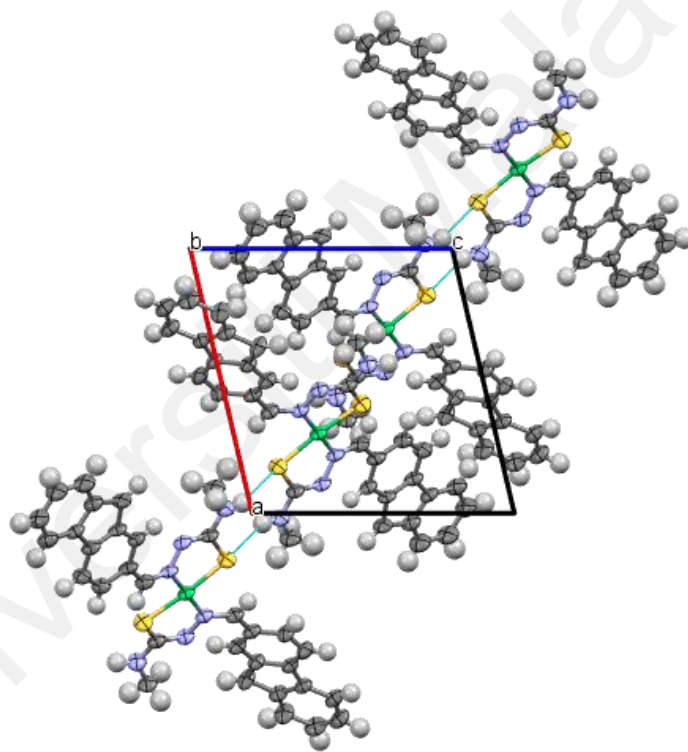


Figure 4.29 Unit cell packing diagram of complex 2 viewed along axis b.

Table 4.16 Crystallographic data summary for complex 2.

Compound	2
Empirical formula	C ₃₂ H ₂₆ N ₆ NiS ₂
Formula weight	617.42
Crystal system	Triclinic
Space group	<i>P</i> 1
Unit cell dimensions	
<i>a</i> (Å)	11.3871(15)
<i>b</i> (Å)	12.0595(16)
<i>c</i> (Å)	12.0850(16)
α (°)	63.353(13)
β (°)	73.689(11)
γ (°)	79.778(11)
<i>V</i> (Å ³)	1421.0(4)
<i>Z</i>	2
<i>F</i> (000)	640
<i>D</i> _{calc} (mg m ⁻³)	1.443
Absorption coefficient, μ (mm ⁻¹)	2.62
<i>T</i> (K)	293
Crystal size (mm)	0.34×0.16×0.13
Reflections collected	8336
Independent reflections (<i>R</i> _{int})	5433 (0.091)
Data/restraints/parameters	5433/0/373
<i>R</i> [<i>F</i> ² > 2 σ (<i>F</i> ²)]	0.111
<i>wR</i> (<i>F</i> ²)	0.320
<i>S</i>	1.08
Largest difference peak and hole (e Å ⁻³)	1.57 and -1.33

Table 4.17 Selected bond lengths (Å) and bond angles (°) for complex 2.

Bond lengths		Bond angles	
Ni1—S1	2.1660 (17)	S1—Ni1—S1'	173.18 (7)
Ni1—S1'	2.1741 (18)	N1—Ni1—S1	85.79 (14)
Ni1—N1	1.927 (4)	N1—Ni1—S1'	94.17 (14)
Ni1—N2'	1.923 (4)	N1'—Ni1—S1	94.16 (14)
S1—C15	1.734 (5)	N1'—Ni1—S1'	86.15 (14)
S1'—C15'	1.728 (5)	N1'—Ni1—N1	177.79 (16)
N1—N2	1.386 (6)	C15—S1—Ni1	95.98 (19)
N1—C14	1.305 (7)	C15'—S1'—Ni1	95.9 (2)
N1'—N2'	1.392 (6)	N2—N1—Ni1	120.8 (3)
N1'—C14'	1.308 (7)	C14—N1—Ni1	124.3 (4)
N2—C15	1.299 (7)	C14—N1—N2	114.9 (4)
N2'—C15'	1.305 (7)	N2'—N1'—Ni1	121.0 (3)
N3—C15	1.336 (7)	C14'—N1'—Ni1	125.0 (4)
N3—C16	1.438 (6)	C14'—N1'—N2'	113.9 (4)
N3'—C15'	1.345 (7)	C15—N2—N1	112.5 (4)
N3'—C16'	1.447 (6)	C15'—N2'—N1'	112.1 (4)
		C15—N3—C16	123.0 (5)
		C15'—N3'—C16'	122.9 (5)
		N2—C15—S1	123.5 (4)
		N2—C15—N3	117.8 (4)
		N3—C15—S1	118.6 (4)
		N2'—C15'—S1'	124.2 (4)
		N2'—C15'—N3'	117.3 (5)
		N3'—C15'—S1'	118.5 (4)

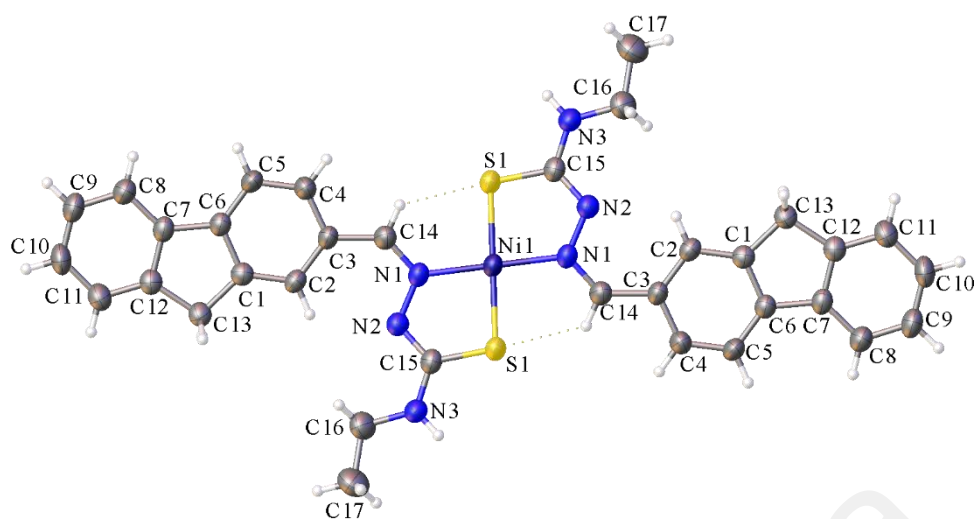


Figure 4.30 Ellipsoid plot of complex 3 drawn at 50 % probability level.

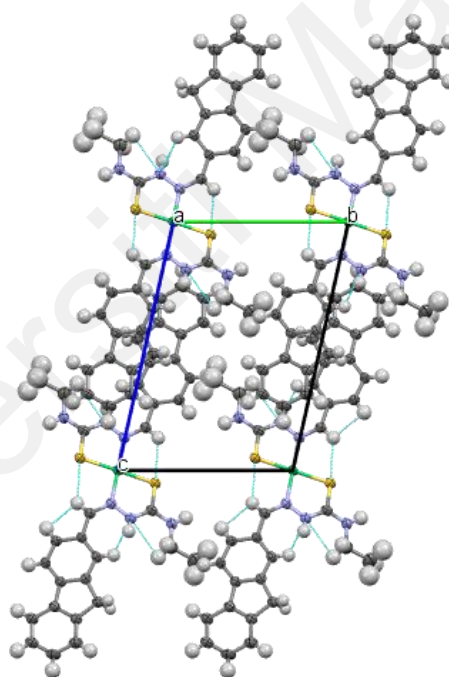


Figure 4.31 Unit cell packing diagram of complex 3 viewed along axis a.

Table 4.18 Crystallographic data summary for complex 3.

Compound	3
Empirical formula	C ₃₄ H ₃₄ N ₆ NiS ₂
Formula weight	649.50
Crystal system	Triclinic
Space group	<i>P</i> 1
Unit cell dimensions	
a (Å)	7.5011(6)
b (Å)	10.2395(10)
c (Å)	13.9044(10)
α (°)	100.746(7)
β (°)	92.780(7)
γ (°)	110.994(8)
V (Å ³)	971.81(16)
Z	1
F(000)	340
D _{calc} (mg m ⁻³)	1.110
Absorption coefficient, μ (mm ⁻¹)	1.94
T (K)	293
Crystal size (mm)	0.34 × 0.16 × 0.13
Reflections collected	3607
Independent reflections (R _{int})	3607 (0.091)
Data/restraints/parameters	3607/0/206
R[F ² > 2σ(F ²)]	0.050
wR(F ²)	0.151
S	0.94
Largest difference peak and hole (e Å ⁻³)	0.44 and -0.35

Table 4.19 Selected bond lengths (Å) and bond angles (°) for complex 3.

Bond lengths		Bond angles	
Ni1—S1 ⁱ	2.1789 (7)	S1 ⁱ —Ni1—S1	180.0
Ni1—S1	2.1789 (7)	N1 ⁱ —Ni1—S1	94.84 (7)
Ni1—N1 ⁱ	1.923 (2)	N1 ⁱ —Ni1—S1 ⁱ	85.15 (7)
Ni1—N1	1.923 (2)	N1—Ni1—S1 ⁱ	94.85 (7)
S1—C15	1.743 (3)	N1—Ni1—S1	85.16 (7)
N2—H2	0.8600	N1 ⁱ —Ni1—N1	180.0
N2—N1	1.394 (3)	C15—S1—Ni1	95.88 (9)
N2—C15	1.297 (3)	C15—N2—N1	112.9 (2)
N1—C14	1.293 (3)	N2—N1—Ni1	119.59 (16)
N3—H4	0.8600	C14—N1—Ni1	124.63 (19)
N3—C15	1.329 (4)	C14—N1—N2	115.8 (2)
N3—C16	1.454 (4)	N2—C15—N3	119.6 (2)
		N3—C15—S1	118.0 (2)

4.4.2 Crystal structures of Nickel complexes of 2,3,4 trihydroxybenzaldehyde thiosemicarbazone derivatives and triphenylphosphine

The crystal data and structure refinement parameters of complexes **4**, **5** and **6** are shown in **Table 4.20**, **4.22** and **4.24**, respectively. Whereas, the selected bond lengths and bond angles of complexes **4**, **5** and **6** and are shown in **Table 4.21**, **4.23** and **4.25**, respectively. Meanwhile, the crystal structures of complexes **4**, **5** and **6** are shown in **Figure 4.32**, **4.34** and **4.36**, respectively. Whilst, the unit cell packing of complexes **4**, **5** and **6** are shown in **Figure 4.33**, **4.35** and **4.37**, respectively.

4.4.2.1 Crystal structures of complexes (4-6)

It is revealed by single crystal X-ray analysis that complexes **4** and **5** crystallised in triclinic crystal system with P1 space group. Whilst, complex **6** was found to have crystallised into a monoclinic lattice with P2₁ space group. All three complexes were four coordinated and displays a square planar geometry. All ligands were found to have coordinated to the metal centre *via* their O,N,S tridentate binding site. The S1-C8 bond lengths for complexes **4**, **5** and **6** were seen at 1.721 (3) Å, 1.714 (3) Å and 1.728 (12) Å, respectively. The bond lengths are similar as those observed in other thiosemicarbazone metal complexes. It is noteworthy that the S1-C8 bond lengths for complexes **4** and **5** were shorter than complex **6**, indicating that the mentioned bond is a double bond in complexes **4** and **5** but a single bond in complex **6** (Bingham et al., 1987). The fact that coordination gives rise to an increase of the single bond character for C-S bond is true in the case of complex **6** (Mathew et al., 1969). Besides, the effect of thione to thiol tautomerization is clearly observed in complex **6**. In addition, the N2-C8 bond lengths were seen at 1.324 (4) Å, 1.328 (4) Å and 1.299 (14) Å for complexes **4**, **5** and **6**, respectively. It is interesting to note that the N2-C8 bond lengths for complexes **4** and **5**

were longer than complex **6**, suggesting that the mentioned bond is a single bond in complexes **4** and **5** but a double bond in complex **6** (Khalaji et al., 2013). Similar bond lengths were observed in thiosemicarbazones reported by previous research, stipulating that ligands **L4** and **L5** were coordinated to the metal in the original thione form but ligand **L6** was coordinated to the metal in its thiolate form. The bite angle for O1-Ni1-N1, N1-Ni-S1, S1-Ni-P1 and O1-Ni-P1 which slightly deviate from the ideal 90 ° reflect that the complexes adopt a distorted square planar geometry. Deviations due to restricted bite angle caused by ligands is common (Elmagbari et al., 2019; Seena et al., 2007). Besides, the O1-Ni-S1 and N1-Ni-P1 bonds were found to intersect at an approximate angle of 180 ° signifying that all complexes are in a distorted square planar geometry. Complex **4** displays detailed intermolecular and intramolecular O-H---Cl, O-H---O and N-H---Cl hydrogen bonding interactions. Also, water molecules were found to bridge adjacent ligands.

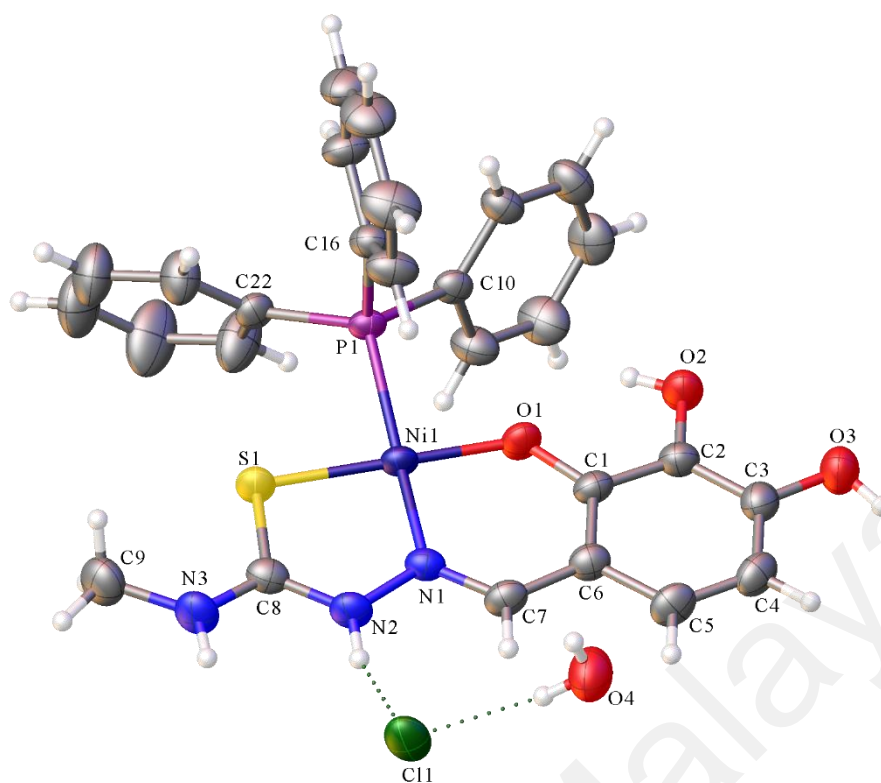


Figure 4.32 Ellipsoid plot of complex 4 drawn at 50 % probability level.

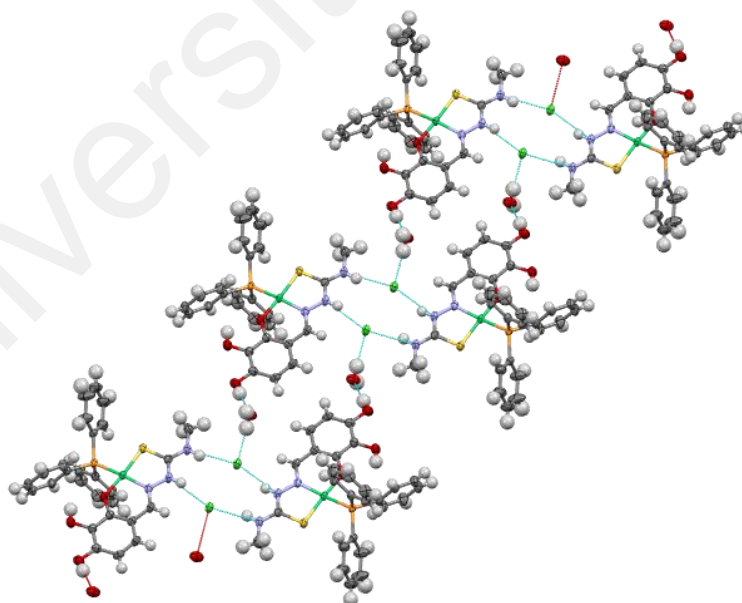


Figure 4.33 Unit cell packing diagram of complex 4 viewed along axis c. Intermolecular and intramolecular O-H...Cl, O-H...O and N-H...Cl hydrogen bonding interactions are displayed. Also, water molecules were found to bridge adjacent ligands.

Table 4.20 Crystallographic data summary for complex 4.

Compound	4
Empirical formula	C ₂₇ H ₂₅ N ₃ NiO ₃ PS.Cl.H ₂ O
Formula weight	614.70
Crystal system	Triclinic
Space group	<i>P</i> 1
Unit cell dimensions	
a (Å)	9.5562 (4)
b (Å)	12.7600 (5)
c (Å)	13.0135 (7)
α (°)	116.839(5)
β (°)	97.172 (4)
γ (°)	94.617(3)
V (Å ³)	1387.92 (12)
Z	2
F(000)	636
D _{calc} (mg m ⁻³)	1.471
Absorption coefficient, μ (mm ⁻¹)	3.46
T (K)	293
Crystal size (mm)	0.10 × 0.10 × 0.05
Reflections collected	8175
Independent reflections (R _{int})	5313 (0.033)
Data/restraints/parameters	5313/0/349
R[F ² > 2σ(F ²)]	0.054
wR(F ²)	0.151
S	1.01
Largest difference peak and hole (e Å ⁻³)	0.97 and -1.08

Table 4.21 Selected bond lengths (Å) and bond angles (°) for complex 4.

Bond lengths (Å)		Bond angles (°)	
Ni1—P1	2.206 (7)	S1—Ni1—P1	90.27 (3)
Ni1—S1	2.148 (7)	O1—Ni1—P1	88.06 (6)
Ni1—O1	1.849 (19)	O1—Ni1—S1	175.68 (8)
Ni1—N1	1.881 (2)	O1—Ni1—N1	94.09 (9)
S1—C8	1.721 (3)	N1—Ni1—P1	168.04 (7)
N1—N2	1.394 (3)	N1—Ni1—S1	88.35 (7)
N1—C7	1.310 (3)	C16—P1—Ni1	107.92 (9)
N2—C8	1.324 (4)	C22—P1—C10	107.68 (12)
N3—C8	1.323 (3)	C10—P1—Ni1	112.51 (8)
N3—C9	1.446 (4)	C22—P1—Ni1	116.75 (8)

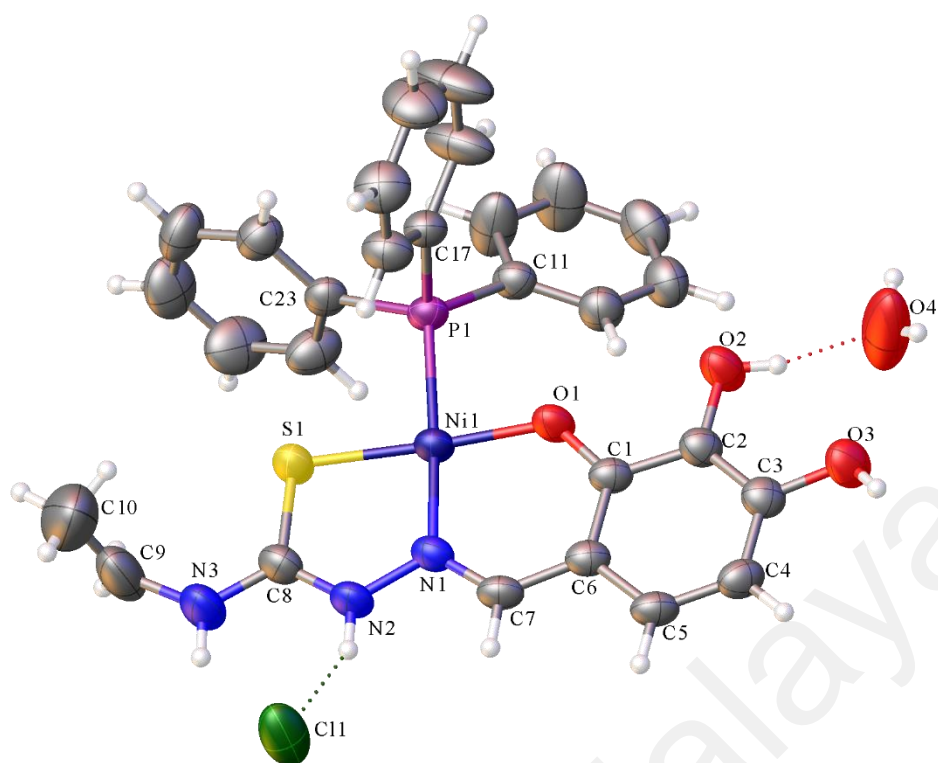


Figure 4.34 Ellipsoid plot of complex 5 drawn at 50 % probability level.

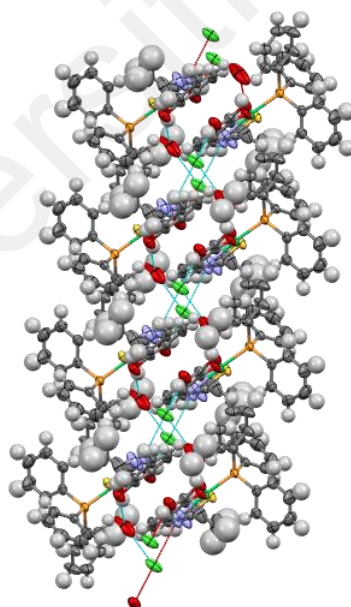


Figure 4.35 Unit cell packing diagram of complex 5 viewed along axis b. N-H...Cl and O-H...Cl hydrogen bonding interactions are observed. Water molecules were found to bridge adjacent ligands.

Table 4.22 Crystallographic data summary for complex 5.

Compound	5
Empirical formula	C ₂₈ H ₂₆ N ₃ NiO ₃ PS.Cl.H ₂ O
Formula weight	627.69
Crystal system	Triclinic
Space group	<i>P</i> 1
Unit cell dimensions	
a (Å)	7.9432 (5)
b (Å)	14.000 (1)
c (Å)	14.2845 (9)
α (°)	107.900(6)
β (°)	91.597 (5)
γ (°)	105.191(6)
V (Å ³)	1448.59 (18)
Z	2
F(000)	615
D _{calc} (mg m ⁻³)	1.360
Absorption coefficient, μ (mm ⁻¹)	2.86
T (K)	293
Crystal size (mm)	0.10 × 0.10 × 0.05
Reflections collected	8468
Independent reflections (R _{int})	5533 (0.029)
Data/restraints/parameters	5533/0/358
R[F ² > 2σ(F ²)]	0.053
wR(F ²)	0.159
S	1.03
Largest difference peak and hole (e Å ⁻³)	0.68 and -0.66

Table 4.23 Selected bond lengths (Å) and bond angles (°) for complex 5.

Bond lengths (Å)		Bond angles (°)	
Ni1—P1	2.2250 (8)	S1—Ni1—P1	89.79 (3)
Ni1—S1	2.1536 (9)	O1—Ni1—P1	88.24 (6)
Ni1—O1	1.846 (2)	O1—Ni1—S1	176.76 (7)
Ni1—N1	1.885 (2)	O1—Ni1—N1	93.92 (10)
S1—C8	1.714 (3)	N1—Ni1—P1	175.21 (8)
N1—N2	1.393 (3)	N1—Ni1—S1	87.86 (8)
N1—C7	1.296 (4)	C17—P1—Ni1	106.74 (10)
N2—C8	1.328 (4)	C11—P1—C23	102.36 (14)
N3—C8	1.328 (4)	C11—P1—Ni1	120.46 (10)
N3—C9	1.462 (6)	C23—P1—Ni1	113.65 (10)

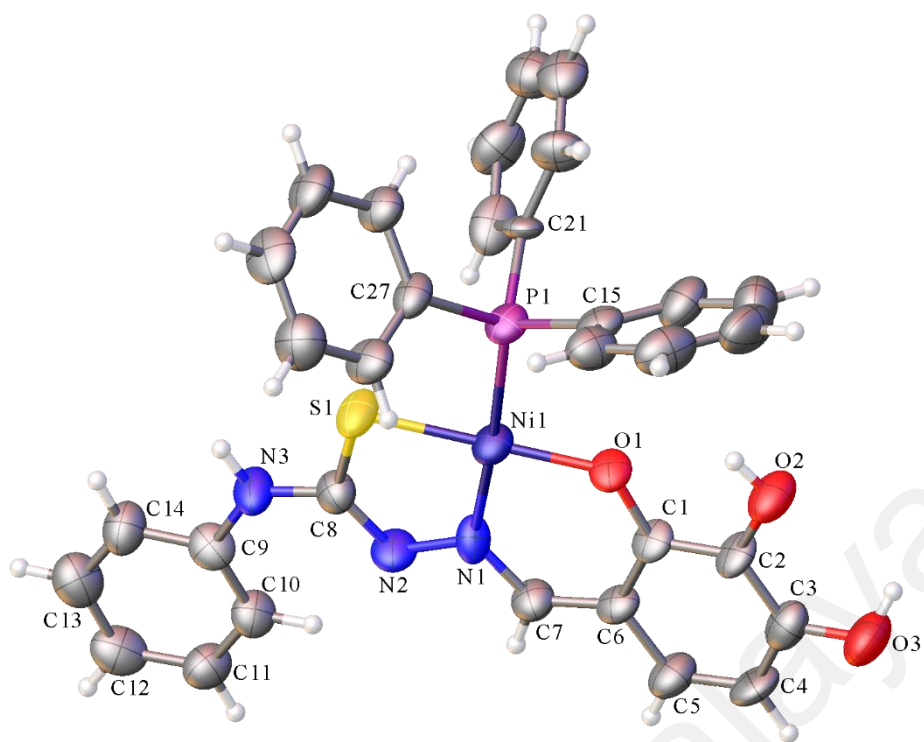


Figure 4.36 Ellipsoid plot of complex 6 drawn at 50 % probability level.

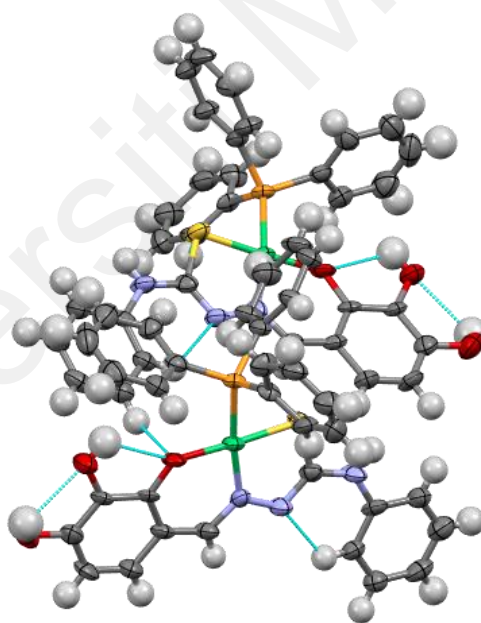


Figure 4.37 Unit cell packing diagram of complex 6 viewed along axis c. N-H, S-H and O-H...O hydrogen bonding interactions are observed.

Table 4.24 Crystallographic data summary for complex 6.

Compound	6
Empirical formula	C ₃₂ H ₂₇ N ₃ NiO ₃ PS
Formula weight	623.30
Crystal system	Monoclinic
Space group	<i>P</i> 2 ₁
Unit cell dimensions	
a (Å)	9.6016 (3)
b (Å)	10.6957 (3)
c (Å)	13.5895 (6)
β (°)	93.499 (3)
V (Å ³)	1392.98 (8)
Z	2
F(000)	646
D _{calc} (mg m ⁻³)	1.486
Absorption coefficient, μ (mm ⁻¹)	2.58
T (K)	293
Crystal size (mm)	0.10 × 0.10 × 0.05
Reflections collected	2486
Independent reflections (R _{int})	1618 (0.031)
Data/restraints/parameters	1618/1/372
R[F ² > 2σ(F ²)]	0.044
wR(F ²)	0.125
S	1.10
Largest difference peak and hole (e Å ⁻³)	0.43 and -0.44

Table 4.25 Selected bond lengths (Å) and bond angles (°) for complex 6.

Bond lengths (Å)		Bond angles (°)	
Ni1—S1	2.132 (3)	S1—Ni1—P1	88.95 (12)
Ni1—P1	2.216 (3)	O1—Ni1—S1	177.4 (2)
Ni1—O1	1.866 (7)	O1—Ni1—P1	89.4 (2)
Ni1—N1	1.900 (9)	O1—Ni1—N1	95.5 (3)
S1—C8	1.728 (12)	N1—Ni1—S1	86.3 (3)
N1—N2	1.370 (12)	N1—Ni1—P1	173.2 (3)
N1—C7	1.326 (14)	C21—P1—Ni1	111.4 (4)
N2—C8	1.299 (14)	C15—P1—C27	104.9 (5)
N3—C8	1.361 (13)	C27—P1—Ni1	115.9 (4)
N3—C9	1.411 (14)	C15—P1—Ni1	114.6 (4)

4.4.3 Crystal structures of Nickel complexes of 2,5 dihydroxybenzaldehyde thiosemicarbazone derivatives and triphenylphosphine

The crystal data and structure refinement parameters of complexes **8**, **9** and **10** are shown in **Table 4.26**, **4.28** and **4.30**, respectively. Whereas, the selected bond lengths and bond angles of complexes **8**, **9** and **10** and are shown in **Table 4.27**, **4.29** and **4.31**, respectively. Meanwhile, the crystal structures of complexes **8**, **9** and **10** are shown in **Figure 4.38**, **4.40** and **4.42**, respectively. Whilst, the unit cell packing of complexes **8**, **9** and **10** are shown in **Figure 4.39**, **4.41** and **4.43**, respectively.

4.4.3.1 Crystal structures of complexes (8-10)

Complexes **8** and **10** crystallised in triclinic crystal system with P1 space group. Whilst, complex **9** was found to have crystallised into a monoclinic lattice with P2₁/c space group. All three complexes were four coordinated and displays a square planar geometry. All ligands were found to have coordinated to the metal centre *via* their O,N,S tridentate binding site in their anionic (**L8** and **L9**) and neutral (**L10**) forms. The longer S1-C8 bond lengths in complexes **8** (1.770 (4) Å) and **9** (1.727 (6) Å) than in complex **10** (1.713 (4) Å) indicates that the mentioned bond is a single bond in complexes **8** and **9** but is a double bond in complex **10**, confirming the coordination of ligands **L8** and **L9** to the metal centre in their anionic thiolate form while ligand **L10** in its neutral thione form. This is further supported by the shorter N2-C8 bond lengths in complexes **8** (1.265 (6) Å) and **9** (1.304 (7) Å) than in complex **10** (1.337 (6) Å), an indication that the mentioned bond length is a double bond in complexes **8** and **9** but is a single bond in complex **10**. This is consistent with the similar results obtained from previous research (Piri et al., 2019; Richardson et al., 2009). The bite angles O1-Ni1-N1, N1-Ni1-S1, S1-Ni-P1 and O1-Ni1-S1 show minor deviations from the ideal 90 ° whereas bite angles O1-Ni-S1 and

N1-Ni1-P1 also show slight divergence from the usual 180° . Deviations in these angles resulted in a distorted square planar geometry around the metal centre (Elamathi et al., 2020; Kalaivani et al., 2012). Various hydrogen bonding interactions were observed from these complexes, for instance, N-H--N, N-H--O and O-H--O. In complexes **9** and **10**, water molecules were seen to bridge adjacent ligands.

Universiti Malaya

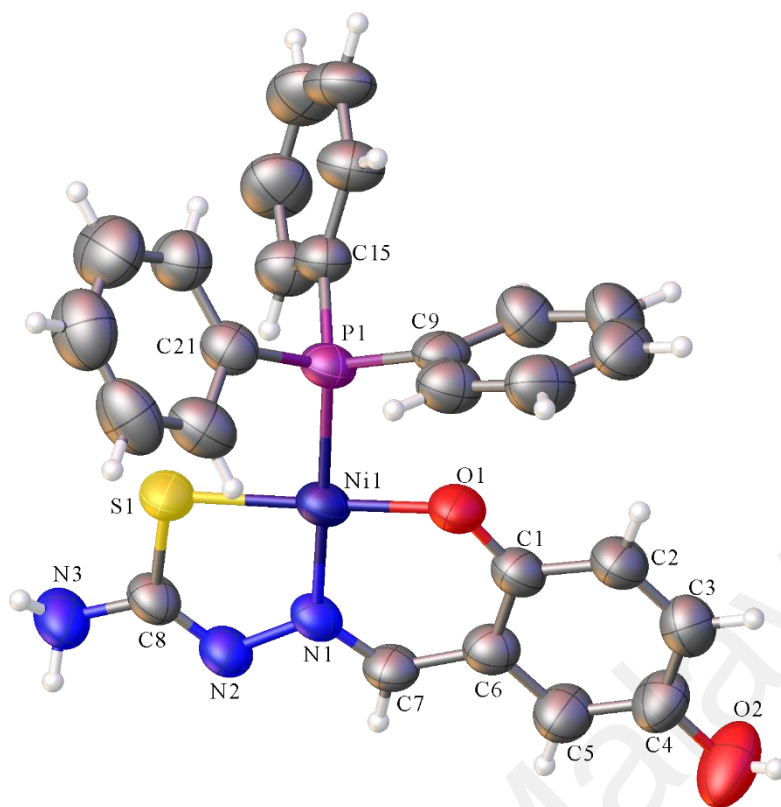


Figure 4.38 Ellipsoid plot of complex 8 drawn at 50 % probability level.

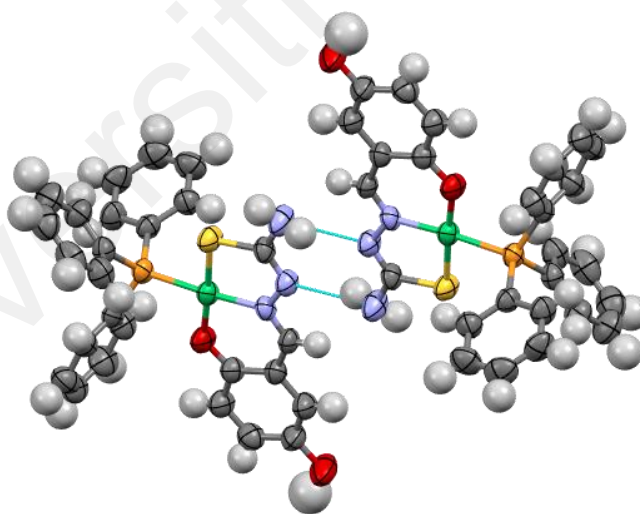


Figure 4.39 Unit cell packing diagram of complex 8 viewed along axis c. Intermolecular N-H...N hydrogen bonding interactions are observed.

Table 4.26 Crystallographic data summary for complex 8.

Compound	8
Empirical formula	C ₂₆ H ₂₂ N ₃ NiO ₂ PS
Formula weight	530.20
Crystal system	Triclinic
Space group	P1
Unit cell dimensions	
a (Å)	9.4082 (7)
b (Å)	9.5239 (5)
c (Å)	19.1383 (9)
α (°)	93.266(4)
β (°)	95.122 (5)
γ (°)	98.085(5)
V (Å ³)	1686.81 (17)
Z	2
F(000)	548
D _{calc} (mg m ⁻³)	1.044
Absorption coefficient, μ (mm ⁻¹)	2.03
T (K)	293
Crystal size (mm)	0.10 x 0.10 x 0.05
Reflections collected	9279
Independent reflections (R _{int})	5903(0.058)
Data/restraints/parameters	5903/108/309
R[F ² > 2σ(F ²)]	0.067
wR(F ²)	0.195
S	0.95
Largest difference peak and hole (e Å ⁻³)	0.54 and -0.57

Table 4.27 Selected bond lengths (Å) and bond angles (°) for complex 8.

Bond length (Å)		Bond angle (°)	
Ni1—S1	2.1375 (13)	S1—Ni1—P1	91.15 (5)
Ni1—P1	2.2044 (11)	O1—Ni1—S1	177.19 (11)
Ni1—O1	1.833 (3)	O1—Ni1—P1	86.54 (10)
Ni1—N1	1.892 (3)	O1—Ni1—N1	94.97 (14)
S1—C8	1.770 (4)	N1—Ni1—S1	87.44 (11)
N1—N2	1.398 (4)	N1—Ni1—P1	175.73 (11)
N1—C7	1.290 (5)	C15—P1—Ni1	111.76 (14)
N2—C8	1.265 (6)	C9—P1—C21	104.8 (2)
N3—C8	1.354 (5)	C21—P1—Ni1	115.74 (13)
		C9—P1—Ni1	112.29 (14)

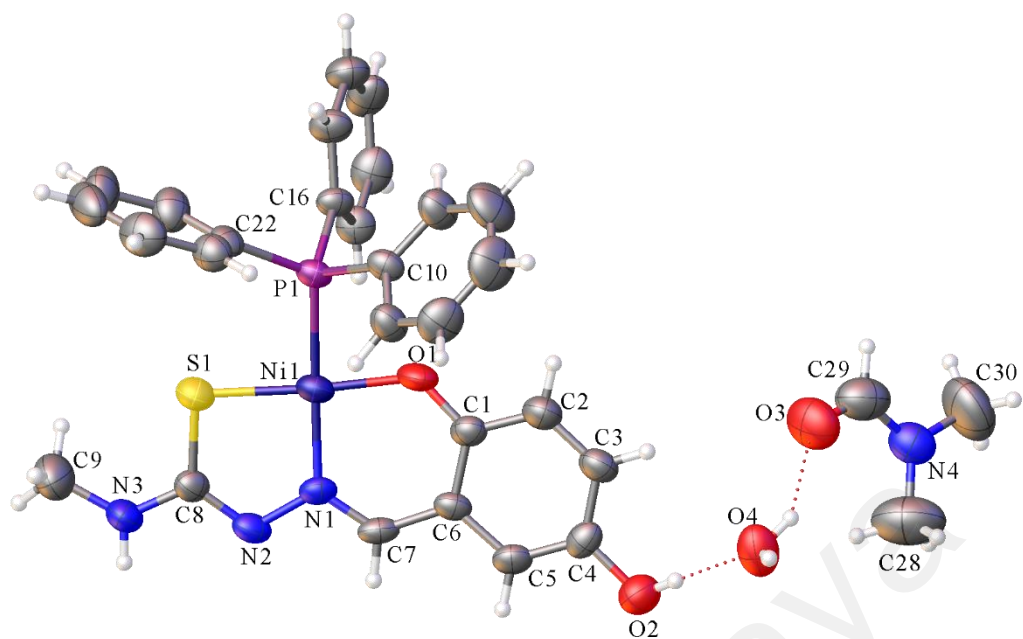


Figure 4.40 Ellipsoid plot of complex 9 drawn at 50 % probability level.

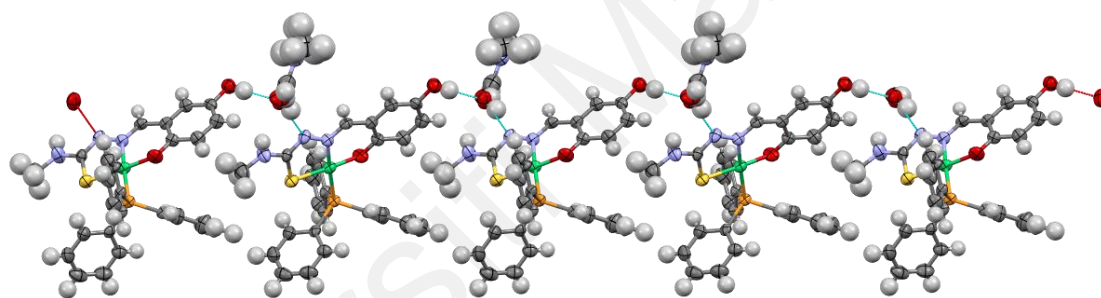


Figure 4.41 Unit cell packing diagram of complex 9 viewed along axis b. Intermolecular N-H...O and O-H...O hydrogen bonding interactions are observed. Water molecules were found to bridge adjacent ligands.

Table 4.28 Crystallographic data summary for complex 9.

Compound	9
Empirical formula	C ₂₇ H ₂₅ N ₃ NiO ₂ PS.H ₂ O.C ₃ H ₇ NO
Formula weight	637.36
Crystal system	Monoclinic
Space group	<i>P</i> 2 ₁ / <i>c</i>
Unit cell dimensions	
a (Å)	9.4664 (7)
b (Å)	23.1655 (9)
c (Å)	14.0907 (7)
β (°)	104.264 (6)
V (Å ³)	2994.7 (3)
Z	4
F(000)	1336
D _{calc} (mg m ⁻³)	1.414
Absorption coefficient, μ (mm ⁻¹)	2.44
T (K)	293
Crystal size (mm)	0.10 x 0.10 x 0.05
Reflections collected	4406
Independent reflections (R _{int})	2093 (0.032)
Data/restraints/parameters	2093/0/377
R[F ² > 2σ(F ²)]	0.055
wR(F ²)	0.160
S	1.07
Largest difference peak and hole (e Å ⁻³)	0.48 and -0.40

Table 4.29 Selected bond lengths (Å) and bond angles (°) for complex 9.

Bond length (Å)		Bond angle (°)	
Ni1—S1	2.1327 (17)	S1—Ni1—P1	93.71 (7)
Ni1—P1	2.1933 (15)	O1—Ni1—S1	174.40 (14)
Ni1—O1	1.823 (5)	O1—Ni1—P1	84.09 (14)
Ni1—N1	1.889 (5)	O1—Ni1—N1	94.9 (2)
S1—C8	1.727 (6)	N1—Ni1—S1	87.67 (19)
N1—N2	1.394 (7)	N1—Ni1—P1	175.34 (14)
N1—C7	1.288 (7)	C16—P1—Ni1	112.7 (2)
N2—C8	1.304 (7)	C22—P1—C10	104.9 (3)
N3—C8	1.353 (8)	C22—P1—Ni1	117.34 (18)
N3—C9	1.418 (8)	C10—P1—Ni1	109.3 (2)

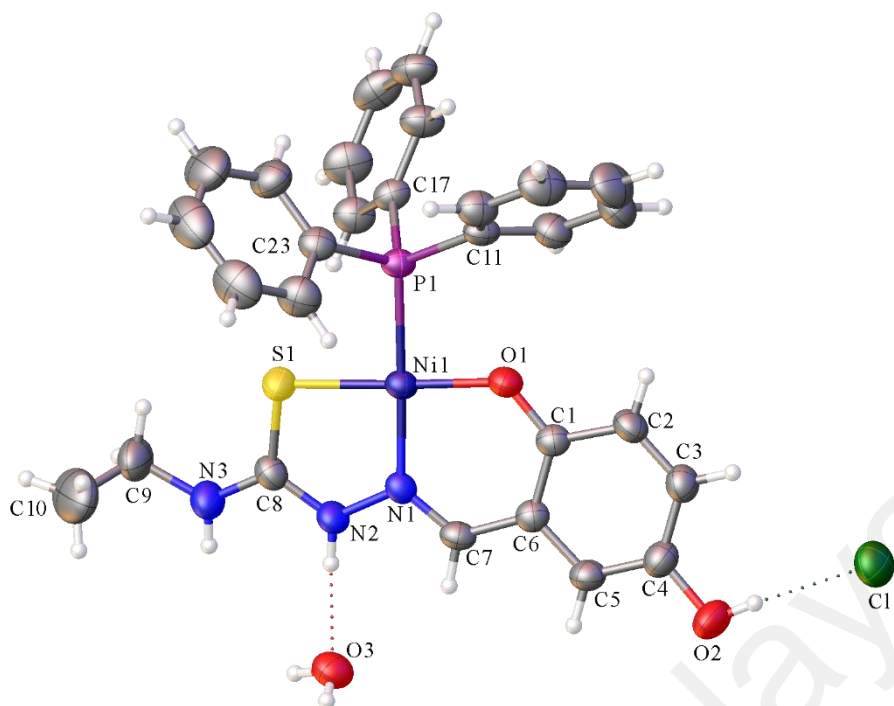


Figure 4.42 Ellipsoid plot of complex 10 drawn at 50 % probability level.

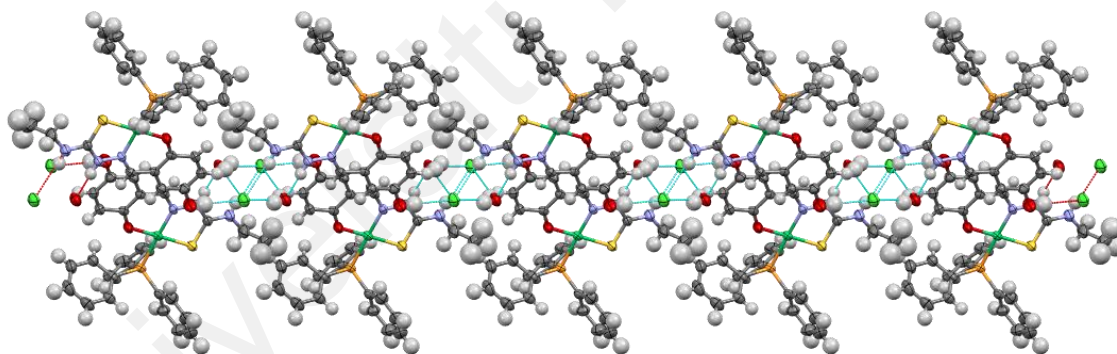


Figure 4.43 Unit cell packing diagram of complex 10 viewed along axis a. Intermolecular N-H...Cl, N-H...O and O-H...Cl hydrogen bonding interactions are observed. Water molecules and chloride ions were found to bridge adjacent ligands.

Table 4.30 Crystallographic data summary for complex 10.

Compound	10
Empirical formula	C ₂₈ H ₂₇ N ₃ NiO ₂ PS.Cl.H ₂ O
Formula weight	653.76
Crystal system	Triclinic
Space group	P1
Unit cell dimensions	
a (Å)	8.8943 (5)
b (Å)	12.0672 (10)
c (Å)	16.2336 (10)
α (°)	99.126(6)
β (°)	105.606 (5)
γ (°)	103.827(6)
V (Å³)	1582.5 (2)
Z	2
F(000)	678
D_{calc} (mg m⁻³)	1.372
Absorption coefficient, μ (mm⁻¹)	3.07
T (K)	293
Crystal size (mm)	0.10 x 0.10 x 0.05
Reflections collected	9294
Independent reflections (R_{int})	6045 (0.050)
Data/restraints/parameters	6045/0/375
R[F² > 2σ(F²)]	0.055
wR(F²)	0.159
S	1.02
Largest difference peak and hole (e Å⁻³)	0.55 and -0.91

Table 4.31 Selected bond lengths (Å) and bond angles (°) for complex 10.

Bond length (Å)		Bond angle (°)	
S1—Ni1	2.1656 (12)	S1—Ni1—P1	90.60 (5)
P1—Ni1	2.2213 (11)	O1—Ni1—S1	177.95 (10)
O1—Ni1	1.836 (3)	O1—Ni1—P1	88.01 (10)
N1—Ni1	1.880 (3)	O1—Ni1—N1	93.59 (14)
C8—S1	1.713 (4)	N1—Ni1—S1	87.83 (10)
N1—N2	1.386 (5)	N1—Ni1—P1	178.11 (10)
C7—N1	1.304 (5)	C17—P1—Ni1	114.70 (13)
C8—N2	1.337 (6)	C23—P1—C11	105.4 (2)
C8—N3	1.319 (6)	C23—P1—Ni1	111.69 (14)
C9—N3	1.455 (7)	C11—P1—Ni1	114.87 (13)

4.5 Biological activities of ligands and metal complexes

4.5.1 Cytotoxic activity of ligands and metal complexes

Section 4.5.1.1 describes in detail the cytotoxic activity of ligands (L1-L3) and their metal complexes (1-3). Whereas section 4.5.1.2 describes in detail the cytotoxic activity of ligands (L4-L7) and their metal complexes (4-7). On the other hand, section 4.5.1.3 describes in detail the cytotoxic activity of ligands (L8-L11) and their metal complexes (8-11).

4.5.1.1 Cytotoxic activity of fluorene-2-carboxaldehyde-N4 thiosemicarbazone ligands (L1-L3) and their metal complexes (1-3)

Three different human cancer cell lines, namely HCT 116, PC-3, and MCF7 were used to determine the cytotoxic activity of ligands and metal complexes *via* MTT assay and the results were shown in Table 4.32. All ligands were inactive against PC-3. As for ligand L1, moderate growth inhibitory effect at 30.46 ± 0.65 and 48.45 ± 3.20 μM was observed when tested with HCT 116 and MCF7, respectively while ligand L2 exhibited potent growth inhibitory effect against HCT 116 at 7.23 ± 1.09 μM , and moderate cytotoxicity against MCF7 with an IC_{50} of 41.14 ± 3.32 μM . Compared to ligands L1, L2 and cisplatin, ligand L3 exhibited the strongest growth inhibitory effect against HCT 116, with an IC_{50} of 0.69 ± 0.13 μM . It was evident that the cytotoxic activity of the ligands increases with an increase in the hydrophobicity of the substituent group attached at the N(3) position (Rebolledo et al., 2005). In this case, the ligand with the ethyl (L3) substituent is the most cytotoxic among the other two ligands. In contrast to its parent ligand (L1), complex 1 was found to show significant improvement in the cytotoxicity against all three cell lines. The complexation of ligand L1 has increased the growth inhibitory effect of complex 1 by more than 3-fold in PC-3, 9-fold in HCT 116, and 3-

fold in MCF7. Particularly, the cytotoxicity of complex **1** against HCT 116 was enhanced to an extent that becoming higher than cisplatin, as depicted from the lower IC₅₀ value of complex **1** ($3.36 \pm 0.21 \mu\text{M}$) than cisplatin ($5.92 \pm 0.79 \mu\text{M}$). Meanwhile, complexes **2** and **3** did not show cytotoxicity (IC₅₀ > 100 μM) against all the tested cell lines, probably due to their higher molecular weights (MW) compared to complex **1** (MW of complex **1**, 603.39; complex **2**, 617.42; complex **3**, 649.50 g/mol). Generally, lower molecular weight compounds (ligands **L2** and **L3**) were found to show higher cytotoxicity than compounds with higher molecular weight (complexes **2** and **3**), and compounds which have molecular weight more than 605 g/mol (complexes **2** and **3**) were mostly cytotoxic inactive, suggesting that the compounds with lower MW are more likely to penetrate through the cell membrane and produce growth inhibitory effect in cancerous cells (Matuszewska et al., 2018; Matuszewska et al., 2019). In the case of ligand **L1** and complex **1**, metal complexation does help to improve cytotoxic activity of ligand **L1**. Altogether, factors such as hydrophobicity and molecular weight of the compounds need to be taken into consideration during the design and synthesis of cytotoxic compounds for anticancer drugs development.

Table 4.32 *In vitro* cytotoxic activity (IC₅₀ values) of ligands (**L1-L3**) and complexes (**1-3**) against three human cancer cell lines.

Compound	IC ₅₀ in μM		
	PC-3	HCT 116	MCF7
L1	>100	30.46 ± 0.65	48.45 ± 3.20
L2	>100	7.23 ± 1.09	41.14 ± 3.32
L3	>100	0.69 ± 0.13	40.34 ± 3.38
1	30.71 ± 0.97	3.36 ± 0.21	15.78 ± 0.74
2	>100	>100	>100
3	>100	>100	>100
Cisplatin*	19.45 ± 0.221	5.92 ± 0.79	4.38 ± 0.50

* Positive control, cisplatin was used as a reference standard. Values were expressed as mean \pm standard deviation (n=3).

4.5.1.2 Cytotoxic activity of 2,3,4-trihydroxybenzaldehyde-N4 thiosemicarbazone ligands (L4-L7) and their metal complexes (4-7)

The cytotoxicity of the ligands and metal complexes was carried out against three human cancer cell lines, namely PC-3, HCT 116 and MCF7, the results are reported in **Table 4.33**. Ligand **L4** was inactive against PC-3 but showed a moderate cytotoxic activity against HCT 116 and MCF7 with IC_{50} 10.34 ± 0.23 and 11.79 ± 0.86 μ M, respectively. Ligand **L5** exhibited a potent growth inhibitory effect against HCT 116 with IC_{50} 5.75 ± 0.49 μ M, which is comparable with cisplatin (IC_{50} 5.92 ± 0.79 μ M), and it also showed a substantial cytotoxicity against MCF7 with an IC_{50} 8.68 ± 0.11 μ M. Both ligands **L6** and **L7** displayed stronger cytotoxicity than cisplatin with IC_{50} 9.82 ± 0.69 and 15.66 ± 2.44 μ M, respectively when tested against PC-3, and they exhibited moderate growth inhibitory effect when tested against HCT 116 (**L3**, IC_{50} 9.82 ± 1.85 μ M; **L4**, IC_{50} 9.75 ± 0.54 μ M). Overall, **L5** exhibited a wider spectrum of cytotoxicity than the other ligands with reference to the result of HCT 116 and MCF7. This is consistent with the previous study that the addition of long aliphatic and lipophilic side chain could enhance the cytotoxicity of the compounds (**L5**), while the introduction of aromatic ring into the compound (**L6** and **L7**) has no significant improvement to its cytotoxicity (Patterson et al., 2014).

Generally, the results showed that the complexation did not improve the cytotoxicity of the parent ligands, except for complexes **4** and **6**. Notably, the complexation of **L4** has significantly enhanced the cytotoxicity of **4** against HCT 116 to an extent that becoming more potent than cisplatin with an IC_{50} 4.26 ± 0.29 μ M. Interestingly, the complexation of **L6** has slightly increased the cytotoxicity and cell line-specificity of the complex **6** towards HCT 116 (IC_{50} 7.07 ± 0.61 μ M). Complex **6** is more hydrophobic than **5**, therefore, it exhibited a stronger cytotoxic activity than the latter (IC_{50} 12.68 ± 0.72 μ M) when tested against HCT 116, indicating once again that cytotoxicity is directly

proportional to hydrophobicity (Pingaew et al., 2010). Previous research on the cytotoxic activity of 2,3-dihydroxybenzaldehyde complexes with ethyl and phenyl substituents showed that the latter exhibited better cytotoxicity when tested against MCF7 and PC-3 cell lines (Shawish et al., 2014). Through this research, it was found that complexes of 2,3,4-trihydroxybenzaldehyde with ethyl and phenyl substituents showed comparable cytotoxic activity with compounds stated in literature and better activity against HCT 116.

Table 4.33 *In vitro* cytotoxic activity (IC₅₀ values) of ligands (L4-L7) and complexes (4-7) against three human cancer cell lines.

Compound	IC ₅₀ in μM		
	PC-3	HCT 116	MCF7
L4	>100	10.34 \pm 0.23	11.79 \pm 0.86
L5	82.47 \pm 4.14	5.75 \pm 0.49	8.68 \pm 0.11
L6	9.82 \pm 0.69	9.82 \pm 1.85	29.70 \pm 0.16
L7	15.66 \pm 2.44	9.75 \pm 0.54	23.80 \pm 1.54
4	>100	4.26 \pm 0.29	13.03 \pm 0.69
5	>100	12.68 \pm 0.72	24.72 \pm 1.59
6	>100	7.07 \pm 0.61	>100
7	>100	>100	>100
Cisplatin*	19.45 \pm 0.73	5.92 \pm 0.79	4.38 \pm 0.50

* Positive control; Values were expressed as the mean \pm standard deviation (n=3) of three independent experiments.

4.5.1.3 Cytotoxic activities of 2,5-dihydroxybenzaldehyde-N4 thiosemicarbazone ligands (L8-L11) and their metal complexes (8-11)

The **Table 4.34** reports the cytotoxicity of the ligands and metal complexes which was carried out against three human cancer cell lines, namely PC-3, HCT 116 and MCF7. Among the ligands tested, ligands **L9** and **L10** were seen to show moderate cytotoxic activity against HCT 116 with IC_{50} 11.51 ± 0.78 and 12.85 ± 0.71 μ M, respectively. A previous study reported that the cytotoxic potency of a compound increases as the alkyl group attached to the N(3) position increases in size, indicating that the alkyl group is a part of the pharmacophore and further suggesting that the cytotoxicity is ruled predominantly by the thiosemicarbazone ligands which are highly cytotoxic (Beckford et al., 2009). In this case, the ligands tested against MCF7 showed an increase in cytotoxic activity, proven by decreasing IC_{50} values in order of **L8** > **L9** > **L10** (**L8**, IC_{50} 48.94 ± 3.74 μ M; **L9**, IC_{50} 39.09 ± 1.03 μ M; **L10**, IC_{50} 19.09 ± 0.20 μ M) as the substituents at the N(3) position increase in size. However, ligand **L11** was found to be inactive when tested against MCF7 due to the fact that the presence of long aliphatic and lipophilic side chain could cause the cytotoxicity of the compounds to be elevated (**L9** and **L10**), while the existence of aromatic ring in a compound may not enhance its cytotoxicity (**L11**) (Patterson et al., 2014).

Overall, the cytotoxicity of parent ligands did not improve after metal complexation, except for complexes **9** and **11**. The results show that the complexation of ligands **L9** and **L10** improved the cytotoxic activity of complexes **9** and **11** when tested against HCT 116 (**9**, IC_{50} 8.82 ± 1.30 μ M; **11**, IC_{50} 8.21 ± 1.20 μ M). It is noteworthy that complexes formed from anionic thiolate ligands (complexes **9** and **11**) showed cytotoxic activity but complex formed from neutral thione ligand (complex **10**) was found inactive when tested against HCT 116. This is because metal complexation by anionic ligands that results in charge neutral metal complexes exhibit improved bioactivity due to the negative charge on the

sulfur atom that functions to enhance the coordination strength (Casas et al., 1998; Paterson & Donnelly, 2011; Teoh et al., 1999). Besides, complex **11** (IC_{50} 8.21 ± 1.20 μ M) displayed slightly better cytotoxicity than complex **9** (IC_{50} 8.82 ± 1.30 μ M) due to increased hydrophobicity of the former than the latter (Pingaew et al., 2010). Evidently, the inactivity of complex **8** towards all three cell lines could be due to reduced hydrophobicity of the complex when compared to its derivatives.

Table 4.34 *In vitro* cytotoxic activity (IC_{50} values) of ligands (L8-L11) and complexes (8-11) against three human cancer cell lines.

Compound	IC_{50} in μ M		
	PC-3	HCT 116	MCF7
L8	19.36 ± 3.69	19.46 ± 2.79	48.94 ± 3.74
L9	41.35 ± 0.78	11.51 ± 0.78	39.09 ± 1.03
L10	>100	12.85 ± 0.71	19.09 ± 0.20
L11	>100	28.09 ± 1.21	>100
8	>100	>100	>100
9	>100	8.82 ± 1.30	>100
10	>100	>100	>100
11	>100	8.21 ± 1.20	>100
Cisplatin*	19.45 ± 0.73	5.92 ± 0.79	4.38 ± 0.50

* Positive control, cisplatin was used as a reference standard. Values were expressed as mean \pm standard deviation (n=3).

4.5.2 Antiplasmodium activity of ligands and metal complexes

Section 4.5.2.1 describes in detail the antiplasmodium activity of ligands (L1-L3) and their metal complexes (1-3). Whereas section 4.5.2.2 describes in detail the antiplasmodium activity of ligands (L4-L7) and their metal complexes (4-7). On the other hand, section 4.5.2.3 describes in detail the antiplasmodium activity of ligands (L8-L11) and their metal complexes (8-11).

4.5.2.1 Antiplasmodium activity of fluorene-2-carboxaldehyde-N4 thiosemicarbazone ligands (L1-L3) and their metal complexes (1-3)

The Table 4.35 reports IC_{50} values of all compounds and goodness of fit accessed by R^2 as whether it is more or lesser than 0.8. Among the compounds tested on *P. falciparum* only complexes 2 and 3 were found to inhibit the parasite growth. Complex 1 was not active against the parasite. Whereas, the IC_{50} values for complexes 2 and 3 were $23.79 \pm 1.09 \mu\text{M}$ and $2.29 \pm 2.19 \mu\text{M}$, respectively. The antimalarial activity of these complexes increases in the order of $2 < 3$. It is obvious that complex 3 inhibits the parasite more than complex 2 as lipophilicity corresponds strongly with antimalarial activity (Kashyap et al., 2017; Walcourt et al., 2004). In other words, the higher the hydrophobicity of the compound, the better its antimalarial activity.

Table 4.35 Antiplasmodium activity (IC₅₀ (μM) values) of ligands (L1-L3) and complexes (1-3) for *P. falciparum* 3D7.

Compound	IC ₅₀ (μM) ^a
L1	>25 ^b
L2	>25 ^b
L3	>25 ^b
1	>25 ^b
2	23.79 ± 1.09
3	2.29 ± 2.19
Chloroquine*	(3.17 ± 0.14) × 10⁻³

^aMean (±SD) from two different experiments which were performed in duplicates each

^bR² < 0.8; * Positive control

Universiti Malaysia

4.5.2.2 Antiplasmodium activity of 2,3,4-trihydroxybenzaldehyde-N4 thiosemicarbazone ligands (L4-L7) and their metal complexes (4-7)

The **Table 4.36** reports the IC_{50} and the goodness of fit of each result, whether it is more or lesser than 0.8. All ligands were inactive against *P. falciparum*, while the complexation of **L5** and **L6** into complexes **5** and **6** has gained pronounced antimalarial activity with IC_{50} 9.88 ± 0.23 and 1.06 ± 0.01 μM , respectively. Similar to the MTT cytotoxicity study, **6** has a higher antimalarial activity than **5**, which again probably due to the higher hydrophobicity of **6** than the latter (Bhattacharjee & Karle, 1996). In contrast with complex **6**, complex **7** is inactive although **7** is also hydrophobic, suggesting that the antimalarial activity can only be improved when the hydrophobicity is attributed by phenyl group (in **6**) but not the longer and larger ethyl phenyl group (in **7**), as the latter tend to lower the activity (Cheng et al., 2002).

Table 4.36 Antiplasmodium activity (IC_{50} (μM) values) of ligands (L4-L7) and complexes (4-7) for *P. falciparum* 3D7.

Compound	IC_{50} (μM) ^a
L4	>25 ^b
L5	>25 ^b
L6	>25 ^b
L7	>25 ^b
4	>25 ^b
5	9.88 ± 0.23
6	1.06 ± 0.01
7	>25 ^b
Chloroquine*	$(3.25 \pm 0.23) \times 10^{-3}$

^a Mean (\pm SD) from two different experiments which were performed in duplicates each

^b $R^2 < 0.8$; * Positive control

4.5.2.3 Antiplasmodium activity of 2,5-dihydroxybenzaldehyde-N4 thiosemicarbazone ligands (L8-L11) and their metal complexes (8-11)

The **Table 4.37** shows the IC₅₀ results obtained. Unfortunately, it was found that all compounds in this series did not inhibit the parasite growth and were antimalarial inactive. Previous studies on thiosemicarbazone complexes have revealed that the presence of hydroxyl group in a compound enhances its absorption rate into cell due to the hydrophilicity of the hydroxyl group (Matsa et al., 2019). However, it was discovered that most Schiff bases with high inhibitory activity arise from its hydroxy substituent being at the *para*-position on the benzaldehyde unit rather than at the *meta*-position (Leigh et al., 2011), explaining the reason behind the inactivity of this group of compounds.

Table 4.37 Antiplasmodium activity (IC₅₀ (μM) values) of ligands (L8-L11) and complexes (8-11) for *P. falciparum* 3D7.

Compound	IC ₅₀ (μM) ^a
L8	>25 ^b
L9	>25 ^b
L10	>25 ^b
L11	>25 ^b
8	>25 ^b
9	>25 ^b
10	>25 ^b
11	>25 ^b
Chloroquine*	$(3.25 \pm 0.23) \times 10^{-3}$

^a Mean (±SD) from two different experiments which were performed in duplicates each

^b R² < 0.8 ; * Positive control

CHAPTER 5: CONCLUSION AND RECOMMENDATIONS

Schiff base ligands and nickel complexes were synthesized from fluorene-2-carboxaldehyde, 2,3,4-trihydroxybenzaldehyde, 2,5-dihydroxybenzaldehyde, thiosemicarbazide, 4-methyl-3-thiosemicarbazide, 4-ethyl-3-thiosemicarbazide, 4-phenyl-3-thiosemicarbazide and 4-(4-ethylphenyl)-3-thiosemicarbazide. The synthesized ligands and complexes were characterized using FT-IR, NMR and X-ray crystallography methods. Complexes of fluorene-2-carboxaldehyde-N₄ thiosemicarbazones exhibited square planar geometry. Complexes of 2,3,4-trihydroxybenzaldehyde-N₄ thiosemicarbazones and 2,5-dihydroxybenzaldehyde-N₄ thiosemicarbazone were found to exhibit distorted square planar geometry due to the presence of triphenylphosphine. These ligands and complexes were tested for their cytotoxic and antimalarial activities.

The feature of the N(3) substituent portrays its cytotoxic and antimalarial activities. Factors such as hydrophobicity and molecular weight have to be considered to determine the biological activities of the compounds in discussion. The higher the hydrophobicity of the compound, the better its cytotoxic and antimalarial activity. However, this is not always true as anomalies in trend may occur. This research proved that compounds with more hydrophobic substituent displayed better cytotoxic and antimalarial activity. In this case, complexes of 2,3,4-trihydroxybenzaldehyde with the ethyl and phenyl substituent showed improved cytotoxic and antimalarial activity. It is noteworthy that the polyhydroxybenzaldehyde with three hydroxyl groups displayed better activity than the polyhydroxybenzaldehyde with two hydroxyl groups. This may be due to the feature of hydroxyl group which enhances solubility. Hence, the greater the number of hydroxyl group, the better the activity of compounds. Hence, compounds of the 2,3,4-trihydroxybenzaldehyde displayed better activity than compounds of 2,5-dihydroxybenzaldehyde. Ligand **L3** and complex **1** may be used to develop a new set of

thiosemicarbazone based anticancer agents since both exhibited higher cytotoxic activity than cisplatin against the HCT 116 cell line. Besides, complexes **4**, **6** and ligand **L5** could be developed as polyhydroxybenzaldehyde based anticancer agents. The cytotoxic activities of complexes **4** and **6** are greater than complexes **9** and **11** when tested against HCT 116 cell line, indicating once again that compounds with hydroxyl group at para position of the benzaldehyde component display higher biological activity.

On the other hand, complex **3** with ethyl substituent which has higher hydrophobicity than complexes **1** and **2** could be a suitable candidate in the study of antimalarial activity. Complexes **5** and **6** could be developed as candidates for studying antimalarial activity as well, and they were found to exhibit both cytotoxicity and antimalarial activity. It is worth mentioning that complexation process has significantly enhanced the biological activities of the ligands, as observed in complexes **1**, **4**, **5**, **6**, **9** and **11**. In future, much focus and importance should be given to compounds similar as complexes **5** and **6** in the development of a single drug with cytotoxic and antimalarial properties. In addition, future studies should focus on the mechanism of action of the synthesized drugs, mechanism of cell death and discovery of new drug targets to overcome the issues of drug toxicity and resistance.

REFERENCES

- Abdul Halim, Nordin, Mohd Abd Razak, Mohd Sofyan, Abdul Halim, Rajab, & Sarip. (2019). Synthesis, characterization, and evaluation of silver (I) complexes with mixed-ligands of thiosemicarbazones and diphenyl (p-tolyl) phosphine as biological agents. *Journal of Coordination Chemistry*, 72(5-7), 879-893.
- Ackerman, Fanwick, Green, John, Running, Swearingen, . . . West. (1999). Structural and spectral studies of copper (II) and nickel (II) complexes of pyruvaldehyde mixed bis {N (4)-substituted thiosemicarbazones}. *Polyhedron*, 18(21), 2759-2767.
- Ackley, Barry, Mounce, Farmer, Springer, Day, . . . Bierbach. (2004). Structure–activity relationships in platinum–acridinylthiourea conjugates: effect of the thiourea nonleaving group on drug stability, nucleobase affinity, and in vitro cytotoxicity. *JBIC Journal of Biological Inorganic Chemistry*, 9(4), 453-461.
- Adediji, Obaleye, & Akinremi. (2012). Ni (II) complex of mefloquine-pyrimethamine: Synthesis, toxicological and antimalarial activities against Plasmodium Berghei. *Journal of Chemical and Pharmaceutical Research*, 4(8), 4066-4072.
- Adsule, Barve, Chen, Ahmed, Dou, Padhye, & Sarkar. (2006). Novel Schiff base copper complexes of quinoline-2 carboxaldehyde as proteasome inhibitors in human prostate cancer cells. *Journal of Medicinal Chemistry*, 49(24), 7242-7246.
- Afrasiabi, Sinn, Chen, Ma, Rheingold, Zakharov, . . . Padhye. (2004). Appended 1, 2-naphthoquinones as anticancer agents 1: synthesis, structural, spectral and antitumor activities of ortho-naphthaquinone thiosemicarbazone and its transition metal complexes. *Inorganica Chimica Acta*, 357(1), 271-278.
- Afrasiabi, Sinn, Lin, Ma, Campana, & Padhye. (2005). Nickel (II) complexes of naphthaquinone thiosemicarbazone and semicarbazone: Synthesis, structure, spectroscopy, and biological activity. *Journal of Inorganic Biochemistry*, 99(7), 1526-1531.
- Afzal, Gul, & Akhter. (2014). π -Conjugated ferrocenyl Schiff base polymers: synthesis, characterization and electrical conductivity. *Journal of Inorganic and Organometallic Polymers and Materials*, 24(2), 321-332.
- Aguiar, Murce, Cortopassi, Pimentel, Almeida, Barros, . . . Krettli. (2018). Chloroquine analogs as antimalarial candidates with potent in vitro and in vivo activity. *International Journal for Parasitology: Drugs and Drug Resistance*, 8(3), 459-464.

- Ajani, Obafemi, Ikpo, Ogunniran, & Nwinyi. (2009). Microwave-assisted synthesis and antibacterial activity of some pyrazol-1-ylquinoxalin-2 (1H)-one derivatives. *Chemistry of Heterocyclic Compounds*, 45(11), 1370-1378.
- Alekseyev, Lagoda, Yakimovich, & Yegorova. (2010). 1, 2, 4-Triazines—products of reaction of thiocarbohydrazide and its alkyl (aryl)-substituted derivatives with 1, 2-dicarbonyl compounds. *Chemistry of Heterocyclic Compounds*, 46(8), 971-982.
- Almendras, Huentupil, Novoa, Roussel, Melis, Smith, & Arancibia. (2019). Trinuclear Ni (II), Pd (II) and Cu (II) complexes containing the 2-hydroxy-benzaldehyde-ferrocenyl-sulfonylhydrazone ligand: synthesis, structural characterization and antiplasmodial evaluation. *Inorganica Chimica Acta*, 496, Article#119050.
- Alomar, Landreau, Allain, Bouet, & Larcher. (2013). Synthesis, structure and antifungal activity of thiophene-2, 3-dicarboxaldehyde bis (thiosemicarbazone) and nickel (II), copper (II) and cadmium (II) complexes: Unsymmetrical coordination mode of nickel complex. *Journal of Inorganic Biochemistry*, 126, 76-83.
- Altura, & Altura. (1996). Role of magnesium in patho-physiological processes and the clinical utility of magnesium ion selective electrodes. *Scandinavian Journal of Clinical and Laboratory Investigation*, 56(sup224), 211-234.
- Amato, Ballistreri, Pappalardo, Sciotto, Tomaselli, & Toscano. (2007). Synthesis and conformational aspects of 20- and 40-membered macrocyclic mono and dinuclear uranyl complexes incorporating salen and (R)-BINOL units. *Tetrahedron*, 63(39), 9751-9757.
- Amoedo, Adrio, Antelo, Martínez, Pereira, Fernández, & Vila. (2006). Synthesis, Characterization, and Crystal Structure Analysis of the First Terdentate [C, N, S] Thiosemicarbazone Complex with a Six-Membered Palladacycle: Influence of Steric Effects on Ring Size. *European Journal of Inorganic Chemistry*, 2006(15), 3016-3021.
- Anastassopoulou, & Theophanides. (1995). The role of metal ions in biological systems and medicine *Bioinorganic chemistry* (pp. 209-218): Springer.
- Andiappan, Sanmugam, Deivanayagam, Karuppasamy, Kim, & Vikraman. (2018). In vitro cytotoxicity activity of novel Schiff base ligand–lanthanide complexes. *Scientific Reports*, 8(1), Article#3054.
- Anjomshoa, Hadadzadeh, Fatemi, & Torkzadeh-Mahani. (2015). A mononuclear Ni (II) complex with 5, 6-diphenyl-3-(2-pyridyl)-1, 2, 4-triazine: DNA- and BSA-binding and anticancer activity against human breast carcinoma cells. *Spectrochimica Acta Part A: Molecular and Biomolecular Spectroscopy*, 136, 205-215.

- Anjum, Palanimuthu, Kalinowski, Lewis, Park, Kovacevic, . . . Richardson. (2019). Synthesis, Characterization, and in Vitro Anticancer Activity of Copper and Zinc Bis (Thiosemicarbazone) Complexes. *Inorganic Chemistry*, 58(20), 13709-13723.
- Arutyunyan, Arutyunyan, Gevorkyan, Gasparyan, Paronikyan, Stepanyan, & Minasyan. (2018). Synthesis and conversions of polyhedral compounds. 32. Synthesis and antibacterial activity of azaadamantane-containing azomethine dihydrochlorides. *Pharmaceutical Chemistry Journal*, 52(5), 419-423.
- Aswin, Mansoor, Logaiya, & Sudhan. (2014). Triphenylphosphine: An efficient catalyst for the synthesis of 4, 6-diphenyl-3, 4-dihydropyrimidine-2 (1H)-thione under thermal conditions. *Journal of King Saud University-Science*, 26(2), 141-148.
- Atteke, Ndong, Aubouy, Maciejewski, Brocard, Lébib, & Deloron. (2003). In vitro susceptibility to a new antimalarial organometallic analogue, ferroquine, of Plasmodium falciparum isolates from the Haut-Ogooue region of Gabon. *Journal of Antimicrobial Chemotherapy*, 51(4), 1021-1024.
- Bahl, Athar, Soares, de Sá, Moreira, Srivastava, . . . Azam. (2010). Structure–activity relationships of mononuclear metal–thiosemicarbazone complexes endowed with potent antiplasmodial and antiamoebic activities. *Bioorganic & Medicinal Chemistry*, 18(18), 6857-6864.
- Balachandran, Haribabu, Jeyalakshmi, Bhuvanesh, Karvembu, Emi, & Awale. (2018). Nickel (II) bis (isatin thiosemicarbazone) complexes induced apoptosis through mitochondrial signaling pathway and G0/G1 cell cycle arrest in IM-9 cells. *Journal of Inorganic Biochemistry*, 182, 208-221.
- Baragaña, Forte, Choi, Hewitt, Bueren-Calabuig, Pisco, . . . Jansen. (2019). Lysyl-tRNA synthetase as a drug target in malaria and cryptosporidiosis. *Proceedings of the National Academy of Sciences*, 116(14), 7015-7020.
- Barnholtz, Lydon, Huang, Venkatesh, Barnes, Ketring, & Jurisson. (2001). Syntheses and Characterization of Gold (III) Tetradentate Schiff Base Complexes. X-ray Crystal Structures of [Au (sal2pn)] Cl[⊖] 2.5 H₂O and [Au (sal2en)] PF₆. *Inorganic Chemistry*, 40(5), 972-976.
- Baruffini, Ruotolo, Bisceglie, Montalbano, Ottonello, Pelosi, . . . Lodi. (2020). Mechanistic insights on the mode of action of an antiproliferative thiosemicarbazone-nickel complex revealed by an integrated chemogenomic profiling study. *Scientific Reports*, 10(1), 1-14.

- Bayrak, Demirbas, Karaoglu, & Demirbas. (2009). Synthesis of some new 1, 2, 4-triazoles, their Mannich and Schiff bases and evaluation of their antimicrobial activities. *European Journal of Medicinal Chemistry*, 44(3), 1057-1066.
- Beckford, Shaloski Jr, Leblanc, Thessing, Lewis-Alleyne, Holder, . . . Seeram. (2009). Microwave synthesis of mixed ligand diimine–thiosemicarbazone complexes of ruthenium (II): biophysical reactivity and cytotoxicity. *Dalton Transactions*(48), 10757-10764.
- Beekman, Woerdenbag, Kampinga, & Konings. (1996). Cytotoxicity of artemisinin, a dimer of dihydroartemisinin, artemisitene and eupatoriopicrin as evaluated by the MTT and clonogenic assay. *Phytotherapy Research*, 10(2), 140-144.
- Bhattacharjee, & Karle. (1996). Molecular electronic properties of a series of 4-quinolinecarbinolamines define antimalarial activity profile. *Journal of Medicinal Chemistry*, 39(23), 4622-4629.
- Bingham, Bögge, Müller, Ainscough, & Brodie. (1987). Synthetic, spectroscopic, and X-ray crystallographic studies on binuclear copper (II) complexes with a tridentate NNS-bonding 2-formylpyridine thiosemicarbazone ligand. The characterization of both neutral and deprotonated co-ordinated ligand structures. *Journal of the Chemical Society, Dalton Transactions*(3), 493-499.
- Biot, Chavain, Dubar, Pradines, Trivelli, Brocard, . . . Dive. (2009). Structure–activity relationships of 4-N-substituted ferroquine analogues: Time to re-evaluate the mechanism of action of ferroquine. *Journal of Organometallic Chemistry*, 694(6), 845-854.
- Bisceglie, Orsoni, Pioli, Bonati, Tarasconi, Rivetti, . . . Pelosi. (2019). Cytotoxic activity of copper (ii), nickel (ii) and platinum (ii) thiosemicarbazone derivatives: interaction with DNA and the H2A histone peptide. *Metallomics*, 11(10), 1729-1742.
- Blunden, Thomas, & Stenzel. (2012). Macromolecular ruthenium complexes as anti-cancer agents. *Polymer Chemistry*, 3(10), 2964-2975.
- Boudhar, Ng, Loh, Chia, Tan, Nosten, . . . Tan. (2016). Overcoming chloroquine resistance in malaria: design, synthesis and structure–activity relationships of novel chemoreversal agents. *European Journal of Medicinal Chemistry*, 119, 231-249.
- Bray, Ferlay, Soerjomataram, Siegel, Torre, & Jemal. (2018). Global cancer statistics 2018: GLOBOCAN estimates of incidence and mortality worldwide for 36 cancers in 185 countries. *CA: A Cancer Journal for Clinicians*, 68(6), 394-424.

- Brockman, Thomson, Bell, & Skipper. (1956). Observations on the antileukemic activity of pyridine-2-carboxaldehyde thiosemicarbazone and thiocarbohydrazone. *Cancer Research*, 16(2), 167-170.
- Bruijninx, & Sadler. (2008). New trends for metal complexes with anticancer activity. *Current Opinion in Chemical Biology*, 12(2), 197-206.
- Bullen, Rogers, & Griffiths. (1978). Role of iron in bacterial infection *Current Topics in Microbiology and Immunology* (pp. 1-35): Springer.
- Butler, & Sadler. (2013). Targeted delivery of platinum-based anticancer complexes. *Current Opinion in Chemical Biology*, 17(2), 175-188.
- Calvert. (2019). The Clinical Development of Carboplatin—A Personal Perspective. *Inorganica Chimica Acta*, Article#118987.
- Campbell. (1975). Transition metal complexes of thiosemicarbazide and thiosemicarbazones. *Coordination Chemistry Reviews*, 15(2-3), 279-319.
- Carcelli, Tegoni, Bartoli, Marzano, Pelosi, Salvalaio, . . . Gandin. (2020). In vitro and in vivo anticancer activity of tridentate thiosemicarbazone copper complexes: Unravelling an unexplored pharmacological target. *European Journal of Medicinal Chemistry*, Article#112266.
- Casas, Garcia-Tasende, & Sordo. (2000). Main group metal complexes of semicarbazones and thiosemicarbazones. A structural review. *Coordination Chemistry Reviews*, 209(1), 197-261.
- Casas, Rodríguez-Argüelles, Russo, Sánchez, Sordo, Vázquez-López, . . . Albertini. (1998). Diorganotin (IV) complexes of pyridoxal thiosemicarbazone: Synthesis, spectroscopic properties and biological activity. *Journal of Inorganic Biochemistry*, 69(4), 283-292.
- Chandra, Ballabh, & Choudhary. (2013). Synthesis, Spectral Characterization of Cu (Ii) and Ni (Ii) Complexes with Thiosemicarbazones and Semicarbazones Derived from Pyridine-2-Carboxaldehyde. *International Journal of Applied Biology and Pharmaceutical Technology*, 4(3), 65-72.
- Chandra, Parmar, & Kumar. (2009). Synthesis, spectroscopic, and antimicrobial studies on bivalent zinc and mercury complexes of 2-formylpyridine thiosemicarbazone. *Bioinorganic Chemistry and Applications*, 2009, Article#851316.
- Chasapis, Loutsidou, Spiliopoulou, & Stefanidou. (2012). Zinc and human health: an update. *Archives of Toxicology*, 86(4), 521-534.

- Chellaian, & Johnson. (2014). Spectral characterization, electrochemical and anticancer studies on some metal (II) complexes containing tridentate quinoxaline Schiff base. *Spectrochimica Acta Part A: Molecular and Biomolecular Spectroscopy*, 127, 396-404.
- Chellan, Nasser, Vivas, Chibale, & Smith. (2010). Cyclopalladated complexes containing tridentate thiosemicarbazone ligands of biological significance: Synthesis, structure and antimalarial activity. *Journal of Organometallic Chemistry*, 695(19), 2225-2232.
- Chellan, Shunmoogam-Gounden, Hendricks, Gut, Rosenthal, Lategan, . . . Smith. (2010). Synthesis, structure and in vitro biological screening of palladium (II) complexes of functionalised salicylaldimine thiosemicarbazones as antimalarial and anticancer agents. *European Journal of Inorganic Chemistry*, 2010(22), 3520-3528.
- Chen, Frezza, Shakya, Cui, Milacic, Verani, & Dou. (2007). Inhibition of the proteasome activity by gallium (III) complexes contributes to their anti-prostate tumor effects. *Cancer Research*, 67(19), 9258-9265.
- Cheng, Shen, Luo, Zhu, Gu, Ji, . . . Chen. (2002). Molecular docking and 3-D-QSAR studies on the possible antimalarial mechanism of artemisinin analogues. *Bioorganic & Medicinal Chemistry*, 10(9), 2883-2891.
- Chinappi, Via, Marcatili, & Tramontano. (2010). On the mechanism of chloroquine resistance in Plasmodium falciparum. *PLoS One*, 5(11), Article#e14064.
- Chrysouli, Banti, Kourkoumelis, Panayiotou, Markopoulos, Tasiopoulos, & Hadjikakou. (2018). Chloro (triphenylphosphine) gold (I) a forefront reagent in gold chemistry as apoptotic agent for cancer cells. *Journal of Inorganic Biochemistry*, 179, 107-120.
- Cini, Bradshaw, & Woodward. (2017). Using titanium complexes to defeat cancer: the view from the shoulders of titans. *Chemical Society Reviews*, 46(4), 1040-1051.
- Coronado, Nadovich, & Spadafora. (2014). Malarial hemozoin: from target to tool. *Biochimica et Biophysica Acta (BBA)-General Subjects*, 1840(6), 2032-2041.
- Çukurovali, Yilmaz, Özmen, & Ahmedzade. (2002). Cobalt (II), copper (II), nickel (II) and zinc (II) complexes of two novel Schiff base ligands and their antimicrobial activity. *Transition Metal Chemistry*, 27(2), 171-176.
- Dabrowiak. (2017). *Metals in medicine*: John Wiley & Sons.

- Dale, Tocher, Dyson, Edwards, & Tocher. (1992). Studies on DNA damage and induction of SOS repair by novel multifunctional bioreducible compounds. II. A metronidazole adduct of a ruthenium-arene compound. *Anti-Cancer Drug Design*, 7(1), 3-14.
- Deshpande, Solomon, Katti, & Prabhakar. (2009). Topological descriptors in modelling antimalarial activity: N 1-(7-chloro-4-quinolyl)-1, 4-bis (3-aminopropyl) piperazine as prototype. *Journal of Enzyme Inhibition and Medicinal Chemistry*, 24(1), 94-104.
- Đilović, Rubčić, Vrdoljak, Pavelić, Kralj, Piantanida, & Cindrić. (2008). Novel thiosemicarbazone derivatives as potential antitumor agents: Synthesis, physicochemical and structural properties, DNA interactions and antiproliferative activity. *Bioorganic & Medicinal Chemistry*, 16(9), 5189-5198.
- Dimopoulos, Seeley, Wolf, & Kafatos. (1998). Malaria infection of the mosquito *Anopheles gambiae* activates immune-responsive genes during critical transition stages of the parasite life cycle. *The EMBO journal*, 17(21), 6115-6123.
- Dixon, & Stockwell. (2014). The role of iron and reactive oxygen species in cell death. *Nature Chemical Biology*, 10(1), 9-17.
- Dolomanov, Bourhis, Gildea, Howard, & Puschmann. (2009). OLEX2: a complete structure solution, refinement and analysis program. *Journal of Applied Crystallography*, 42(2), 339-341.
- Dorozhkin, & Epple. (2002). Biological and medical significance of calcium phosphates. *Angewandte Chemie International Edition*, 41(17), 3130-3146.
- Dougan, & Sadler. (2007). The design of organometallic ruthenium arene anticancer agents. *CHIMIA International Journal for Chemistry*, 61(11), 704-715.
- Dyson. (2007). Systematic design of a targeted organometallic antitumour drug in pre-clinical development. *CHIMIA International Journal for Chemistry*, 61(11), 698-703.
- Eby, & Eby. (2006). Rapid recovery from major depression using magnesium treatment. *Medical Hypotheses*, 67(2), 362-370.
- Eğlence-Bakır, Sacan, Şahin, Yanardag, & Ülküseven. (2019). Dioxomolybdenum (VI) complexes with 3-methoxy salicylidene-N-alkyl substituted thiosemicarbazones. Synthesis, characterization, enzyme inhibition and antioxidant activity. *Journal of Molecular Structure*, 1194, 35-41.

- Ekengard, Glans, Cassells, Fogeron, Govender, Stringer, . . . Doverbratt. (2015). Antimalarial activity of ruthenium (II) and osmium (II) arene complexes with mono-and bidentate chloroquine analogue ligands. *Dalton Transactions*, 44(44), 19314-19329.
- Elamathi, Fronczek, Madankumar, & Prabhakaran. (2020). Synthesis and spectral characterizations of water soluble Cu (ii) complexes containing N-heterocyclic chelates: cell-proliferation, antioxidant and nucleic acid/serum albumin interactions. *New Journal of Chemistry*, 44(10), 4158-4170.
- Elmagbari, Hammouda, Jackson, & Bonomo. (2019). Stability, solution structure and X-ray crystallography of a copper (II) diamide complex. *Inorganica Chimica Acta*, 498, Article#119132.
- Esteves-Souza, Pissinate, da Graça Nascimento, Grynberg, & Echevarria. (2006). Synthesis, cytotoxicity, and DNA-topoisomerase inhibitory activity of new asymmetric ureas and thioureas. *Bioorganic & Medicinal Chemistry*, 14(2), 492-499.
- Fang, Jia, Dong, Xin, & Zhang. (2018). Syntheses, characterization and reactivity of dinuclear ruthenium-nickel complexes with hexane-2, 5-dione bis (thiosemicarbazonato) ligands. *Journal of Organometallic Chemistry*, 871, 122-129.
- Farrell. (2002). Biomedical uses and applications of inorganic chemistry. An overview. *Coordination Chemistry Reviews*, 232(1-2), 1-4.
- Fatih, Staines, Siner, Ahmed, Woon, Pasini, . . . Krishna. (2013). Susceptibility of human Plasmodium knowlesi infections to anti-malarials. *Malaria Journal*, 12(1), Article#425.
- Fatondji, Kpoviessi, Gbaguidi, Bero, Hannaert, Quetin-Leclercq, . . . Accrombessi. (2013). Structure–activity relationship study of thiosemicarbazones on an African trypanosome: Trypanosoma brucei brucei. *Medicinal Chemistry Research*, 22(5), 2151-2162.
- Ferrari, Bisceglie, Pelosi, Sassi, Tarasconi, Cornia, . . . Pinelli. (2002). Synthesis, characterization and X-ray structures of new antiproliferative and proapoptotic natural aldehyde thiosemicarbazones and their nickel (II) and copper (II) complexes. *Journal of Inorganic Biochemistry*, 90(3-4), 113-126.
- Finch, Liu, Cory, Cory, & Sartorelli. (1999). Triapine (3-aminopyridine-2-carboxaldehyde thiosemicarbazone; 3-AP): an inhibitor of ribonucleotide reductase with antineoplastic activity. *Advances in Enzyme Regulation*, 39, 3-12.

- Forsen, & Kordel. (1994). Calcium in biological systems (pp. 107): University Science Books: Mill Valley, CA.
- Gabano, Ravera, & Osella. (2009). The drug targeting and delivery approach applied to Pt-antitumour complexes. A coordination point of view. *Current Medicinal Chemistry*, 16(34), 4544-4580.
- Galluzzi, Senovilla, Vitale, Michels, Martins, Kepp, . . . Kroemer. (2012). Molecular mechanisms of cisplatin resistance. *Oncogene*, 31(15), 1869-1883.
- Gao, Gong, Zhang, Du, Cao, & Zhao. (2020). A novel cyclopalladated ferrocene derivative: Synthesis, single crystal structure and evaluation of in vitro antitumor activity. *Journal of Molecular Structure*, 1200, Article#127077.
- Güveli, Özdemir, Ülküseven, & Bal-Demirci. (2016). Divalent nickel complexes of thiosemicarbazone based on 5-bromosalicylaldehyde and triphenylphosphine: Experimental and theoretical characterization. *Polyhedron*, 113, 16-24.
- Haribabu, Jeyalakshmi, Arun, Bhuvanesh, Perumal, & Karvembu. (2015). Synthesis, DNA/protein binding, molecular docking, DNA cleavage and in vitro anticancer activity of nickel (II) bis (thiosemicarbazone) complexes. *RSC Advances*, 5(57), 46031-46049.
- Harper, Krause-Heuer, Grant, Manohar, Garbutcheon-Singh, & Aldrich-Wright. (2010). Advances in platinum chemotherapeutics. *Chemistry—A European Journal*, 16(24), 7064-7077.
- Held, Supan, Salazar, Tinto, Bonkian, Nahum, . . . Sirima. (2015). Ferroquine and artesunate in African adults and children with Plasmodium falciparum malaria: a phase 2, multicentre, randomised, double-blind, dose-ranging, non-inferiority study. *The Lancet Infectious Diseases*, 15(12), 1409-1419.
- Heng, Sinniah, Teoh, Sim, Ng, Cheah, & Tan. (2015). Synthesis of a DNA-targeting nickel (II) complex with testosterone thiosemicarbazone which exhibits selective cytotoxicity towards human prostate cancer cells (LNCaP). *Spectrochimica Acta Part A: Molecular and Biomolecular Spectroscopy*, 150, 360-372.
- Hoelz, Calil, Nonato, Pinheiro, & Boechat. (2018). Plasmodium falciparum dihydroorotate dehydrogenase: A drug target against malaria. *Future Medicinal Chemistry*, 10(15), 1853-1874.
- Hyde. (2005). Drug-resistant malaria. *Trends in Parasitology*, 21(11), 494-498.

- Immel, Groth, Huhn, & Öhlschläger. (2011). Titanium salen complexes displays strong antitumor properties in vitro and in vivo in mice. *PLoS One*, 6(3), Article#e17869.
- Isab, & Al-Arfaj. (1991). Interaction of palladium (II) with DL-selenamethionine in acidic aqueous solution. *Transition Metal Chemistry*, 16(3), 304-307.
- John, Sreekanth, Rajakannan, Ajith, & Kurup. (2004). New copper (II) complexes of 2-hydroxyacetophenone N (4)-substituted thiosemicarbazones and polypyridyl co-ligands: structural, electrochemical and antimicrobial studies. *Polyhedron*, 23(16), 2549-2559.
- Johnstone, Wilson, & Lippard. (2013). Monofunctional and higher-valent platinum anticancer agents. *Inorganic Chemistry*, 52(21), 12234-12249.
- Jouad, Riou, Allain, Khan, & Bouet. (2001). Synthesis, structural and spectral studies of 5-methyl 2-furaldehyde thiosemicarbazone and its Co, Ni, Cu and Cd complexes. *Polyhedron*, 20(1-2), 67-74.
- Kalaivani, Prabhakaran, Ramachandran, Dallemer, Paramaguru, Renganathan, . . . Natarajan. (2012). Influence of terminal substitution on structural, DNA, protein binding, anticancer and antibacterial activities of palladium (II) complexes containing 3-methoxy salicylaldehyde-4 (N) substituted thiosemicarbazones. *Dalton Transactions*, 41(8), 2486-2499.
- Kalaivani, Saranya, Poornima, Prabhakaran, Dallemer, Padma, & Natarajan. (2014). Biological evaluation of new nickel (II) metallates: Synthesis, DNA/protein binding and mitochondrial mediated apoptosis in human lung cancer cells (A549) via ROS hypergeneration and depletion of cellular antioxidant pool. *European Journal of Medicinal Chemistry*, 82, 584-599.
- Kashyap, Chetia, & Rudrapal. (2017). Synthesis, Antimalarial Activity Evaluation and Drug likeness Study of Some New Quinoline-Lawsone Hybrids. *Indian Journal of Pharmaceutical Sciences*, 78(6), 801-809.
- Kaya, Erçağ, & Koca. (2020). New square-planar nickel (II)-triphenylphosphine complexes containing ONS donor ligands: Synthesis, characterization, electrochemical and antioxidant properties. *Journal of Molecular Structure*, 1206, Article#127653.
- Kelland. (2007). The resurgence of platinum-based cancer chemotherapy. *Nature Reviews Cancer*, 7(8), 573-584.
- Keller. (1993). Arene ruthenium complexes as anticancer agents. *Metal Complexes in Cancer Chemotherapy*, VCH Weinheim, 187.

- Khalaji, Grivani, Rezaei, Fejfarova, & Dusek. (2013). Synthesis and Characterization of Zinc (II) Complexes with 3, 4-Dimethoxybenzaldehyde Thiosemicarbazone: The Crystal Structure of [Zn (34-MBTSC) 2Cl₂]. *Phosphorus, Sulfur, and Silicon and the Related Elements*, 188(8), 1119-1126.
- Khan, Kumar, Joshi, Iqbal, & Saleem. (2008). Synthesis and in vitro antibacterial activity of new steroidal thiosemicarbazone derivatives. *European Journal of Medicinal Chemistry*, 43(9), 2029-2034.
- Khan, & Yusuf. (2009). Synthesis, spectral studies and in vitro antibacterial activity of steroidal thiosemicarbazone and their palladium (Pd (II)) complexes. *European Journal of Medicinal Chemistry*, 44(5), 2270-2274.
- Khanye, Smith, Lategan, Smith, Gut, Rosenthal, & Chibale. (2010). Synthesis and in vitro evaluation of gold (I) thiosemicarbazone complexes for antimalarial activity. *Journal of Inorganic Biochemistry*, 104(10), 1079-1083.
- King, De Ryck, Kaminski, Valade, Stables, & Kohn. (2011). Defining the structural parameters that confer anticonvulsant activity by the site-by-site modification of (R)-N'-benzyl 2-amino-3-methylbutanamide. *Journal of Medicinal Chemistry*, 54(19), 6432-6442.
- Klayman, Bartosevich, Griffin, Mason, & Scovill. (1979). 2-Acetylpyridine thiosemicarbazones. 1. A new class of potential antimalarial agents. *Journal of Medicinal Chemistry*, 22(7), 855-862.
- Klayman, Scovill, Bartosevich, & Mason. (1979). 2-Acetylpyridine thiosemicarbazones. 2. N₄, N₄-Disubstituted derivatives as potential antimalarial agents. *Journal of Medicinal Chemistry*, 22(11), 1367-1373.
- Koram, & Molyneux. (2007). When is "malaria" malaria? The different burdens of malaria infection, malaria disease, and malaria-like illnesses. *American Journal of Tropical Medicine and Hygiene*, 77(6), 1-5.
- Kosaisavee, Suwanarusk, Nosten, Kyle, Barrends, Jones, . . . Lek-Uthai. (2006). Plasmodium vivax: isotopic, PicoGreen, and microscopic assays for measuring chloroquine sensitivity in fresh and cryopreserved isolates. *Experimental parasitology*, 114(1), 34-39.
- Kotkar, & Juneja. (2013). Synthesis, Characterization, and Antimicrobial Studies of N, O Donor Schiff Base Polymeric Complexes. *Journal of Chemistry*, 2013, Article#479343.

- Kumar, Sarala, Siddikha, Vanitha, Babu, & Reddy. (2018). Synthesis, Characterization Antimicrobial and Antioxidant Activities of 2, 4-dihydroxybenzaldehyde-4-phenyl-3-thiosemicarbazone (DHBPTSC) and its Pd (II), Ni (II) dppm Mixed ligand and Cu (II) complex having heterocyclic bases. *Journal of Applied Pharmaceutical Science*, 8(04), 071-078.
- Kumar, & Trivedi. (2016). A review on role of nickel in the biological system. *Internationa Journal of Current Microbiology and Applied Sciences*, 5(3), 719-727.
- Kyu, Stein, Pinto, Rakovac, Weber, Purnat, . . . Biryukov. (2018). Causes of death among children aged 5–14 years in the WHO European Region: a systematic analysis for the Global Burden of Disease Study 2016. *The Lancet Child & Adolescent Health*, 2(5), 321-337.
- Lambotte. (1932). L'utilisation du magnesium comme materiel perdu dans l'osteosynthèse. *Bull Mem Soc Nat Chir*, 28(3), 1325-1334.
- Latheef, Manoj, & Kurup. (2007). Synthesis and spectral characterization of zinc (II) complexes of N (4)-substituted thiosemicarbazone derived from salicylaldehyde: Structural study of a novel–OH free Zn (II) complex. *Polyhedron*, 26(15), 4107-4113.
- Leigh, Raines, Castillo, & Duhme-Klair. (2011). Inhibition of xanthine oxidase by thiosemicarbazones, hydrazones and dithiocarbazates derived from hydroxy-substituted benzaldehydes. *ChemMedChem*, 6(6), 1107-1118.
- Lewis, Liu, Seymour, Magnusen, Erves, Arca, . . . Fronczek. (2012). Synthesis, characterisation, and preliminary in vitro studies of vanadium (IV) complexes with a Schiff base and thiosemicarbazones as mixed ligands. *European Journal of Inorganic Chemistry*, 2012(4), 664-677.
- Liberta, & West. (1992). Antifungal and antitumor activity of heterocyclic thiosemicarbazones and their metal complexes: current status. *Biometals*, 5(2), 121-126.
- Liu, Cheng, Frost, & Dong. (2013). The mineral tooeleite Fe₆ (AsO₃)₄SO₄ (OH) 4·4H₂O—An infrared and Raman spectroscopic study—environmental implications for arsenic remediation. *Spectrochimica Acta Part A: Molecular and Biomolecular Spectroscopy*, 103, 272-275.
- Liu, Qin, Zhai, Zhang, Gu, Tang, . . . Chen. (2019). Antimalarial drug pyrimethamine plays a dual role in antitumor proliferation and metastasis through targeting DHFR and TP. *Molecular Cancer Therapeutics*, 18(3), 541-555.

- Lobana, Khanna, Hundal, Butcher, & Castineiras. (2009). Mono- and di-nuclear complexes of thiosemicarbazones with copper (I): Synthesis, spectroscopy and structures. *Polyhedron*, 28(18), 3899-3906.
- Lobana, Sharma, Bawa, & Khanna. (2009). Bonding and structure trends of thiosemicarbazone derivatives of metals—an overview. *Coordination Chemistry Reviews*, 253(7-8), 977-1055.
- Lopez-Garriga, Babcock, & Harrison. (1986). Factors influencing the C: N stretching frequency in neutral and protonated Schiff's bases. *Journal of the American Chemical Society*, 108(23), 7241-7251.
- Lovejoy, & Lippard. (2009). Non-traditional platinum compounds for improved accumulation, oral bioavailability, and tumor targeting. *Dalton Transactions*(48), 10651-10659.
- Lu, Du, Guo, Jiang, Zeng, & Zang. (2011). Two oxovanadium complexes incorporating thiosemicarbazones: synthesis, characterization, and DNA-binding studies. *Journal of Coordination Chemistry*, 64(7), 1229-1239.
- MacDiarmid, Mugridge, Weiss, Phillips, Burn, Paulin, . . . Pattison. (2007). Bacterially derived 400 nm particles for encapsulation and cancer cell targeting of chemotherapeutics. *Cancer Cell*, 11(5), 431-445.
- Macrae, Bruno, Chisholm, Edgington, McCabe, Pidcock, . . . Wood. (2008). Mercury CSD 2.0 - new features for the visualization and investigation of crystal structures. *Journal of Applied Crystallography*, 41(2), 466-470.
- Marchewka, Debrus, Pietraszko, Barnes, & Ratajczak. (2003). Crystal structure, vibrational spectra and nonlinear optical properties of L-histidinium-L-tartrate hemihydrate. *Journal of Molecular Structure*, 656(1-3), 265-273.
- Maret. (2013). Zinc and human disease *Interrelations between essential metal ions and human diseases* (pp. 389-414): Springer.
- Martins, Baruah, Kramarczyk, Saluta, Day, Kucera, & Bierbach. (2001). Design, synthesis, and biological activity of a novel non-cisplatin-type platinum-acridine pharmacophore. *Journal of Medicinal Chemistry*, 44(25), 4492-4496.
- Mathew, & Palenik. (1969). Crystal structure of bis (1-isoquinolinecarboxaldehyde thiosemicarbazonato) nickel (II) monohydrate. *Journal of the American Chemical Society*, 91(23), 6310-6314.

- Matsa, Makam, Kaushik, Hoti, & Kannan. (2019). Thiosemicarbazone derivatives: Design, synthesis and in vitro antimalarial activity studies. *European Journal of Pharmaceutical Sciences*, 137, Article#104986.
- Matuszewska, Jaszek, Stefaniuk, Ciszewski, & Matuszewski. (2018). Anticancer, antioxidant, and antibacterial activities of low molecular weight bioactive subfractions isolated from cultures of wood degrading fungus *Cerrena unicolor*. *PLoS One*, 13(6), Article#e0197044.
- Matuszewska, Stefaniuk, Jaszek, Pięt, Zając, Matuszewski, . . . Bancierz. (2019). Antitumor potential of new low molecular weight antioxidative preparations from the white rot fungus *Cerrena unicolor* against human colon cancer cells. *Scientific Reports*, Article#1975.
- Mazzei, Dondero, Balbi, & Bonora. (2001). Synthesis of unsymmetrical methylene derivatives of benzopyran-4-ones from mannich bases. *Journal of Heterocyclic Chemistry*, 38(2), 499-501.
- Melis, Barnett, Wiesner, Nordlander, & Smith. (2020). Quinoline-triazole half-sandwich iridium (III) complexes: synthesis, antiplasmodial activity and preliminary transfer hydrogenation studies. *Dalton Transactions*.
- Mirabelli, Johnson, Sung, Faucette, Muirhead, & Crooke. (1985). Evaluation of the in vivo antitumor activity and in vitro cytotoxic properties of auranofin, a coordinated gold compound, in murine tumor models. *Cancer Research*, 45(1), 32-39.
- Mombo-Ngoma, Supan, Dal-Bianco, Missinou, Matsiegui, Salazar, . . . Kombila. (2011). Phase I randomized dose-ascending placebo-controlled trials of ferroquine-a candidate anti-malarial drug-in adults with asymptomatic *Plasmodium falciparum* infection. *Malaria journal*, 10(1), Article#53.
- Mostafa, El-Asmy, & El-Shahawi. (2000). Ruthenium (II) 2-hydroxybenzophenone N (4)-substituted thiosemicarbazone complexes. *Transition Metal Chemistry*, 25(4), 470-473.
- Munakata, Zhong, Ino, Kuroda-Sowa, Maekawa, Suenaga, & Oiji. (2001). 1-D cyano-bridged heterometallic complexes consisting of 1, 4, 8, 11-tetraazacyclotetradecanesilver (II) and tetracyanopalladium (II) or tetracyanoplatinum (II). *Inorganica Chimica Acta*, 317(1-2), 268-275.
- Muthukumar, & Viswanathamurthi. (2010). Synthesis, spectral characterization and catalytic studies of new ruthenium (II) chalcone thiosemicarbazone complexes. *Open Chemistry*, 8(1), 229-240.

- Nandal, Deep, Singh, Kaushik, SL, Narasimhan, . . . Sharma. (2019). Synthesis of Metal Complexes of Primaquine and In-vitro Antimalarial Evaluation Against Plasmodium falciparum. *Current Bioactive Compounds*, 15(6), 631-636.
- Naß, & Efferth. (2019). Development of artemisinin resistance in malaria therapy. *Pharmacological Research*, Article#104275.
- Navarro, Castro, Martínez, & Delgado. (2011). The mechanism of antimalarial action of [Au (CQ)(PPh₃)] PF₆: structural effects and increased drug lipophilicity enhance heme aggregation inhibition at lipid/water interfaces. *Journal of Inorganic Biochemistry*, 105(2), 276-282.
- Oliveira, Notario, da Silva, & Monte. (2017). Vapour pressures, enthalpies and Gibbs energies of formation and sublimation of fluorene-2-carboxaldehyde. *The Journal of Chemical Thermodynamics*, 111, 65-71.
- Ott, & Gust. (2007). Non platinum metal complexes as anti-cancer drugs. *Archiv der Pharmazie: An International Journal Pharmaceutical and Medicinal Chemistry*, 340(3), 117-126.
- Padhye, & Kauffman. (1985). Transition metal complexes of semicarbazones and thiosemicarbazones. *Coordination Chemistry Reviews*, 63, 127-160.
- Padmanaban, Nagaraj, & Rangarajan. (2007). Drugs and drug targets against malaria. *Current Science*, 92(11), 1545-1555.
- Paterson, & Donnelly. (2011). Copper complexes of bis (thiosemicarbazones): from chemotherapeutics to diagnostic and therapeutic radiopharmaceuticals. *Chemical Society Reviews*, 40(5), 3005-3018.
- Patterson, Miller, Miles, Stewart, Melanson, Vogels, . . . Westcott. (2014). Synthesis, characterization and anticancer properties of (salicylaldiminato) platinum (II) complexes. *Inorganica Chimica Acta*, 415, 88-94.
- Pearce, Rolfe, Russell, Tse, Whittaker, Fuchs, & Thurecht. (2014). Development of a polymer theranostic for prostate cancer. *Polymer Chemistry*, 5(24), 6932-6942.
- Pereira, Curra, & Garcia. (2018). Ubiquitin proteasome system as a potential drug target for malaria. *Current Topics in Medicinal Chemistry*, 18(5), 315-320.
- Pingaew, Prachayasittikul, & Ruchirawat. (2010). Synthesis, cytotoxic and antimalarial activities of benzoyl thiosemicarbazone analogs of isoquinoline and related compounds. *Molecules*, 15(2), 988-996.

- Piri, Moradi–Shoeili, & Assoud. (2019). Ultrasonic assisted synthesis, crystallographic, spectroscopic studies and biological activity of three new Zn (II), Co (II) and Ni (II) thiosemicarbazone complexes as precursors for nano-metal oxides. *Inorganica Chimica Acta*, 484, 338-346.
- Pohl, Wheeler, & Murray. (2013). Sodium and potassium in health and disease *Interrelations between essential metal ions and human diseases* (pp. 29-47): Springer.
- Popović-Bijelić, Kowol, Lind, Luo, Himo, Enyedy, . . . Gräslund. (2011). Ribonucleotide reductase inhibition by metal complexes of Triapine (3-aminopyridine-2-carboxaldehyde thiosemicarbazone): a combined experimental and theoretical study. *Journal of Inorganic Biochemistry*, 105(11), 1422-1431.
- Prabhakaran, Kalaivani, Huang, Poornima, Padma, Dallemer, & Natarajan. (2013). DNA binding, antioxidant, cytotoxicity (MTT, lactate dehydrogenase, NO), and cellular uptake studies of structurally different nickel (II) thiosemicarbazone complexes: synthesis, spectroscopy, electrochemistry, and X-ray crystallography. *JBIC Journal of Biological Inorganic Chemistry*, 18(2), 233-247.
- Prabhu, & Ramesh. (2013). Synthesis and structural characterization of palladium (II) thiosemicarbazone complex: application to the Buchwald–Hartwig amination reaction. *Tetrahedron Letters*, 54(9), 1120-1124.
- Prasad, Rao, Mohan, Singh, Prakash, & Rao. (2009). Synthesis, Spectral and Electrochemical Studies of Co (II) and Zn (II) Complexes of a Novel Schiff base Derived from Pyridoxal. *Synthesis and Reactivity in Inorganic, Metal-Organic, and Nano-Metal Chemistry*, 39(3), 129-132.
- Prylutska, Panchuk, Gołuński, Skivka, Prylutsky, Hurmach, . . . Piosik. (2017). C 60 fullerene enhances cisplatin anticancer activity and overcomes tumor cell drug resistance. *Nano Research*, 10(2), 652-671.
- Raj, & Kurup. (2007). N-2-Hydroxy-4-methoxyacetophenone-N'-4-nitrobenzoyl hydrazine: synthesis and structural characterization. *Spectrochimica Acta Part A: Molecular and Biomolecular Spectroscopy*, 66(4-5), 898-903.
- Raman, Ravichandran, & Thangaraja. (2004). Copper (II), cobalt (II), nickel (II) and zinc (II) complexes of Schiff base derived from benzil-2, 4-dinitrophenylhydrazone with aniline. *Journal of Chemical Sciences*, 116(4), 215-219.
- Ramdzan, Ismail, & Zanib. (2020). Prevalence of malaria and its risk factors in Sabah, Malaysia. *International Journal of Infectious Diseases*, 91, 68-72.

- Rebecca, Nicastrì, Fennelly, Chude, Barber-Rotenberg, Ronghe, . . . Goldman. (2019). PPT1 promotes tumor growth and is the molecular target of chloroquine derivatives in cancer. *Cancer Discovery*, 9(2), 220-229.
- Rebolledo, Vieites, Gambino, Piro, Castellano, Zani, . . . Beraldo. (2005). Palladium (II) complexes of 2-benzoylpyridine-derived thiosemicarbazones: spectral characterization, structural studies and cytotoxic activity. *Journal of Inorganic Biochemistry*, 99(3), 698-706.
- Reena, & Kurup. (2010). Copper (II) complexes derived from di-2-pyridyl ketone-N4-phenyl-3-semicarbazone: Synthesis and spectral studies. *Spectrochimica Acta Part A: Molecular and Biomolecular Spectroscopy*, 76(3-4), 322-327.
- Richardson, Kalinowski, Richardson, Sharpe, Lovejoy, Islam, & Bernhardt. (2009). 2-Acetylpyridine thiosemicarbazones are potent iron chelators and antiproliferative agents: redox activity, iron complexation and characterization of their antitumor activity. *Journal of Medicinal Chemistry*, 52(5), 1459-1470.
- Rodríguez-Argüelles, Sánchez, Ferrari, Fava, Pelizzi, Pelosi, . . . Pinelli. (1999). Transition-metal complexes of isatin- β -thiosemicarbazone. X-ray crystal structure of two nickel complexes. *Journal of Inorganic Biochemistry*, 73(1-2), 7-15.
- Rogolino, Bacchi, De Luca, Rispoli, Sechi, Stevaert, . . . Carcelli. (2015). Investigation of the salicylaldehyde thiosemicarbazone scaffold for inhibition of influenza virus PA endonuclease. *JBIC Journal of Biological Inorganic Chemistry*, 20(7), 1109-1121.
- Rosenberg, Vancamp, Trosko, & Mansour. (1969). Platinum compounds: a new class of potent antitumor agents. *Nature*, 222(5191), 385-386.
- Rosenthal. (1998). Proteases of malaria parasites: new targets for chemotherapy. *Emerging Infectious Diseases*, 4(1), Article#49.
- Rosu, Pahontu, Pasculescu, Georgescu, Stanica, Curaj, . . . Leabu. (2010). Synthesis, characterization antibacterial and antiproliferative activity of novel Cu (II) and Pd (II) complexes with 2-hydroxy-8-R-tricyclo [7.3. 1.0. 2, 7] tridecane-13-one thiosemicarbazone. *European Journal of Medicinal Chemistry*, 45(4), 1627-1634.
- Russell, Chalfein, Prasetyorini, Kenangalem, Piera, Suwanarusk, . . . Cheng. (2008). Determinants of in vitro drug susceptibility testing of Plasmodium vivax. *Antimicrobial Agents and Chemotherapy*, 52(3), 1040-1045.

- Salam, Alam, Sarker, & Rahman. (2018). Synthesis, spectroscopic characterization, crystal structure, and anti-bacterial activity of diorganotin (IV) complexes with 5-bromo-2-hydroxybenzaldehyde-N (4)-ethylthiosemicarbazone. *Journal of Coordination Chemistry*, 71(10), 1593-1605.
- Sava, Alessio, Bergamo, & Mestroni. (1999). Sulfoxide ruthenium complexes: non-toxic tools for the selective treatment of solid tumour metastases *Metallopharmaceuticals I* (pp. 143-169): Springer.
- Scheiber, Dringen, & Mercer. (2013). Copper: effects of deficiency and overload *Interrelations between essential metal ions and human diseases* (pp. 359-387): Springer.
- Schnegg, & Kirchgessner. (1976). Absorption and metabolic efficiency of iron in nickel deficiency. *International Journal for Vitamin and Nutrition Research.*, 46(1), 96-99.
- Scovill, Klayman, & Franchino. (1982). 2-Acetylpyridine thiosemicarbazones. 4. Complexes with transition metals as antimalarial and antileukemic agents. *Journal of Medicinal Chemistry*, 25(10), 1261-1264.
- Seenaa, & Kurup. (2007). Spectral and structural studies of mono-and binuclear copper (II) complexes of salicylaldehyde N (4)-substituted thiosemicarbazones. *Polyhedron*, 26(4), 829-836.
- Seenaa, & Kurup. (2008). Synthesis, spectral and structural studies of zinc (II) complexes of salicylaldehyde N (4)-phenylthiosemicarbazone. *Spectrochimica Acta Part A: Molecular and Biomolecular Spectroscopy*, 69(3), 726-732.
- Sekhon, & Bimal. (2012). Transition metal-based anti-malarial. *Journal of Pharmaceutical Education and Research*, 20112(3), 52-63.
- Shabbir, Akhter, Ashraf, Ismail, Habib, & Mirza. (2017). Nickel (II) and palladium (II) triphenylphosphine complexes incorporating tridentate Schiff base ligands: Synthesis, characterization and biocidal activities. *Journal of Molecular Structure*, 1149, 720-726.
- Shawish, & Bashir. (2014). *Synthesis, characterization and biological studies of nickel (II) complexes containing thiosemicarbazone and thiourea derivatives/Hana Bashir Mohammed Shawish*. Universiti Malaya.
- Shawish, Maah, Halim, & Shaker. (2016). Synthesis, characterization and structural studies of binuclear nickel(II) complexes derived from dihydroxybenzaldehyde

thiosemicarbazones, bridged by 1,2-bis(diphenylphosphino)ethane. *Arabian Journal of Chemistry*, 9, S1935-S1942.

Shawish, Maah, & Ng. (2010). 1-(2, 3, 4-Trihydroxybenzylidene)-4-ethylthiosemicarbazide. *Acta Crystallographica Section E: Structure Reports Online*, 66(5), o1151-o1151.

Shawish, Paydar, Looi, Wong, Movahed, Halim, . . . Maah. (2014). Nickel (II) complexes of polyhydroxybenzaldehyde N4-thiosemicarbazones: synthesis, structural characterization and antimicrobial activities. *Transition Metal Chemistry*, 39(1), 81-94.

Shawish, Wong, Wong, Loh, Looi, Hassandarvish, . . . Paterson. (2014). Nickel (II) complex of polyhydroxybenzaldehyde N4-thiosemicarbazone exhibits anti-inflammatory activity by inhibiting NF- κ B transactivation. *PLoS One*, 9(6), Article#e100933.

Sigel, Sigel, & Sigel. (2013). *Interrelations between essential metal ions and human diseases* (Vol. 13): Springer.

Silva, Becceneri, Solcia, Santiago, Moreira, Neto, . . . Netto. (2020). Cytotoxic and apoptotic effects of ternary silver (i) complexes bearing 2-formylpyridine thiosemicarbazones and 1, 10-phenanthroline. *Dalton Transactions*, 49(16), 5264-5275.

Simon, Kunishima, Vibert, & Lorber. (1979). Inhibitory effects of a new oral gold compound on HeLa cells. *Cancer*, 44(6), 1965-1975.

Singh. (2019). Metal complexes as antimalarial potential: A review.

Singh, Bharti, Naqvi, & Azam. (2004). Synthesis, characterization and in vitro Antiamoebic Activity of 5-nitrothiophene-2-carboxaldehyde thiosemicarbazones and their Palladium (II) and Ruthenium (II) Complexes. *European Journal of Medicinal Chemistry*, 39(5), 459-465.

Singh, Butcher, & Singh. (2008). Synthesis and X-ray structural studies of N'-(pyridine-3-carbonyl) hydrazinecarbodithioic acid ethyl ester (H₂pchc) and [Mn (Hpchc) 2 (o-phen)]. *Polyhedron*, 27(17), 3451-3460.

Singh, & Dikshit. (1995). Synthesis and characterization of mixed ligand copper (I) complexes containing halides, triphenylarsine and N, N-dimethyl-N'-phenylthiourea (dmptH), N, N-dibutyl-N'-phenylthiourea (dbptH) or 1, 3-thiazolidine-2-thione (tzdtH). The X-ray crystal structure of [Cu (PPh₃) 2 (dmptH) Cl]. *Polyhedron*, 14(13-14), 1799-1807.

- Sîrbu, Palamarciuc, Babak, Lim, Ohui, Enyedy, . . . Ang. (2017). Copper (II) thiosemicarbazone complexes induce marked ROS accumulation and promote nrf2-mediated antioxidant response in highly resistant breast cancer cells. *Dalton Transactions*, 46(12), 3833-3847.
- Sobiesiak, Cieślak, Krolewska, Kaźmierczak-Barańska, Pasternak, & Budzisz. (2016). Thiosemicarbazone-derived copper (II), cobalt (II) and nickel (II) complexes as potential anticancer agents: nuclease activity, cytotoxicity and apoptosis studies. *New Journal of Chemistry*, 40(11), 9761-9767.
- Sreekanth, Joseph, Fun, & Kurup. (2006). Formation of manganese (II) complexes of substituted thiosemicarbazones derived from 2-benzoylpyridine: Structural and spectroscopic studies. *Polyhedron*, 25(6), 1408-1414.
- Staiger, Pietak, Huadmai, & Dias. (2006). Magnesium and its alloys as orthopedic biomaterials: a review. *Biomaterials*, 27(9), 1728-1734.
- Summers. (2019). A structural chemistry perspective on the antimalarial properties of thiosemicarbazone metal complexes. *Mini Reviews in Medicinal Chemistry*, 19(7), 569-590.
- Süss-Fink. (2010). Arene ruthenium complexes as anticancer agents. *Dalton Transactions*, 39(7), 1673-1688.
- Sutradhar, Mukherjee, Drew, & Ghosh. (2007). Simple general method of generating non-oxo, non-amavadine model octacoordinated vanadium (IV) complexes of some tetradentate ONNO chelating ligands from various oxovanadium (IV/V) compounds and structural characterization of one of them. *Inorganic Chemistry*, 46(12), 5069-5075.
- Sutton, McGusty, Walz, & DiMartino. (1972). Oral gold. Antiarthritic properties of alkylphosphinegold coordination complexes. *Journal of Medicinal Chemistry*, 15(11), 1095-1098.
- Suwonkerd, Ritthison, Ngol, Tainchum, Bangs, & Chareonviriyahap. (2013). Anopheles mosquitoes—new insights into malaria vectors. *Vector Biology and Malaria Transmission in Southeast Asia*. New York: InTech Open, 273-325.
- Swaminathan. (2003). Magnesium metabolism and its disorders. *The Clinical Biochemist Reviews*, 24(2), 47.
- Swaminathan, Fonseca, Alam, & Shah. (2007). The role of iron in diabetes and its complications. *Diabetes Care*, 30(7), 1926-1933.

- Tan, Seng, Lim, Cheah, Ng, Koo, . . . Maah. (2012). Towards a selective cytotoxic agent for prostate cancer: Interaction of zinc complexes of polyhydroxybenzaldehyde thiosemicarbazones with topoisomerase I. *Polyhedron*, 38(1), 275-284.
- Tate, Bell, D RACKHAM, Wright, Barrett, & Croft. (2014). N-Myristoyltransferase as a potential drug target in malaria and leishmaniasis. *Parasitology*, 141(1), Article#37.
- Teoh, Ang, Fun, & Ong. (1999). Synthesis, crystal structure and biological activity of thiophene-2-carboxaldehyde thiosemicarbazone and its tin complexes. *Journal of Organometallic Chemistry*, 580(1), 17-21.
- Tilley, Straimer, Gnädig, Ralph, & Fidock. (2016). Artemisinin action and resistance in *Plasmodium falciparum*. *Trends in Parasitology*, 32(9), 682-696.
- Tittal, Ghule, Kumar, Kumar, Lal, & Kumar. (2020). Design, synthesis, biological activity, molecular docking and computational studies on novel 1, 4-disubstituted-1, 2, 3-Triazole-Thiosemicarbazone hybrid molecules. *Journal of Molecular Structure*, 1209, Article#127951.
- Todorich, Pasquini, Garcia, Paez, & Connor. (2009). Oligodendrocytes and myelination: the role of iron. *Glia*, 57(5), 467-478.
- Tomma. (2017). Synthesis of New Schiff Bases and 2, 3-Disubstituted 1, 3-Thiazolidin-4-one Derivatives Containing Benzothiazole Moiety. *Ibn AL-Haitham Journal For Pure and Applied Science*, 24(2).
- Tran Buu, Duong Ba, Khoi Nguyen Hoang, Vu Quoc, Duong Khanh, Oanh Doan Thi, & Van Meervelt. (2019). Synthesis and redetermination of the crystal structure of salicylaldehyde N(4)-morpholiniothiosemicarbazone. *Acta Crystallographica Section E*, 75(9), 1389-1393.
- Tserga, Nandwani, Edvall, Bulla, Patel, Canlon, . . . Baguley. (2019). The genetic vulnerability to cisplatin ototoxicity: a systematic review. *Scientific Reports*, 9(1), 3455.
- Tunçel, & Serin. (2005). Synthesis and Characterization of Copper (II), Nickel (II) and Cobalt (II) Complexes with Azo-Linked Schiff Base Ligands. *Synthesis and Reactivity in Inorganic, Metal-Organic and Nano-Metal Chemistry*, 35(3), 203-212.
- Udhayakumari, Velmathi, Venkatesan, & Wu. (2015). A pyrene-linked thiourea as a chemosensor for cations and simple fluorescent sensor for picric acid. *Analytical Methods*, 7(3), 1161-1166.

- Vandresen, Falzirolli, Batista, da Silva-Giardini, de Oliveira, Catharino, . . . da Silva. (2014). Novel R-(+)-limonene-based thiosemicarbazones and their antitumor activity against human tumor cell lines. *European Journal of Medicinal Chemistry*, 79, 110-116.
- Walcourt, Loyevsky, Lovejoy, Gordeuk, & Richardson. (2004). Novel aroylhydrazone and thiosemicarbazone iron chelators with anti-malarial activity against chloroquine-resistant and-sensitive parasites. *The International Journal of Biochemistry & Cell Biology*, 36(3), 401-407.
- Wang, & Guo. (2013). Targeting and delivery of platinum-based anticancer drugs. *Chemical Society Reviews*, 42(1), 202-224.
- Weckler, & Lutz. (1996). Near-infrared spectra of M (OH) Cl (M= Ca, Cd, Sr), Zn (OH) F, γ -Cd (OH) 2, Sr (OH) 2, and brucite-type hydroxides M (OH) 2 (M= Mg, Ca, Mn, Fe, Co, Ni, Cd). *Spectrochimica Acta Part A: Molecular and Biomolecular Spectroscopy*, 52(11), 1507-1513.
- West, Liberta, Padhye, Chikate, Sonawane, Kumbhar, & Yerande. (1993). Thiosemicarbazone complexes of copper (II): structural and biological studies. *Coordination Chemistry Reviews*, 123(1-2), 49-71.
- Westrip. (2010). publCIF: software for editing, validating and formatting crystallographic information files. *Journal of Applied Crystallography*, 43(4), 920-925.
- Wheate, Walker, Craig, & Oun. (2010). The status of platinum anticancer drugs in the clinic and in clinical trials. *Dalton Transactions*, 39(35), 8113-8127.
- Yıldız, Kılıç, & Hökelek. (1998). Intramolecular hydrogen bonding and tautomerism in Schiff bases. Part I. Structure of 1, 8-di [N-2-oxyphenyl-salicylidene]-3, 6-dioxaoctane. *Journal of Molecular Structure*, 441(1), 1-10.
- Yu, Kalinowski, Kovacevic, Siafakas, Jansson, Stefani, . . . Richardson. (2009). Thiosemicarbazones from the old to new: iron chelators that are more than just ribonucleotide reductase inhibitors. *Journal of Medicinal Chemistry*, 52(17), 5271-5294.
- Zambelli, & Ciurli. (2013). Nickel and human health *Interrelations between essential metal ions and human diseases* (pp. 321-357): Springer.
- Zeglis, Divilov, & Lewis. (2011). Role of metalation in the topoisomerase II α inhibition and antiproliferation activity of a series of α -heterocyclic-N4-substituted thiosemicarbazones and their Cu (II) complexes. *Journal of Medicinal Chemistry*, 54(7), 2391-2398.

Zhang, Lin, Hu, Song, Shen, & Gui. (2013). Interaction with biomacromolecules and antiproliferative activities of Mn (II), Ni (II), Zn (II) complexes of demethylcantharate and 2, 2'-bipyridine. *Spectrochimica Acta Part A: Molecular and Biomolecular Spectroscopy*, 110, 100-107.

Universiti Malaya

LIST OF PUBLICATIONS AND PAPERS PRESENTED

Publication

1. **Savir, S.**, Wei, Z. J., Liew, J. W. K., Vythilingam, I., Lim, Y. A. L., Saad, H. M., ... & Tan, K. W. (2020). Synthesis, cytotoxicity and antimalarial activities of thiosemicarbazones and their nickel (II) complexes. *Journal of Molecular Structure*, Article#128090.
2. **Savir, S.**, Liew, J. W. K., Vythilingam, I., Lim, Y. A. L., Tan, C. H., Sim, K. S., ... & Tan, K. W. (2021). Nickel (II) Complexes with Polyhydroxybenzaldehyde and O, N, S tridentate Thiosemicarbazone ligands: Synthesis, Cytotoxicity, Antimalarial Activity, and Molecular Docking Studies. *Journal of Molecular Structure*, Article#130815.

Papers Presented

1. **Savir, S.**, Wei, Z. J., Liew, J. W. K., Vythilingam, I., Lim, Y. A. L., Saad, H. M., ... & Tan, K. W. (2019). *Synthesis and antimalarial activities of metal complexes of thiosemicarbazones*. Paper presented at the 7th Asian Conference on Coordination Chemistry (ACCC), 15-18 October 2019, PWTC, Kuala Lumpur, Malaysia.